

Appendix I

Corrected Emission Spectra

A relatively limited number of corrected emission spectra are available. In this Appendix we include the well-documented corrected spectra. It is not possible to state which are the "most correct." Corrected spectra can be interchanged from photons per wavenumber interval $I(\bar{\nu})$ to photons per wavelength interval $I(\lambda)$ using $I(\lambda) = I(\bar{\nu})\lambda^{-2}$, followed by normalization of the peak intensity to unity. Most of the compounds listed below satisfy the suggested criteria for emission spectral standards, which are as follows:

1. Broad wavelength emission with no fine structure
2. Chemically stable, easily available and purified
3. High quantum yield
4. Emission spectrum independent of excitation wavelength
5. Completely depolarized emission.

I. EMISSION SPECTRA STANDARDS FROM 300 TO 800 NM

Corrected emission spectra on the wavelength scale were reported for six readily available fluorophores in neat solvents (Table I.1). The emission spectra of these standards overlap, providing complete coverage from 300 to 800 nm. For convenience the numerical values of the emission spectra are given in Table I.2. The values are plotted in Figure I.1, and the chemical structures are given in Figure I.2. These correct spectra cover almost all needed wavelengths. It is recommended that these spectra be adopted as the accepted standards for determination of instrument

corrections factors and for calculation of corrected emission spectra.

2. β -CARBOLINE DERIVATIVES AS FLUORESCENCE STANDARDS

Corrected emission spectra of the carboline derivatives shown in Figure I.3 and I.4 were published.² All compounds were measured in 0.1 N H_2SO_4 , except for 2-methyl-harmine, which was measured in 0.01 N H_2SO_4 , 25°C. Corrected emission spectra were reported in graphical form (Figure I.3) and in numerical form (Table I.3). Quantum yields and lifetimes were also reported (Table I.4). Quantum yields were determined relative to quinine sulfate in 1.0

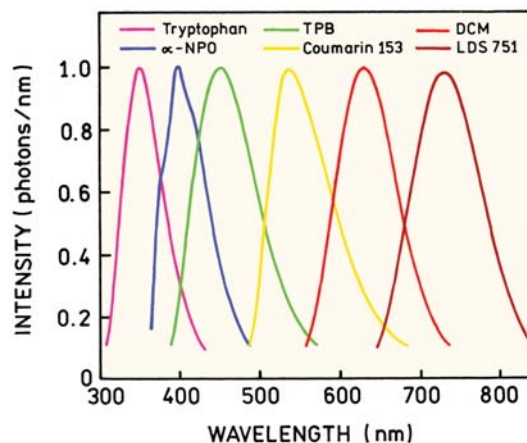


Figure I.1. Corrected emission spectra of six standards from [1]. From left to right the spectra are for tryptophan, α -NPO, TPB, coumarin, DCM, and LDS 751.

Table I.1. Properties of the Emission Intensity Standards*

Probe	CAS	Solvent	Excitation	Emission range
Tryptophan	54-12-6	Water	265	310–428
α -NPO	846-63-9	Methanol	315	364–486
TPB	1450-63-1	Cyclohexane	340	390–570
Coumarin 153	53518-18-6	Methanol	400	486–678
DCM	51325-91-8	Methanol	460	556–736
LDS 751	N/A	Methanol	550	646–844

*CAS number (Chemical Abstract Service registry number) provides a unique identification for each fluorophore. The excitation wavelength and emission range is reported in nm. LDS-751 is a proprietary material of Exciton Inc. (Dayton, OH) and is similar to Styrl 8. Coumarin 153 is also referred to as Coumarin 540A (Exciton). From [1].

Table I.2. Normalized Emission Intensities for Each Emission Standard (emission wavelength is reported in nm and intensity given in photons/nm)

Tryptophan		NPO		TPB		Coumarine 153		DCM		LDS 751	
nm	int.	nm	int.	nm	int.	nm	int.	nm	int.	nm	int.
310	0.111	364	0.162	390	0.11	486	0.118	556	0.1	646	0.101
312	0.149	366	0.247	392	0.137	488	0.142	558	0.115	648	0.114
314	0.194	368	0.342	394	0.167	490	0.169	560	0.132	650	0.128
316	0.242	370	0.433	396	0.199	492	0.2	562	0.148	652	0.143
318	0.299	372	0.509	398	0.235	494	0.235	564	0.168	654	0.159
320	0.357	374	0.571	400	0.271	496	0.274	566	0.19	656	0.177
322	0.417	376	0.618	402	0.31	498	0.315	568	0.214	658	0.196
324	0.485	378	0.656	404	0.35	500	0.36	570	0.238	660	0.216
326	0.547	380	0.69	406	0.393	502	0.407	572	0.266	662	0.238
328	0.611	382	0.725	408	0.436	504	0.458	574	0.303	664	0.26
330	0.675	384	0.764	410	0.478	506	0.509	576	0.331	666	0.284
332	0.727	386	0.813	412	0.525	508	0.56	578	0.353	668	0.308
334	0.771	388	0.864	414	0.571	510	0.613	580	0.38	670	0.334
336	0.814	390	0.915	416	0.62	512	0.665	582	0.412	672	0.361
338	0.86	392	0.959	418	0.663	514	0.715	584	0.444	674	0.388
340	0.906	394	0.988	420	0.699	516	0.762	586	0.478	676	0.416
342	0.928	396	0.999	422	0.735	518	0.806	588	0.513	678	0.445
344	0.957	398	1	424	0.773	520	0.847	590	0.548	680	0.474
346	0.972	400	0.991	426	0.805	522	0.882	592	0.584	682	0.504
348	0.996	402	0.978	428	0.834	524	0.914	594	0.62	684	0.534
350	1	404	0.959	430	0.864	526	0.941	596	0.659	686	0.564
352	0.999	406	0.94	432	0.887	528	0.962	598	0.696	688	0.594
354	0.987	408	0.921	434	0.91	530	0.979	600	0.732	690	0.624
356	0.972	410	0.901	436	0.931	532	0.99	602	0.763	692	0.653
358	0.946	412	0.886	438	0.951	534	0.997	604	0.79	694	0.682
360	0.922	414	0.87	440	0.963	536	1	606	0.818	696	0.711
362	0.892	416	0.855	442	0.976	538	1	608	0.842	698	0.738
364	0.866	418	0.835	444	0.985	540	0.996	610	0.869	700	0.765
366	0.837	420	0.803	446	0.991	542	0.991	612	0.893	702	0.791
368	0.798	422	0.773	448	0.998	544	0.981	614	0.915	704	0.815
370	0.768	424	0.743	450	0.999	346	0.97	616	0.934	706	0.839
372	0.728	426	0.708	452	1	548	0.958	618	0.953	708	0.86
374	0.697	428	0.676	454	0.993	550	0.944	620	0.968	710	0.881
376	0.663	430	0.644	456	0.987	552	0.929	622	0.98	712	0.899
378	0.627	432	0.611	458	0.981	554	0.914	624	0.989	714	0.916
380	0.592	434	0.58	460	0.969	556	0.898	626	0.995	716	0.931
382	0.558	436	0.55	462	0.957	558	0.884	628	0.999	718	0.946
384	0.523	438	0.521	464	0.944	560	0.867	630	1	720	0.956
386	0.492	440	0.494	466	0.931	562	0.852	632	0.998	722	0.965

[continued]

Table I.2, cont'd

388	0.461	442	0.467	468	0.915	564	0.835	634	0.994	724	0.973
390	0.43	444	0.441	470	0.896	566	0.818	636	0.986	726	0.978
392	0.404	446	0.418	472	0.879	568	0.801	638	0.978	728	0.982
394	0.375	448	0.394	474	0.856	570	0.785	640	0.964	730	0.984
396	0.348	450	0.371	476	0.835	572	0.768	642	0.952	732	0.983
398	0.323	452	0.349	478	0.816	574	0.75	644	0.938	734	0.982
400	0.299	454	0.326	480	0.796	576	0.729	646	0.923	736	0.977
402	0.279	456	0.306	482	0.775	578	0.712	648	0.904	738	0.971
404	0.259	458	0.285	484	0.752	580	0.69	650	0.886	740	0.963
406	0.239	460	0.266	486	0.727	582	0.672	652	0.867	742	0.954
408	0.222	462	0.248	488	0.706	584	0.653	654	0.843	744	0.943
410	0.204	464	0.232	490	0.68	586	0.634	656	0.821	746	0.931
412	0.19	466	0.216	492	0.657	588	0.615	658	0.795	748	0.917
414	0.176	468	0.201	494	0.633	590	0.596	660	0.771	750	0.902
416	0.163	470	0.187	496	0.609	592	0.576	662	0.745	752	0.885
418	0.151	472	0.174	498	0.586	594	0.557	664	0.718	754	0.868
420	0.139	474	0.162	500	0.564	596	0.538	666	0.694	756	0.849
422	0.128	476	0.151	502	0.542	598	0.518	668	0.666	758	0.83
424	0.118	478	0.14	504	0.521	600	0.501	670	0.639	760	0.81
426	0.109	480	0.131	506	0.499	602	0.483	672	0.613	762	0.789
428	0.101	482	0.122	508	0.476	604	0.465	674	0.586	764	0.767
		484	0.113	510	0.456	606	0.447	676	0.559	766	0.745
		486	0.105	512	0.437	608	0.43	678	0.534	768	0.722
				514	0.419	610	0.414	680	0.509	770	0.699
				516	0.4	612	0.398	682	0.485	772	0.676
				518	0.382	614	0.383	684	0.46	774	0.653
				520	0.364	616	0.368	686	0.431	776	0.63
				522	0.348	618	0.355	688	0.407	778	0.606
				524	0.332	620	0.341	690	0.391	780	0.583
				526	0.318	622	0.328	692	0.371	782	0.56
				528	0.302	624	0.315	694	0.355	784	0.537
				530	0.289	626	0.303	696	0.336	786	0.514
				532	0.274	628	0.292	698	0.319	788	0.492
				534	0.261	630	0.28	700	0.302	790	0.47
				536	0.249	632	0.269	702	0.284	792	0.449
				538	0.237	634	0.258	704	0.268	794	0.428
				540	0.226	636	0.248	706	0.254	796	0.407
				542	0.215	638	0.239	708	0.239	798	0.387
				544	0.205	640	0.229	710	0.225	800	0.368
				546	0.194	642	0.219	712	0.212	802	0.349
				548	0.184	644	0.211	714	0.199	804	0.331
				550	0.175	646	0.204	716	0.188	806	0.313
				552	0.166	648	0.195	718	0.177	808	0.296
				554	0.158	650	0.188	720	0.166	810	0.28
				556	0.15	652	0.18	722	0.156	812	0.264
				558	0.143	654	0.173	724	0.147	814	0.249
				560	0.135	656	0.166	726	0.138	816	0.234
				562	0.129	658	0.159	728	0.131	818	0.221
				564	0.122	660	0.152	730	0.123	820	0.207
				566	0.116	662	0.146	732	0.116	822	0.195
				568	0.11	664	0.14	734	0.109	824	0.183
				570	0.105	666	0.134	736	0.103	826	0.171
						668	0.129			828	0.16
						670	0.124			830	0.15
						672	0.118			832	0.14
						674	0.113			834	0.131
						676	0.108			836	0.122
						678	0.104			838	0.114
										840	0.106
										842	0.099
										844	0.092

Table I.3. Normalized and Corrected Fluorescence Spectra for Nor-harmane, Harmane, Harmine, 2-Methyl Harmine, and Harmaline in H₂SO₄ Aqueous Solutions (0.1 N H₂SO₄ for nor-harmane, harmane, harmine and 2-methyl harmine and 0.01 N for harmaline)*

Wave length (nm)	Nor-harmane or β -carboline		Harmine	2-Methyl harmine	Harmaline
		Harmane			
400				0.63	
405				0.76	0.53
410				0.87	0.68
415		0.56		0.93	0.78
420		0.70		0.98	0.89
425	0.54	0.81		1.00	0.95
430	0.67	0.90		0.99	0.98
433					1.00
435	0.79	0.97		0.94	0.99
440	0.90	1.00		0.97**	0.97
445	0.96	0.98		0.80	0.90
450	0.99	0.94		0.73	0.84
454	1.00				
455	0.99	0.88		0.64	0.76
460	0.98	0.82		0.54	0.66
465	0.96	0.76		0.48	0.59
470	0.93	0.69			0.52
475	0.87	0.61			0.44
480	0.83	0.56			0.86
485	0.78	0.50			0.92
490	0.73				0.96
495	0.67				0.98
498					1.00
500	0.61				0.99
505	0.54				0.97
510					0.96
515					0.92
520					0.89
525					0.83
530					0.77
535					0.74
540					0.71
550					0.59
560					0.49

*From [2].

**This number is in question.

Table I.4. Quantum Yields and Lifetimes of the β -Carboline Standards^a (from [2])

Compound	Quantum yield	Lifetime (ns)
Nor-harmane	0.58 ± 0.02	21.2
Harmane	0.83 ± 0.03	20.0 ± 0.5
Harmine	0.45 ± 0.03	6.6 ± 0.2
2-Methylharmine	0.45 ± 0.03	6.5 ± 0.2
Harmaline	0.32 ± 0.02	5.3 ± 0.2

^aSame conditions as in Table I.3.

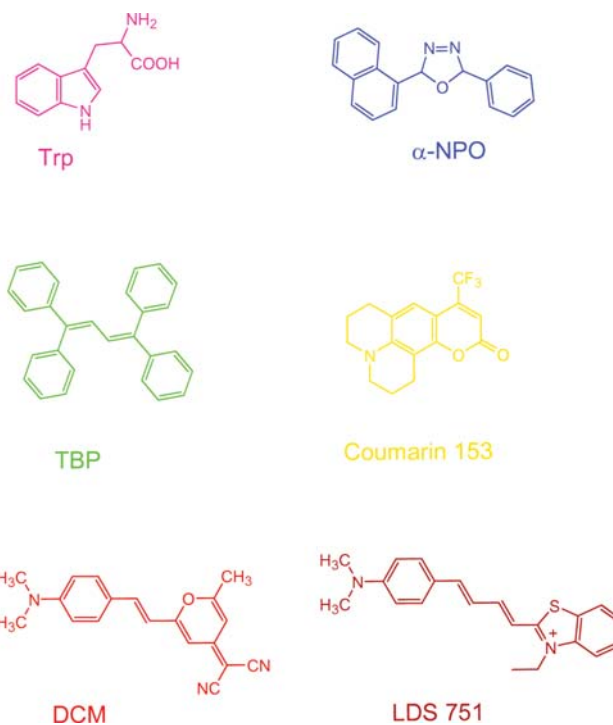


Figure I.2. Chemical structure of the emission spectra standards.

N H₂SO₄, with $Q = 0.546$. Corrected spectra are in relative quanta per wavelength interval. A second corrected emission spectrum of nor-harmane (β -carboline) was also reported (Table I.5).³ The spectral properties of β -carboline are similar to quinine sulfate. While the polarization of the β -carboline standards was not measured, these values are likely to be near zero given the lifetimes near 20 ns (Table I.4).

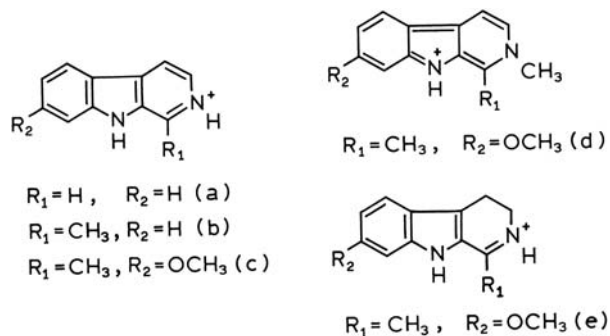


Figure I.3. β -Carboline standards. Cationic species structures: (a) β -carboline or nor-harmane, (b) harmane, (c) harmine, (d) 2-methyl harmine, and (e) harmaline. Revised from [2]. Copyright © 1992, with permission from Elsevier Science.

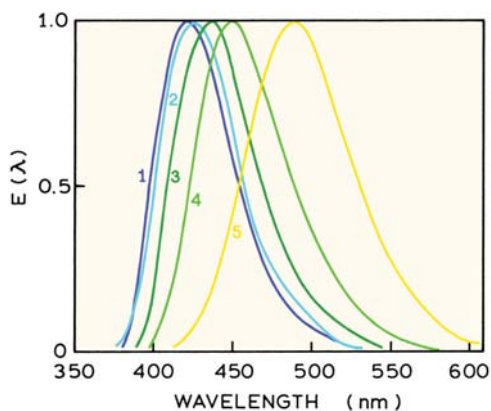


Figure I.4. Corrected and normalized fluorescence spectra for some β -carboline derivatives: (1) harmine 0.1 N H_2SO_4 ; (2) 2-methyl harmine 0.1 N H_2SO_4 ; (3) harmine 0.1 N H_2SO_4 ; (4) nor-harmine 0.1 N H_2SO_4 ; (5) harmaline 0.01 N H_2SO_4 . Revised from [2]. Copyright © 1992, with permission from Elsevier Science.

3. CORRECTED EMISSION SPECTRA OF 9,10-DIPHENYLANTHRACENE, QUININE, AND FLUORESCIN

Corrected spectra in quanta per wavelength interval $I(\lambda)$ were published for these three compounds⁴ (Figure I.5 and Table I.6). The emission spectrum for quinine was found to be at somewhat shorter wavelengths than that published by Melhuish.⁵

4. LONG-WAVELENGTH STANDARDS

Corrected emission spectra in relative quanta per wavelength interval were reported⁴ for quinine sulfate (QS), 3-

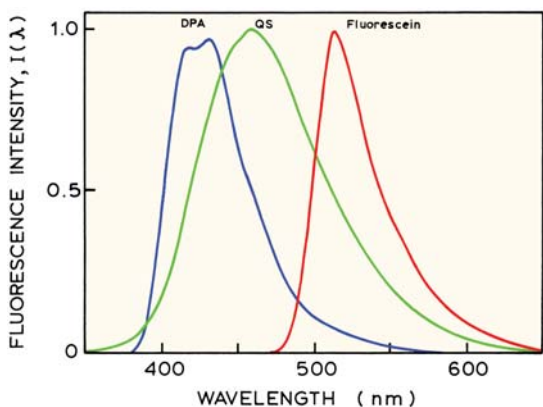


Figure I.5. Corrected emission spectra in relative photons per wavelength interval $I(\lambda)$ for 9,10-diphenylanthracene, quinine sulfate, and fluorescein. From [4].

Table I.5. Corrected Emission Intensities for β -Carboline in 1.0 N H_2SO_4 at 25°C^a

Wave-length (nm)	Corrected intensity	Wave-length (nm)	Corrected intensity
380	0.001	510	0.417
390	0.010	520	0.327
400	0.068	530	0.255
410	0.243	540	0.193
420	0.509	550	0.143
430	0.795	560	0.107
440	0.971	570	0.082
450	1.000	580	0.059
460	0.977	590	0.044
470	0.912	600	0.034
480	0.810	610	0.025
490	0.687	620	0.019
500	0.540	630	0.011

^aExcitation at 360 nm. From [3].

aminophthalimide (3-APT), and N,N-dimethylamino-m-nitrobenzene (N,N-DMAMB). Chemical structures are shown in Figure I.6. These standards are useful because they extend the wavelength range to 750 nm (Figure I.7).

Table I.6. Corrected Emission Spectra in Relative Quanta per Wavelength Interval (from [4])

Quinine sulfate ^a		Fluorescein ^b		DPA ^c	
λ (nm)	$I(\lambda)$	λ (nm)	$I(\lambda)$	λ (nm)	$I(\lambda)$
310	0	470	0	380	0
350	4	480	7	390	39
380	18	490	151	400	423
400	151	495	360	412	993
410	316	500	567	422	914
420	538	505	795	432	1000
430	735	510	950	440	882
440	888	512	1000	450	607
445	935	515	985	460	489
450	965	520	933	470	346
455	990	525	833	480	222
457.2	1000	530	733	490	150
460	998	540	533	500	103
465	979	550	417	550	4
470	951	560	333	600	0
475	916	570	233		
480	871	580	167		
490	733	600	83		
500	616	620	42		
520	408	640	17		
550	171	650	8		
600	19	670	0		
650	3				
700	0				

^aQuinine sulfate was in 1.0 N H_2SO_4 , excitation at 346.5.

^bFluorescein (Uranine) was in 0.1 N NaOH, excitation at 322 nm.

^c9,10-diphenylanthracene (DPA) was in benzene, excitation at 385 nm.

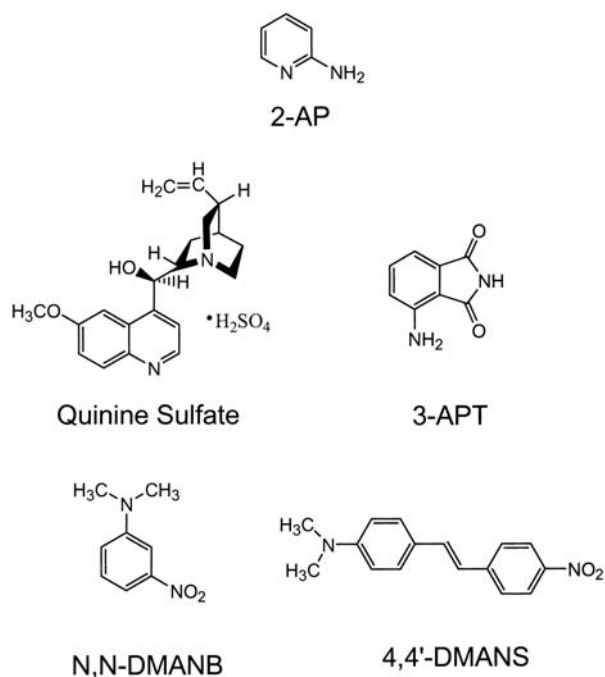


Figure I.6. Chemical structure of fluorophores used as spectral standards.

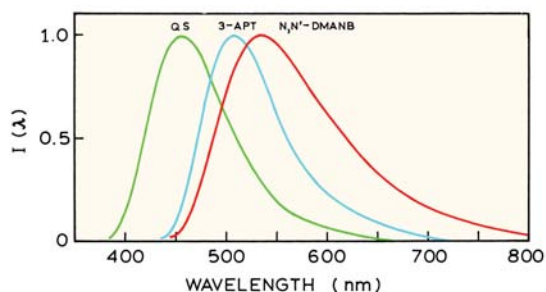


Figure I.7. Corrected emission spectra in relative quanta per wavelength interval $I(\lambda)$. The quinine sulfate (QS) was in 0.1 N H_2SO_4 . 3-aminophthalimide (3-APT) was in 0.1 N H_2SO_4 . N,N-dimethylamino-m-nitrobenzene (N,N-DMANB) was in 70% n-hexane, 30% benzene. Modified from [4].

The data were not reported in numerical form. These corrected emission spectra $I(\lambda)$ were in agreement with that reported earlier⁶ in relative quanta per wavenumber ($I(\bar{\nu})$), following the appropriate transformation.

A more complete set of corrected spectra,^{6,7} in $I(\bar{\nu})$ per wavenumber interval, are summarized numerically in Figure I.8 and Table I.7. These data contain an additional standard, 4-dimethylamino-4'-nitrostilbene (4,4'-DMANS), which extends the wavelength range to 940 nm. These spectra are plotted on the wavenumber scale in Figure I.8. For

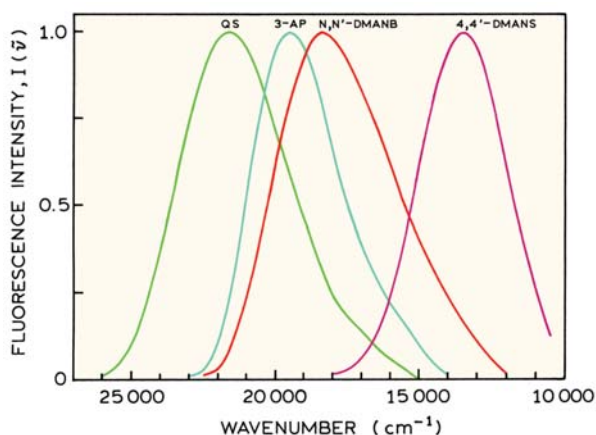


Figure I.8. Corrected emission spectra in relative quanta per wavenumber interval $I(\bar{\nu})$. See Table I.6 for additional details. Data from [6] and [7].

convenience the data were transformed to the wavelength scale, and are shown in Figure I.9 and Table I.8. In summarizing these corrected spectra we omitted β -naphthol, whose emission spectrum depends on pH and buffer concentration. Because these factors change its spectral shape, naphthol is not a good standard.

5. ULTRAVIOLET STANDARDS

2-aminopyridine (Figure I.10) has been suggested as a standard from 315 to 480 nm,^{8,9} which covers most but not all of the wavelengths needed for tryptophan fluorescence

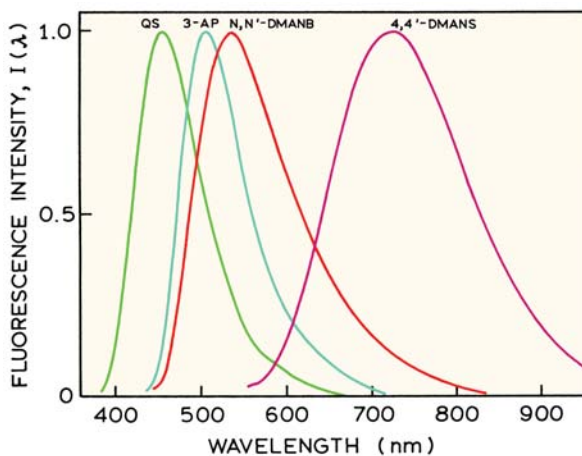


Figure I.9. Corrected emission spectra in relative quanta per wavelength interval $I(\lambda)$. See Table I.5 for additional details. Data from [6] and [7].

Table I.7. Corrected Emission Spectra in Relative Quanta per Wavenumber Interval

Quinine sulfate ^b		3-APT ^c		N,N'-DMANB ^d		4,4'-DMANS ^e	
$\bar{\nu}$ (cm ⁻¹)	<i>I</i> ($\bar{\nu}$)	$\bar{\nu}$ (cm ⁻¹)	<i>I</i> ($\bar{\nu}$)	$\bar{\nu}$ (cm ⁻¹)	<i>I</i> ($\bar{\nu}$)	$\bar{\nu}$ (cm ⁻¹)	<i>I</i> ($\bar{\nu}$)
15.0	0	14.0	1.5	12.0	2.0	10.5	12.5
15.25	1.5	14.25	3.0	12.25	4.0	10.75	18.5
15.5	3.0	14.5	5.0	12.5	6.0	11.0	24.5
15.75	4.5	14.75	7.5	12.75	8.5	11.25	32.5
16.0	6.0	15.0	10.0	13.0	11.0	11.5	41.5
16.25	7.5	15.25	13.0	13.25	13.5	11.75	50.5
16.5	9.5	15.5	16.0	13.5	17.0	12.0	60.0
16.75	11.5	15.75	19.0	13.75	20.0	12.25	70.5
17.0	14.0	16.0	22.0	14.0	23.5	12.5	80.5
17.25	16.0	16.25	25.5	14.25	27.5	12.75	89.0
17.5	18.0	16.5	29.5	14.5	31.0	13.0	95.0
17.75	20.5	16.75	33.5	14.75	35.5	13.25	98.5
18.0	24.0	17.0	38.5	15.0	40.5	13.5	100.0
18.25	28.5	17.25	44.0	15.25	45.0	13.75	98.0
18.5	34.5	17.5	50.0	15.5	50.0	14.0	94.0
18.75	40.5	17.75	56.5	15.75	55.5	14.25	88.0
19.0	46.0	18.0	65.0	16.0	61.5	14.5	81.0
19.25	52.5	18.25	73.0	16.25	68.0	14.75	72.0
19.5	58.5	18.5	82.5	16.5	73.0	15.0	61.5
19.75	65.0	18.75	90.0	16.75	78.0	15.25	51.0
20.0	71.5	19.0	95.0	17.0	82.5	15.5	41.0
20.25	78.5	19.25	98.5	17.25	87.0	15.75	32.0
20.5	84.5	19.5	100.0	17.5	91.5	16.0	24.0
20.75	90.0	19.75	98.5	17.75	95.0	16.25	17.5
21.0	95.0	20.0	94.5	18.0	97.5	16.5	13.0
21.25	98.5	20.25	87.5	18.25	99.5	16.75	9.0
21.5	100.0	20.5	77.5	18.5	99.5	17.0	6.0
21.75	99.5	20.75	66.0	18.75	97.5	17.25	4.0
22.0	98.0	21.0	53.0	19.0	93.5	17.5	2.5
22.25	94.5	21.25	39.5	19.25	87.0	17.75	2.0
22.5	89.0	21.5	28.0	19.5	80.0	18.0	1.5
22.75	82.5	21.75	17.5	19.75	71.5		
23.0	74.0	22.0	11.0	20.0	61.0		
23.25	65.5	22.25	6.0	20.25	51.0		
23.5	55.5	22.5	3.0	20.5	41.5		
23.75	46.0	22.75	1.5	20.75	32.5		
24.0	37.5	23.0	1.0	21.0	23.5		
24.25	29.5			21.25	16.0		
24.5	21.0			21.5	10.5		
24.75	15.0			21.75	6.0		
25.0	10.5			22.0	3.0		
25.25	6.5			22.25	2.0		
25.5	4.0			22.5	1.5		
25.75	2.5						
26.0	1.0						
Max.		Max.		Max.		Max.	
21.6	100.0	19.5	100.0	18.4	100.0	13.5	100.0

^aAll listings are in 10³ cm⁻¹, that is, 13.5 is 13,500 cm⁻¹.

^bQuinine sulfate (10⁻³ M) in 0.1 N H₂SO₄, 20°C.

^c3-aminophthalimide (5 x 10⁻⁴ M) in 0.1 N H₂SO₄, 20°C.

^dN,N-dimethylamino-m-nitrobenzene (10⁻⁴ M) in 30% benzene, 70% n-hexane, 20°C.

^e4-dimethylamino-4'-nitrostilbene in o-dichlorobenzene, 20°C.

Table I.8. Corrected Emission Spectra in Relative Quanta per Wavelength Interval^f

Quinine sulfate ^b		3-APT ^c		N,N-DMANB ^d		4,4'-DMANS ^e	
λ (nm) ^a	$I(\lambda)$	λ (nm)	$I(\lambda)$	λ (nm)	$I(\lambda)$	λ (nm)	$I(\lambda)$
384.6	1.4	434.8	1.4	444.4	2.2	555.6	2.6
388.3	3.5	439.6	2.0	449.4	2.9	563.4	3.4
392.2	5.5	444.4	4.0	454.5	4.2	571.4	4.1
396.0	8.7	449.4	7.7	459.8	8.3	579.7	6.4
400.0	13.8	454.5	13.9	465.1	14.2	588.2	9.4
404.0	19.4	459.8	21.5	470.6	21.1	597.0	13.6
408.2	26.6	465.1	33.7	476.2	30.2	606.1	19.1
412.4	36.6	470.6	46.4	481.9	40.8	615.4	24.9
416.7	45.5	476.2	60.8	487.8	50.9	625.0	33.2
421.1	54.7	481.9	74.0	493.8	61.0	634.9	42.8
425.5	64.6	487.8	84.8	500.0	71.2	645.2	53.2
430.1	74.6	493.8	93.4	506.3	81.4	655.7	64.0
434.8	82.5	500.0	98.4	512.8	88.7	666.7	74.7
439.6	90.0	506.3	100.0	519.5	94.1	678.0	84.5
444.4	95.0	512.8	99.0	526.3	98.5	689.7	91.9
449.4	98.6	519.5	95.0	533.3	100.0	701.8	96.4
454.5	100.0	526.3	89.2	540.5	99.3	714.3	99.4
459.8	99.2	533.3	82.3	547.9	96.7	727.3	100.0
465.1	97.5	540.5	73.5	555.6	92.2	740.7	98.4
470.6	93.8	547.9	63.3	563.4	87.3	754.7	93.3
476.2	88.3	555.6	54.8	571.4	81.8	769.2	86.7
481.9	81.7	563.4	46.3	579.7	75.5	784.3	78.1
487.8	74.9	571.4	39.9	588.2	69.6	800.0	67.9
493.8	67.9	579.7	34.1	597.0	63.8	816.3	57.1
500.0	60.3	588.2	29.0	606.1	58.0	833.3	46.6
506.3	53.4	597.0	24.5	615.4	52.4	851.1	37.6
512.8	46.9	606.1	20.9	625.0	45.9	869.6	29.6
519.5	41.0	615.4	17.5	634.9	40.2	888.9	22.2
526.3	35.0	625.0	14.7	645.2	35.0	909.1	16.0
533.3	30.0	634.9	12.3	655.7	30.5	930.2	11.5
540.5	24.9	645.2	10.0	666.7	26.6	952.4	7.4
547.9	20.0	655.7	7.9	678.0	22.5		
555.6	16.4	666.7	5.9	689.7	19.0		
563.4	13.6	678.0	4.2	701.8	16.3		
571.4	11.6	689.7	2.7	714.3	13.4		
579.7	10.0	701.8	1.6	727.3	11.0		
588.2	8.5	714.3	0.8	740.7	9.0		
597.0	6.8			754.7	6.9		
606.1	5.5			769.2	5.4		
615.4	4.2			784.3	4.0		
625.0	3.2			800.0	2.7		
634.9	2.4			816.3	1.8		
645.2	1.5			833.3	0.8		
655.7	0.7						
666.7	0.0						

^a Calculated from Table I.7.^b Quinine sulfate (10^{-3} M) in 0.1 N H₂SO₄, 20°C.^c 3-aminophthalimide (5×10^{-4} M) in 0.1 N H₂SO₄, 20°C.^d N,N'-dimethylamino-m-nitrobenzene (10^{-4} M) in 30% benzene, 70% m-heptane, 20°C^e 4-dimethylamino-4'-nitrostilbene in o-dichlorobenzene, 20°C.^f Calculated from Table I.7 using $I(\lambda) = \lambda^{-2} I(\bar{\nu})$, followed by normalization of the peak intensity to 100.

Table I.9. Corrected Emission Spectrum of 2-Aminopyridine^a

$\bar{\nu}$ (cm ⁻¹)	$I(\bar{\nu})$	λ (nm)	$I(\lambda)^b$
20,800	0.010	480.8	0.006
21,500	0.038	465.1	0.024
22,200	0.073	450.5	0.049
23,000	0.133	434.8	0.095
23,800	0.264	420.2	0.202
24,700	0.450	404.9	0.371
25,600	0.745	390.6	0.660
26,600	0.960	375.9	0.918
27,200	1.00	367.7	1.00
27,800	0.939	359.7	0.981
28,900	0.587	346.0	0.663
30,150	0.121	331.7	0.149
31,000	0.033	322.6	0.049

^a10⁻⁵ M in 0.1 N₂SO₄. From [10] and [11].

^bCalculated using $I(\lambda) = I(\bar{\nu})\lambda^{-2}$ followed by normalization of the maximum to unity.

(Table I.9 and Figure I.10). Corrected emission spectra have been reported¹⁰ for phenol and the aromatic amino acids, phenylalanine, tyrosine and tryptophan (Figure I.11).

6. ADDITIONAL CORRECTED EMISSION SPECTRA

Corrected spectra as $I(\bar{\nu})$ versus $\bar{\nu}$ can be found in the compendium by Berlman.¹¹ Included in that volume are a number of UV-emitting species including indole and phenol, which can be used to obtain corrected emission spectra of proteins. For convenience Berlman's spectra for phenol and

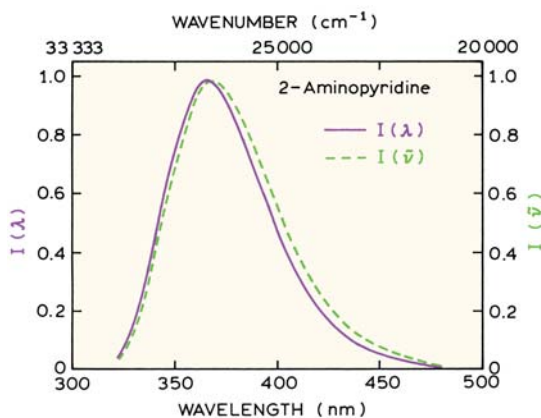


Figure I.10. Corrected emission spectra of 2-aminopyridine in relative quanta per wavenumber interval $I(\bar{\nu})$ and per wavelength interval $I(\lambda)$. See Table I.8 for additional details. From [8] and [9].

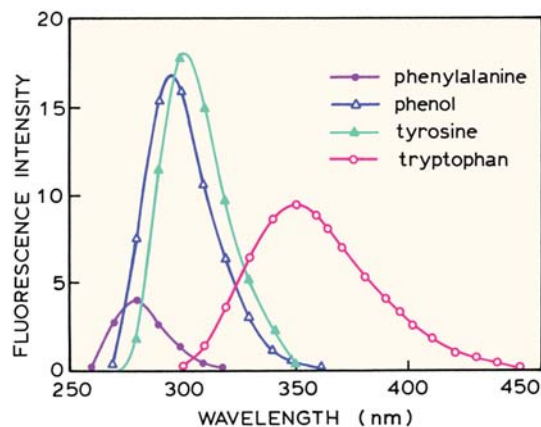


Figure I.11. Corrected emission spectrum $I(\lambda)$ for phenylalanine (●), phenol (Δ), tyrosine (▲), and tryptophan (○). The areas underneath the curves are proportional to the quantum yields. Data from [10].

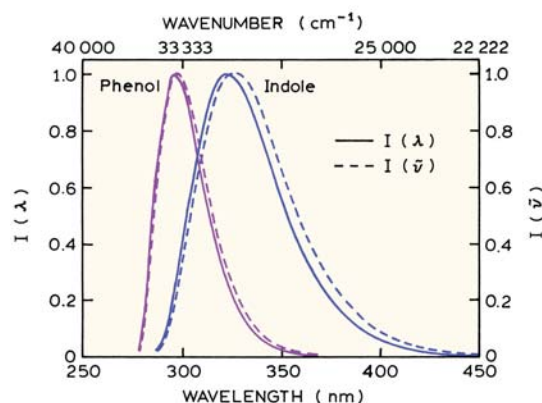


Figure I.12. Corrected emission spectra of phenol in methanol and indole in ethanol. From [11].

indole are provided as Figure I.12. Cresyl violet in methanol has been proposed as a quantum yield and emission spectral standard for red wavelengths.¹² In methanol at 22°C the quantum yield of cresyl violet is reported to be 0.54, with an emission maximum near 614 nm. The use of quinine as a standard has occasionally been questioned.¹³⁻¹⁶ Additional discussion about corrected emission spectra can be found in [17-20].

REFERENCES

1. Gardecki JA, Maroncelli M. 1998. Set of secondary emission standards for calibration of the spectral responsibility in emission spectroscopy. *Appl Spectrosc* **52**:1179-1189.

2. Pardo A, Reyman D, Poyato JML, Medina F. 1992. Some β -carboline derivatives as fluorescence standards. *J Luminesc* **51**:269–274.
3. Ghiggino KP, Skilton PF, Thistlethwaite PJ. 1985. β -Carboline as a fluorescence standard. *J Photochem* **31**:113–121.
4. Heller CA, Henry RA, McLaughlin BA, Bliss DE. 1974. Fluorescence spectra and quantum yields: quinine, uranine, 9,10-diphenylanthracene, and 9,10-bis(phenylethynyl) anthracenes. *J Chem Eng Data* **19**(3):214–219.
5. Melhuish WH. 1960. A standard fluorescence spectrum for calibrating spectro-fluorophotometers. *J Phys Chem* **64**:762–764.
6. Lippert EN, Nägele W, Seibold-Blankenstein I, Staiger W, Voss W. 1959. Messung von fluoreszenzspektren mit hilfe von spektralphotometern und vergleichsstandards. *Z Anal Chem* **170**:1–18.
7. Schmillen A, Legler R. 1967. *Landolt-Börnstein*, Vol. 3: *Lumineszenz Organischer Substanzen*. Springer-Verlag, New York, pp. 228–229.
8. Testa AC. 1969. Fluorescence quantum yields and standards. *Am Instrum Co, Newsl Luminesc* **4**(4):1–3.
9. Rusakowicz R, Testa AC. 1968. 2-aminopyridine as a standard for low wavelength spectrofluorimetry. *J Phys Chem* **72**:2680–2681.
10. Chen RF. 1967. Fluorescence quantum yields of tryptophan and tyrosine. *Anal Lett* **1**:35–42.
11. Berlman IB. 1971. *Handbook of fluorescence spectra of aromatic molecules*, 2nd ed, Academic Press, New York.
12. Magde D, Brannon JH, Cremers TL, Olmsted J. 1979. Absolute luminescence yield of cresyl violet: a standard for the red. *J Phys Chem* **83**(6):696–699.
13. Chen RF. 1967. Some characteristics of the fluorescence of quinine. *Anal Biochem* **19**:374–387.
14. Fletcher AN. 1968. Fluorescence emission band shift with wavelength of excitation. *J Phys Chem* **72**:2742–2749.
15. Itoh K, Azumi T. 1973. Shift of emission band upon excitation at the long wavelength absorption edge: a preliminary survey for quinine and related compounds. *Chem Phys Lett* **22**(2):395–399.
16. Gill JE. 1969. The fluorescence excitation spectrum of quinine bisulfate. *Photochem Photobiol* **9**:313–322.
17. Melhuish WH. 1972. Absolute spectrofluorometry. *J Res Natl Bur Stand* **76A**:547–560.
18. Credi A, Prodi L. 1996. Correction of luminescence intensity measurements in solution: a simple method to standard spectrofluorimeters. *EPA Newsl* **58**:50–59.
19. Eaton DF. 1988. Reference materials for fluorescence measurement. *Pure Appl Chem* **60**(7):1107–1114.
20. Zwinkels JC, Gauthier F. 1999. Instrumentation, standards, and procedures used at the National Research Council of Canada for high-accuracy fluorescence measurements. *Anal Chimica Acta* **380**:193–209.

Appendix II

Fluorescence Lifetime Standards

It is valuable to have fluorophores of known lifetimes for use as lifetime standards in time-domain or frequency-domain measurements. Perhaps more important than the actual lifetime is knowledge that the fluorophore displays single-exponential decays. Such fluorophores are useful for testing the time-resolved instruments for systematic errors. We summarized the results from several laboratories on lifetime standards. There is no attempt to compare the values, or to evaluate that values are more reliable. Much of the data is from this laboratory because it was readily available with all the experimental details.

I. NANOSECOND LIFETIME STANDARDS

A series of scintillator fluorophores were characterized as standards for correcting timing errors in photomultiplier

Table II.1. Nanosecond Reference Fluorophores

Compound ^a	Emission wavelength range	τ (ns) ^b
<i>p</i> -Terphenyl ^c	310–412	1.05
PPD	310–440	1.20
PPO	330–480	1.40
POPOP	370–540	1.35
(Me) ₂ POPOP	390–560	1.45

^aThe abbreviations are: PPD, 2,5-diphenyl-1,3,4-oxadiazole; PPO, 2,5-diphenyloxazole; POPOP, *p*-bis[2-(5-phenyloxazolyl)]benzene; dimethyl or (Me)₂POPOP, 1,4-bis-2-(4-methyl-5-phenyloxazolyl)-benzene.

^bThese values are judged to be accurate to ± 0.2 ns at 10 and 30 MHz. From [1].

tubes.¹ While the decay times were only measured at one or two frequencies, these compounds are thought to display single-exponential decays in ethanol. The decay times are in equilibrium with air, and are not significantly sensitive to temperature (Table II.1). These excitation wavelengths range from 280 to 360 nm, and the emission wavelengths range from 300 to 500 nm (Figure II.1).

One of our most carefully characterized intensity decays is for PPD in ethanol at 20°C, in equilibrium with air.² The frequency response was measured with a GHz frequency-domain instrument. No deviations from a single-exponential decay were detected over the entire range of frequencies (Figure II.2).

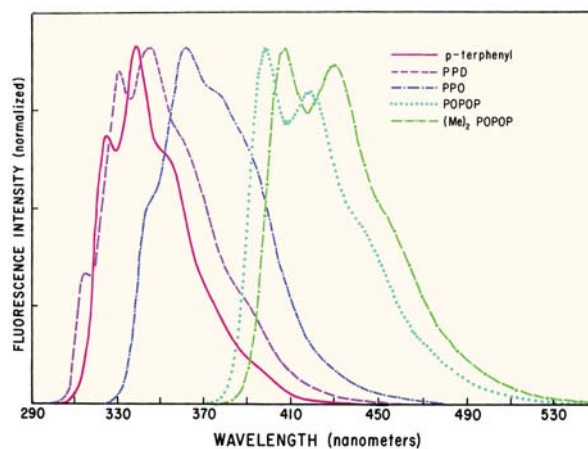


Figure II.1. Emission spectra of nanosecond lifetime reference fluorophores. Reprinted from [1]. Copyright © 1981, with permission from Elsevier Science.

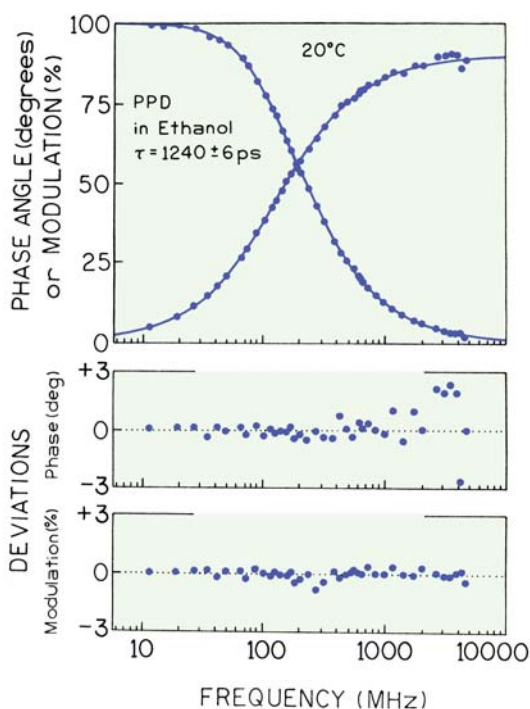


Figure II.2. PPD in ethanol as a single-decay-time standard, in ethanol in equilibrium with air. Reprinted with permission from [2]. Copyright © 1990, American Institute of Physics.

2. PICOSECOND LIFETIME STANDARDS

Derivatives of dimethylamino-stilbene were characterized as lifetime standards with subnanosecond lifetimes³ (Figure II.3). Excitation wavelengths range up to 420 nm, and emission wavelengths from 340 to over 500 nm (Figure II.4).

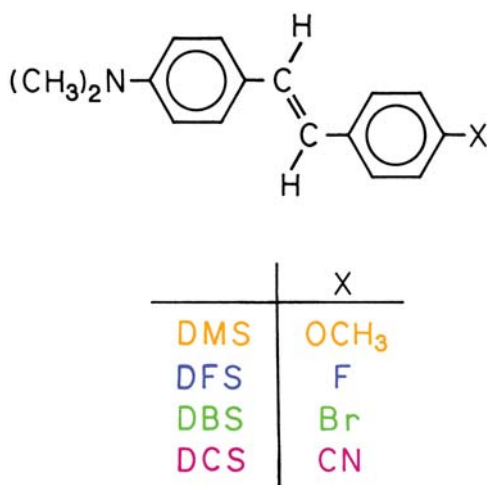


Figure II.3. Picosecond lifetime standard fluorophores. From [3].

APPENDIX II ■ FLUORESCENCE LIFETIME STANDARDS

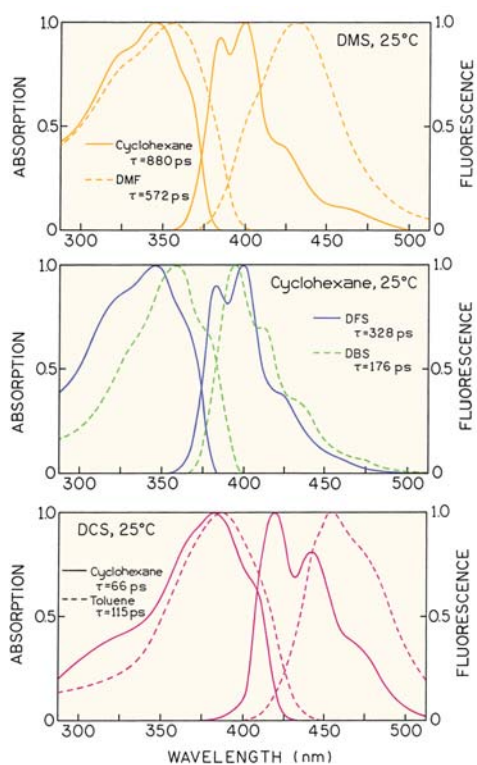


Figure II.4. Top: Absorption and fluorescence spectra of DMS in cyclohexane (solid) and N,N'-dimethylformamide (dashed) at 25°C. **Middle:** Absorption and fluorescence spectra of DFS (solid) and DBS (dashed) in cyclohexane at 25°C. **Bottom:** Absorption and fluorescence spectra of DCS in cyclohexane (solid) and toluene (dashed) at 25°C. Revised from [3].

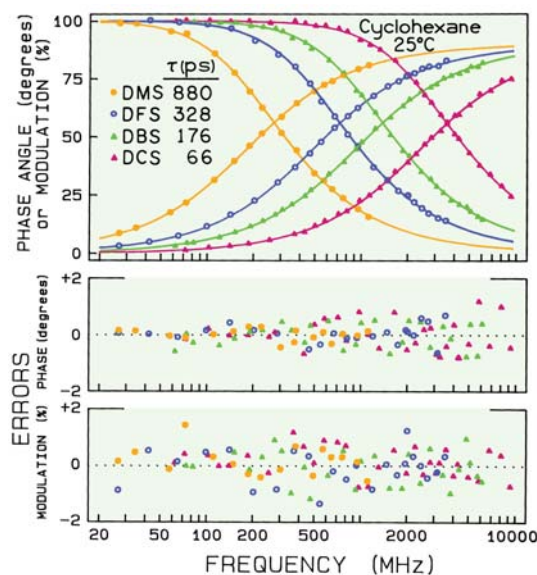


Figure II.5. Representative frequency response of the picosecond lifetime standards. From [3].

Table II.2. Picosecond Lifetime Standards^a

Compound	No. ^a	Sol-vent ^b	Q ^c	T (°C)	τ (ps)
DMS	1	C	0.59	25	880
	2	C	-	37	771
	3	T	0.32	25	740
	4	T	-	5	921
	5	DMF	0.27	25	572
	6	EA	0.15	25	429
DFS	7	C	-	25	328
	8	C	-	37	252
	9	T	0.16	25	305
	10	T	-	5	433
DBS	11	C	0.11	25	176
	12	C	-	37	133
	13	T	0.12	25	168
	14	T	-	5	248
DCS	15	C	0.06	25	66
	16	C	-	37	57
	17	T	0.06	25	115
	18	T	-	5	186

^aFrom [3]. Numbers refer to Figure II.6. These results were obtained from frequency-domain measurements.

^bC, cyclohexane; T, toluene; DMF, dimethylformamide; EA, ethyl acetate. The excitation wavelength was 365 nm.

^cQuantum yields.

Representative frequency responses show that the intensity decays are all single exponentials (Figure II.5). The solutions are all in equilibrium with air. The decay times range from 57 to 921 ps (Table II.2 and Figure II.6).

Rose Bengal can serve as a picosecond lifetime standard at longer wavelengths (Figure II.7). Rose Bengal can

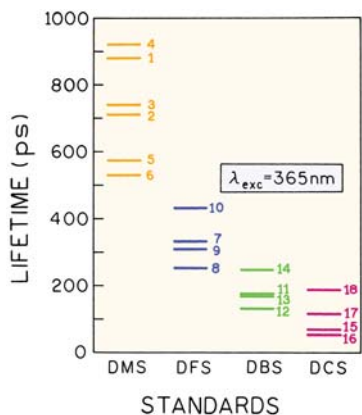


Figure II.6. Lifetimes of the picosecond standards. From [3].

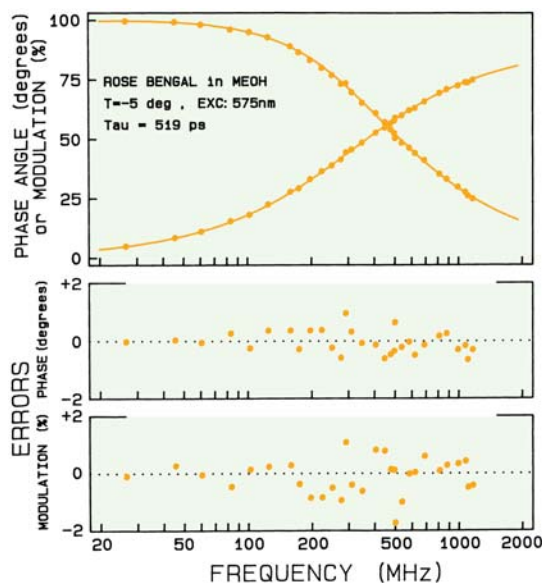


Figure II.7. Rose Bengal as long-wavelength picosecond lifetime standard. For additional lifetime data on Rose Bengal see [4].

also be used as a standard for a short rotational correlation time (Figure II.8).

3. REPRESENTATIVE FREQUENCY-DOMAIN INTENSITY DECAYS

It can be useful to have access to the actual lifetime data. Representative frequency-domain data for single-exponen-

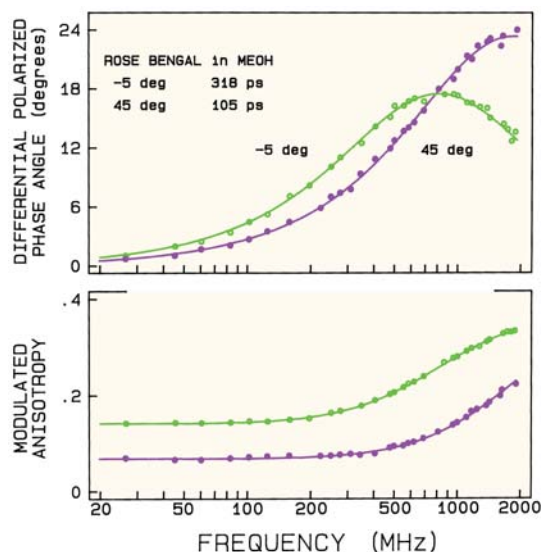


Figure II.8. Rose Bengal as a picosecond correlation time standard. For additional data on Rose Bengal see [4].

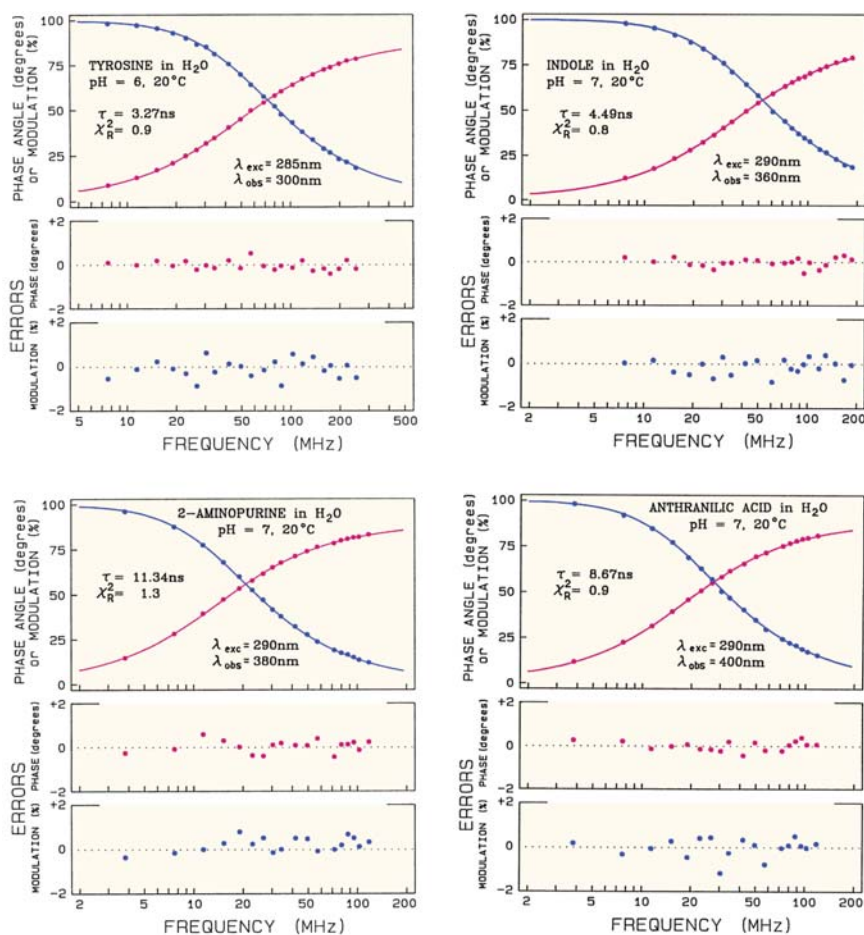


Figure II.9. Representative frequency-domain intensity decays. From [5].

Table II.3. Time-Domain Single Lifetime Standards^a

Compound	Solvent, 20°C	Emission (nm)	τ (ns)
PPO	cyclohexane (D)	440	1.42
PPO	cyclohexane (U)	440	1.28
Anthracene	cyclohexane (D)	405	5.23
Anthracene	cyclohexane (U)	405	4.10
1-cyanonaphthalene	hexane (D)	345	18.23
1-methylindole	cyclohexane (D)	330	6.24
3-methylindole	cyclohexane (D)	330	4.36
3-methylindole	ethanol (D)	330	8.17
1,2-dimethylindole	ethanol (D)	330	5.71

^aFrom [13]. These results were obtained using time-correlated single-photon counting.

^bD = degassed; U = undegassed.

tial decays as shown in Figure II.9. All samples are in equilibrium with air.⁵ Additional frequency-domain data on sin-

gle-decay-time fluorophores are available in the literature,^{6–10} and a cooperative report between several laboratories on lifetime standards is in preparation.¹¹

4. TIME-DOMAIN LIFETIME STANDARDS

The need for lifetime standards for time-domain measurements has been recognized for some time.¹² A number of laboratories have suggested samples as single-decay-time standards.^{13–17} The data are typically reported only in tables (Tables II.3 to II.5), so representative figures are not available. The use of collisional quenching to obtain different lifetimes^{17–18} is no longer recommended for lifetime standards due to the possibility of transient effects and non-exponential decays. Quinine is not recommended as a lifetime standard due to the presence of a multi-exponential decay.^{19–20}

Table II.4. Single-Exponential Lifetime Standards

Sample ^a	λ_{em} (nm)	τ (ns ^a)
Anthracene	380	5.47
PPO	400	1.60
POPOP	400	1.38
9-cyanoanthracene	440	14.76

^aAll samples in ethanol. The lifetimes were measured by time-correlated single-photon counting. From [14]. The paper is unclear on purging, but the values seem consistent with degassed samples.

Table II.5. Single-Exponential Standards^a

Fluorophore	τ (ns)
POPOP in cyclohexane	1.14 ± 0.01
POPOP in EtOH	1.32 ± 0.01
POPOP in aq EtOH	0.87 ± 0.01
Anthracene in EtOH	4.21 ± 0.02
9-Cyanoanthracene in EtOH	11.85 ± 0.03

^aAll measurements were at 25°C, in equilibrium with air, by time-correlated single photon counting. From [17].

Appendix III

Additional Reading

It is not possible in a single volume to completely describe the molecular photophysics and the application of fluorescence spectroscopy. The following books are recommended for additional details on specialized topics. This listing is not intended to be inclusive, and the author apologizes for absence of important citations.

I. TIME-RESOLVED MEASUREMENTS

- Chemical applications of ultrafast spectroscopy* 1986. Fleming, GR. Oxford University Press, New York.
- Excited state lifetime measurements* 1983. Demas JN. Academic Press, New York, pp. 267.
- Time-correlated single photon counting* 1984. O'Connor DV, Phillips D. Academic Press, New York.
- Topics in fluorescence spectroscopy*. Vol 1. 1991. Lakowicz JR, ed. Plenum Press, New York.

2. SPECTRA PROPERTIES OF FLUOROPHORES

- Energy transfer parameters of aromatic compounds*. 1973. Berlman IB. Academic Press, New York.
- Biological techniques: fluorescent and luminescent probes for biological activity*. 1999. Mason WT. Academic Press, New York.
- Handbook of fluorescence spectra of aromatic molecules*, 2nd ed. 1971. Berlman IB. Academic Press, New York.
- Handbook of fluorescent probes and research chemicals*, 9th ed. 2003. Haugland RP, ed. Molecular Probes Inc.
- Landolt-Börnstein: zahlenwerte und funktionen aus naturwissenschaften und technik*. 1967. Serie N. Springer-Verlag, Berlin.
- Molecular luminescence spectroscopy: methods and applications: part 1*. 1985. Schulman SG, ed. John Wiley & Sons, New York.
- Molecular luminescence spectroscopy: methods and applications: part 2*. 1988. Schulman SG, ed. John Wiley & Sons, New York.
- Molecular luminescence spectroscopy: methods and applications: part 3*. 1993. Schulman SG, ed. John Wiley & Sons, New York.

- Organic luminescent materials*. 1984. Krasovitskii BM, Bolotin BM (Vopian VG, transl). VCH Publishers, Germany.
- Practical fluorescence*, 2nd ed. 1990. Guilbault GG, ed. Marcel Dekker, New York.

3. THEORY OF FLUORESCENCE AND PHOTOPHYSICS

- Photophysics of aromatic molecules*. 1970. Birks JB. Wiley Interscience, New York.
- Organic molecular photophysics*, Vol 1. 1973. Birks JB, ed. John Wiley & Sons, New York.
- Organic molecular photophysics*, Vol 2. 1975. Birks JB, ed. John Wiley & Sons, New York.
- Fotoluminescencja roztworow*. 1992. Kowski A. Wydawnictwo Naukowe PWN, Warszawa.

The 1970 and 1973 books by Birks are classic works that summarize organic molecular photophysics. These books start by describing fluorescence from a quantum mechanical perspective, and contain valuable detailed tables and figures that summarize spectral properties and photophysical parameters. Unfortunately, these books are no longer in print, but they may be found in some libraries.

4. REVIEWS OF FLUORESCENCE SPECTROSCOPY

- Methods in enzymology*, Vol. 278: *Fluorescence spectroscopy*. 1997. Brand L, Johnson ML. Academic Press, New York.
- Molecular fluorescence, phosphorescence, and chemiluminescence spectrometry*. 2004. Powe AM, Fletcher KA, St. Luce NN, Lowry M, Neal S, McCarroll ME, Oldham PB, McGown LB, Warner IM. *Anal Chem* **76**:4614–4634. This review is published about every two years.

Resonance energy transfer: theory and data. 1991. Wieb Van Der Meer B, Coker G, Chen S-Y. Wiley-VCH, New York.

Topics in fluorescence spectroscopy, Vol 2: *Principles*. 1991. Lakowicz JR, ed. Plenum Press, New York. Provides information on the biochemical applications of anisotropy, quenching, energy transfer, least-square analysis, and oriented systems.

Topics in fluorescence spectroscopy, Vol 3: *Biochemical applications*. 1992. Lakowicz JR, ed. Plenum Press, New York. Describes the spectral properties of intrinsic biological fluorophores and labeled macromolecules. There are chapters on proteins, membranes and nucleic acids.

Topics in fluorescence spectroscopy, Vol 7: *DNA technology 2003*. Lakowicz JR, ed. Kluwer Academic/Plenum Publishers, New York.

5. BIOCHEMICAL FLUORESCENCE

Analytical use of fluorescent probes in oncology. 1996. Kohen E, Hirschberg JG, eds. Plenum Press, New York.

Applications of fluorescence in the biomedical sciences. 1986. Taylor DL, Waggoner AS, Murphy RF, Lanni F, Birge RR, eds. Alan R. Liss, New York.

Biophysical and biochemical aspects of fluorescence spectroscopy. 1991. Dewey TG, ed. Plenum Press, New York.

Biotechnology applications of microinjection, microscopic imaging, and fluorescence. 1993. Bach PH, Reynolds CH, Clark JM, Mottley J, Poole PL, eds. Plenum Press, New York.

Fluorescent and luminescent probes for biological activity: a practical guide to technology for quantitative real-time analysis, 2nd ed. 1999. Mason WT, ed. Academic Press, San Diego.

Fluorometric analysis in biomedical chemistry. 1987. Ichinose N, Schwedt G, Schnepel FM, Adachi K. John Wiley & Sons.

Fluorescence spectroscopy. 1997. Brand L, Johnson ML, eds. Academic Press, New York.

Methods in cell biology, Vol 58: *Green fluorescent proteins*. 1999. Sullivan KF, Kay SA, eds. Academic Press, San Diego.

Spectroscopic membrane probes, Vol 1. 1988. Loew LM, ed. CRC Press, Boca Raton, FL.

Spectroscopic membrane probes, Vol 2. 1988. Loew LM, ed. CRC Press, Boca Raton, FL.

Spectroscopic membrane probes, Vol 3. 1988. Loew LM, ed. CRC Press, Boca Raton, FL.

6. PROTEIN FLUORESCENCE

Fluorescence and phosphorescence of proteins and nucleic acids. 1967. Konev SV. (Udenfriend S, transl). Plenum Press, New York.

Luminescence of polypeptides and proteins. 1971. Longworth JW. In *Excited states of proteins and nucleic acids*, pp. 319–484. Steiner RF, Weinryb I, eds. Plenum Press, New York.

Luminescent spectroscopy of proteins. 1993. Permyakov EA. CRC Press, Boca Raton, FL.

Ultraviolet spectroscopy of proteins. 1981. Demchenko AP. Springer-Verlag, New York.

7. DATA ANALYSIS AND NONLINEAR LEAST SQUARES

Data reduction and error analysis for the physical sciences, 2nd ed. 1992. Bevington PR, Robinson DK. McGraw-Hill, Boston.

Evaluation and propagation of confidence intervals in nonlinear, asymmetrical variance spaces: analysis of ligand binding data. 1983. Johnson ML. *Biophys J* **44**:101–106.

An introduction to error analysis. 1982. Taylor JR. University Science Books, California.

Methods in enzymology, Vol 240: *Numerical computer methods*. 1994. Johnson ML, Brand L, eds. Academic Press, New York.

Methods in enzymology, Vol 210: *Numerical computer methods*. 1992. Brand L, Johnson ML, eds. Academic Press, New York.

Statistics in spectroscopy. 1991. Mark H, Workman J. Academic Press, New York.

8. PHOTOCHEMISTRY

Essentials of molecular photochemistry. 1991. Gilbert A, Baggott J. CRC Press, Boca Raton, FL.

Fundamentals of photoinduced electron transfer. 1993. Kavarnos GJ. VCH Publishers, New York.

Modern molecular photochemistry. 1978. Turro NJ. Benjamin/Cummings Publishing, San Francisco.

Photochemistry and photophysics, Vol 1. 1990. Rabek JF. CRC Press, Boca Raton, FL.

Photochemistry and photophysics, Vol 2. 1990. Rabek JF. CRC Press, Boca Raton, FL.

Photochemistry and photophysics, Vol 3. 1991. Rabek JF. CRC Press, Boca Raton, FL.

Principles and applications of photochemistry. 1988. Wayne RP. Oxford University Press, New York.

For most applications of fluorescence, photochemical effects are to be avoided. However, it can be valuable to understand that chemical reactions occur in the excited state.

9. FLOW CYTOMETRY

Flow cytometry. 1992. Givan AL. Wiley-Liss, New York.

Practical flow cytometry. 2nd ed. 1988. Shapiro HM. Alan R. Liss, New York.

10. PHOSPHORESCENCE

Phosphorimetry: theory, instrumentation, and applications. 1990. Hurlbut RJ. VCH Publishers, New York.

11. FLUORESCENCE SENSING

Chemical sensors and biosensors for medical and biological applications. 1998. Spichiger-Keller UE. Wiley-VCH, Weinheim.

Sensors and actuators B. 1996. Part 1: Plenary and Parallel Sessions; Part 2: Poster Sessions. Kunz RE, ed. Proceedings of the Third European Conference on Optical Chemical Sensors and Biosensors. Europt(R)ode III. Elsevier Publishers, New York.

Topics in fluorescence spectroscopy, Vol 4: *Probe design and chemical sensing*. 1994. Lakowicz JR, ed. Plenum Press, New York.

Biosensors in the body—continuous in vivo monitoring. 1997. Fraser DM, ed. Biomaterials Science and Engineering Series, Wiley, New York.

12. IMMUNOASSAYS

Applications of fluorescence in immunoassays. 1991. Hemmila IA. John Wiley & Sons, New York.

Luminescence immunoassay and molecular applications. 1990. Van Dyke K, Van Dyke R. CRC Press, Boca Raton, FL.

13. APPLICATIONS OF FLUORESCENCE

Analytical use of fluorescent probes in oncology. 1996. Kohen E, Hirschberg JG, eds. Plenum Press, New York.

Fluorescent chemosensors for ion and molecule recognition. 1992. Czarnik AW, ed. ACS Symposium Series, Vol 538.

Fluorescent probes in cellular and molecular biology. 1994. Slavik J. CRC Press, Boca Raton, FL.

Fluorescence microscopy and fluorescent probes. 1996. Slavik J, ed. Plenum Press, New York.

Fluorescence spectroscopy. 1993. Wolfbeis OS, ed. Springer-Verlag, New York.

Sensors and actuators B: chemical. 1994. Baldini F, ed. Elsevier Press. Vol B2.(1–3).

Applied fluorescence in chemistry, biology and medicine. 1999. Rettig W, Strehmel B, Schrader S, Seifert H. Springer, New York.

New trends in fluorescence spectroscopy. 2001. Valeur B, Brochon J-C, eds. Springer, New York.

Fluorescence spectroscopy, imaging, and probes. 2002. Kraayenhof R, Visser AJWG, Gerritsen HC, eds. Springer, New York.

14. MULTIPHOTON EXCITATION

Topics in fluorescence spectroscopy, Vol 5: *Non-linear and two-photon induced fluorescence*. 1997. Lakowicz JR, ed. Plenum Press, New York.

Fluorescence microscopy and fluorescent probes, Vol 2. 1998. Slavik J, ed. Plenum Press, New York.

15. INFRARED AND NIR FLUORESCENCE

Infrared absorbing dyes. 1990. Matsuoka M. Plenum Press, New York.

Phthalocyanines: properties and applications. 1989. Leznoff CC, Lever ABP, eds. VCH Publishers, New York.

Near-infrared dyes for high technology applications. 1998. Daehne S, Resch-Genger U, and Wolfbeis OS, eds. Kluwer Academic Publishers, Boston.

16. LASERS

Fundamentals of laser optics. 1994. Iga K. (Miles RB, tech ed). Plenum Press, New York.

Principles of lasers, 4th ed. 1998. Svelto O. (Hanna DC, ed, transl) Plenum Press, New York.

An introduction to laser spectroscopy. 2002. Andrews DL, Deminov AA, eds. Kluwer Academic/Plenum Publishers, New York.

Laser spectroscopy: basic concepts and instrumentation, 3rd ed. 2003. Demtroder W. Springer, New York.

17. FLUORESCENCE MICROSCOPY

Chemical analysis: a series of monographs on analytical chemistry and its applications. 1996. Fluorescence Imaging Spectroscopy and Microscopy, Vol 137. Wang XF, and Herman B, eds. John Wiley & Sons, New York.

Fluorescence imaging spectroscopy and microscopy. 1996. Wang XF, Herman B. John Wiley & Sons, New York.

Handbook of confocal microscopy, 2nd ed. 1995. Pawley JB, ed. Plenum Press, New York. See also the First Edition, 1990.

Methods in cell biology, Vol 38: *Cell biological applications of confocal microscopy*. 1993. Matsumoto B, ed. Academic Press, New York.

Methods in cell biology, Vol 40: *A practical guide to the study of calcium in living cells*. 1994. Nuccitelli R, ed. Academic Press, New York.

Optical microscopy, emerging methods and applications. 1993. Herman B, Lemasters JJ. Academic Press, New York.

Optical microscopy for biology. 1990. Herman B, Jacobson K, eds. Wiley-Liss, New York.

Fluorescent microscopy and fluorescent probes, Vol 2. 1998. Slavik J, ed. Plenum, New York.

18. METAL-LIGAND COMPLEXES AND UNUSUAL LUMOPHORES

Molecular level artificial photosynthetic materials. 1997. Meyer GJ, ed. John Wiley & Sons, New York.

Photochemistry of polypyridine and porphyrin complexes. 1992. Kalyanasundaram K. Academic Press, New York.

Ru(II) polypyridine complexes: photophysics, photochemistry, electrochemistry, and chemiluminescence. 1988. Juris A, Balzani V, Barigelletti F, Campagna S, Belser P, Von Zelewsky A. *Coord Chem Rev* **84**:85–277.

19. SINGLE-MOLECULE DETECTION

Selective spectroscopy of single molecules. 2003. Osad'ko IS. Springer, New York.

Single molecule detection in solution methods and applications. 2002. Zander Ch, Enderlein J, Keller RA, eds. Wiley-Vch, Darmstadt, Germany.

Single molecule spectroscopy: Nobel conference letters. 2001. Rigler R, Orrit M, and Basche T. Springer, New York.

20. FLUORESCENCE CORRELATION SPECTROSCOPY

Fluorescence correlation spectroscopy theory and applications. 2001. Rigler R, Elson ES. Springer, New York.

21. BIOPHOTONICS

Methods in enzymology, Vol. 360: *Biophotonics, part a 2003*. Marriott G, Parker I, eds. Academic Press, New York.

Methods in Enzymology, Vol. 361: *Biophotonics part b 2003*. Marriott G, Parker I, eds. Academic Press, New York.

Introduction to biophotonics. 2003. Prasad PN, Wiley-Interscience, New York.

22. NANOPARTICLES

Nanoparticles. 2004. Rotello V, ed. Kluwer Academic/Plenum Publishers, New York.

Optical properties of semiconductor nanocrystals. 1998. Gaponenko SV. Cambridge University Press, New York.

23. METALLIC PARTICLES

Electronic excitations at metal surfaces. 1997. Liebsch A. Plenum Press, New York.

Metal nanoparticles synthesis, characterization, and applications. 2002. Feldheim DL, Foss CA, eds. Marcel Dekker, New York.

24. BOOKS ON FLUORESCENCE

Introduction to fluorescence spectroscopy. 1999. Sharma A, Schulman SG, eds. Wiley-Interscience, New York.

Molecular fluorescence principles and applications. 2002. Valeur B. Wiley-VCH, New York.

Who's who in fluorescence 2004. 2004. Geddes CD, Lakowicz JR, eds. Kluwer Academic/Plenum Publishers, New York.

Answers to Problems

CHAPTER I

- A1.1. A. The natural lifetimes and radiative decay rates can be calculated from the quantum yields and experimental lifetimes:

$$\tau_N(\text{eosin}) = \tau/Q = \frac{3.1}{0.65} = 4.77 \text{ ns} \quad (1.18)$$

$$\tau_N(\text{EB}) = \tau Q = \frac{0.61}{0.12} = 5.08 \text{ ns} \quad (1.19)$$

Hence eosin and erythrosin B have similar natural lifetimes and radiative decay rates (eq. 1.3). This is because both molecules have similar absorption and emission wavelengths and extinction coefficients (eq. 1.4).

The non-radiative decay rates can be calculated from eq. 1.2, which can be rearranged to

$$\frac{1}{\tau} - \frac{1}{\tau_N} = k_{nr} \quad (1.20)$$

For eosin and erythrosin B the non-radiative decay rates are $1.1 \times 10^8 \text{ s}^{-1}$ and $1.44 \times 10^9 \text{ s}^{-1}$, respectively. The larger non-radiative decay rate of erythrosin B is the reason for its shorter lifetime and lower quantum yield than eosin.

- B. The phosphorescence quantum yield (Q_p) can be estimated from an expression analogous to eq. 1.1:

$$Q_p = \frac{\Gamma_p}{\Gamma_p + k_{nr}} \quad (1.21)$$

Using the assumed natural lifetime of 10 ms, and $k_{nr} = 1 \times 10^8 \text{ s}^{-1}$, $Q_p = 10^{-6}$. If k_{nr} is larger, Q_p is still smaller, so that Q_p ; 10^{-7} for ErB. This explains why it is difficult to observe phosphorescence at room temperature: most of the molecules that undergo intersystem crossing return to the ground state by non-radiative paths prior to emission.

- A1.2. The quantum yield (Q_2) of S_2 can be estimated from

$$Q_2 = \frac{\Gamma}{\Gamma + k_{nr}} \quad (1.22)$$

The value of k_{nr} is given by the rate of internal conversion to S_1 , 10^{13} s^{-1} . Using $\Gamma = 2.1 \times 10^8$, one can estimate $Q_2 = 2 \times 10^{-5}$. Observation of emission from S_2 is unlikely because the molecules relax to S_1 prior to emission from S_2 .

- A1.3. The energy spacing between the various vibrational energy levels is revealed by the emission spectrum of perylene (Figure 1.3). The individual emission maxima (and hence vibrational energy levels) are about 1500 cm^{-1} apart. The Boltzmann distribution describes the relative number of perylene molecules in the 0 and 1 vibrational states. The ratio (R) of molecules in each state is given by

$$R = e^{-\Delta E/kT} \quad (1.23)$$

where ΔE is the energy difference, k is the Boltzmann constant, and T is the temperature in degrees kelvin (K). Assuming a room temperature of 300 K, this ratio is about 0.01. Hence most molecules will be present in the lowest vibrational state, and light absorption results mainly from molecules in this energy level. Because of the larger energy difference between S_0 and S_1 , essentially no fluorophores can populate S_1 as a result of thermal energy.

- A1.4. A. The anisotropy of the DENS-labeled protein is given by eq. 1.10. Using $\tau = \theta$, the steady-state anisotropy is expected to be 0.15.
- B. If the protein binds to the larger antibody, its rotational correlation time will increase to 100 ns or longer. Hence the anisotropy will be 0.23 or higher. Such increases in anisotropy upon antigen–antibody binding are the basis of the fluorescence polarization immunoassays, which are used to detect drugs, peptides, and small proteins in clinical samples.
- A1.5. The dependence of transfer efficiency on distance (r) between a donor and acceptor can be calculated using eq. 1.12 (Figure 1.41). At $r = R_0$ the efficiency is 50%; at $r = 0.5R_0$, $E = 0.98$; and at $r = 2R_0$, $E = 0.02$.

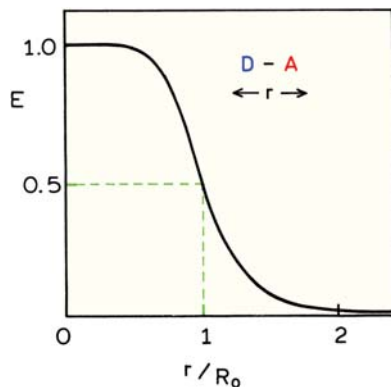


Figure 1.41. Effect of donor-to-acceptor distance on transfer efficiency.

- A1.6. The distance can be calculated for the relative quantum yield of the donor in the presence or absence of the acceptor. The data in Figure 1.37 reveal a relative tryptophan intensity of 0.37, assuming the anthraniloyl group does not contribute at 340 nm. A transfer efficiency of 63% corresponds (see eq. 1.12) to a distance of $r = 0.92R_0 = 27.7 \text{ \AA}$.

In reality the actual calculation is more complex, and the tryptophan intensity needs to be corrected for anthraniloyl emission.⁴² When this is done the transfer efficiency is found to be about 63%, and the distance near 31.9 \AA .

- A1.7. The changes in λ_{\max} , K , and r shown in Figure 1.38 are the result of the tryptophan residue being exposed to or shielded from the water. Increases in

λ_{\max} and K indicate increased exposure to water, and decreases in λ_{\max} and K indicate decreases in exposure to water. Increases and decreases in r indicate a less mobile and more mobile tryptophan residue, respectively. The three parameter values show a cyclical behavior with a period of about 3.5 amino acid residues per cycle. This suggests that the MLCK peptide is in an α -helical state when bound to calmodulin (Figure 1.42). The spectral changes seen in Figure 1.38 are the result of the tryptophan residue being alternately exposed to water or shielded between the MLCK peptide and calmodulin as its position is shifted along the peptide chain.

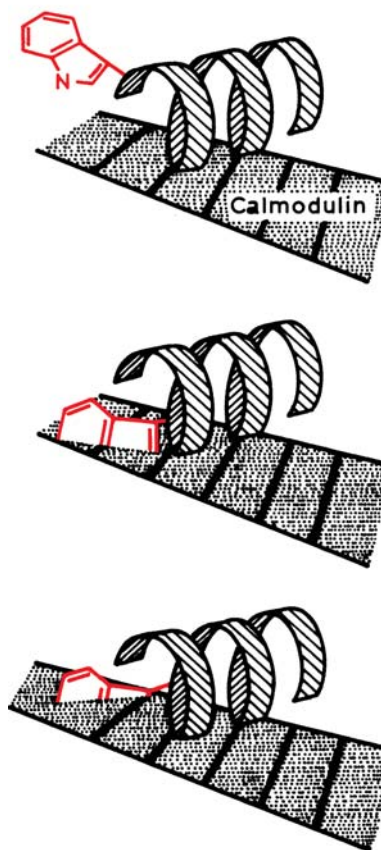


Figure 1.42. Schematic of the interactions of the O-helical MLCK peptide with calmodulin. The position of the single tryptophan residue is moved along the helix in 16 synthetic peptides. Reprinted with permission from [40]. (O'Neil KT, Wolfe HR, Erickson-Vitanen S, DeGrado WF. 1987. Fluorescence properties of calmodulin-binding peptides reflect O-helical periodicity. *Science* 236:1454–1456, Copyright © 1987, American Association for the Advancement of Science.)

A1.8. Figure 1.40 shows that the donor intensity increases and the acceptor intensity decreases upon addition of cAMP and PKI. These spectral changes indicate a decrease in RET. The donor and acceptor must move further apart when the protein binds cAMP or PKI. According to publications⁴³ the C and R subunits remain associated in the presence of cAMP, but change this relative conformation (Figure 1.43). PKI was said to dissociate the subunit.

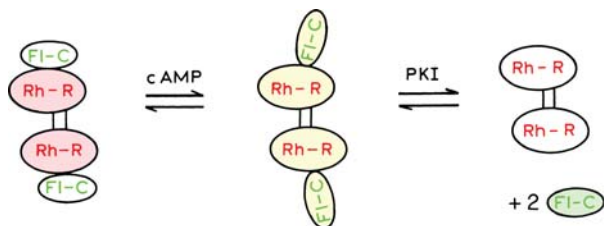


Figure 1.43. Effect of cAMP and protein kinase inhibitor (PKI) on the structure and association of cAMP-dependent protein kinase. The holoenzyme consists of two catalytic and two regulatory subunits.

CHAPTER 2

- A2.1. The true optical density is 10. Because of stray light the lowest percent transmission (%T) you can measure is 0.01%. The %T of the rhodamine solution is much less than 0.01%. In fact $I/I_0 = 10^{-10}$ and $\%T = 10^{-8}\%$. Hence your instrument will report an optical density of 4.0. The calculated concentration of rhodamine B would be 4×10^{-5} M, 2.5-fold less than the true concentration.
- A2.2. The concentrations of solutions are 10^{-5} and 10^{-7} M, respectively. A 1% error in %T means the OD can be

$$OD = \log \frac{I_0}{I} = \log \frac{1}{0.51} \text{ or } \log \frac{1}{0.49} \quad (2.13)$$

Hence the concentration can be from 0.97×10^{-5} to 1.03×10^{-5} M.

For the more dilute solution, the 1% error results in a large error in the concentration:

$$OD = \log \frac{I_0}{I} = \log \frac{1.00}{1.00} \text{ or } \log \frac{1.0}{0.98} \quad (2.14)$$

The measured OD ranges from 0 to 0.009, so the calculated concentration ranges from 0 to 2.9×10^{-7} M. This shows that it is difficult to determine the concentration from low optical densities. In contrast, it is easy to obtain emission spectra with optical densities near 0.003.

CHAPTER 3

- A3.1. Binding of the protein to membranes or nucleic acids could be detected by several types of measurements. The most obvious experiment would be to look for changes in the intrinsic tryptophan fluorescence upon mixing with lipid bilayers or nucleic acids. In the case of membranes one might expect the tryptophan emission to shift to shorter wavelengths due to shielding of the indole moiety from water. The blue shift of the emission is also likely to be accompanied by an increase in the tryptophan emission intensity. In the case of nucleic acids, tryptophan residues are typically quenched when bound to DNA, so that a decrease in the emission intensity is expected.

Anisotropy measurements of the tryptophan emission could also be used to detect binding. In this case it is difficult to predict the direction of the changes. In general one expects binding to result in a longer correlation time and higher anisotropy (see eq. 1.10), and an increase of the tryptophan anisotropy is likely upon binding to proteins. However, the anisotropy increase may be smaller than expected if the tryptophan lifetime increases on binding to the membranes (eq. 1.10).

In the case of protein binding to nucleic acids, it is difficult to predict the anisotropy change. The tryptophan residues would now be in two states, free (F) and bound (B), and the anisotropy given by

$$r = r_F f_F + r_B f_B, \quad (3.2)$$

where f_F and f_B represent the fraction of the total fluorescence from the protein in each state. If the protein is completely quenched on binding to DNA, then the anisotropy will not change because $f_B = 0$. If the protein is partially quenched the anisotropy will probably increase, but less than expected due to the small contribution of the DNA-bound protein by the total fluorescence.

Energy transfer can also be used to detect protein binding. Neither DNA nor model membranes possess chromophores that can serve as acceptors for the tryptophan fluorescence. Hence it is necessary to add extrinsic probes. Suitable acceptors would be probes that absorb near 350 nm, the emission maximum of most proteins. Numerous membranes and nucleic-acid probes absorb near 350 nm. The membranes could be labeled with DPH (Figure 1.18), which absorbs near 350 nm. If the protein is bound to DPH-labeled membranes, its emission would be quenched by resonance energy transfer to DPH. Similarly, DNA could be labeled with DAPI (Figure 3.23). An advantage of using RET is that through-space quenching occurs irrespective of the details of the binding interactions. Even if there were no change in the intrinsic tryptophan emission upon binding to lipids or nucleic acids, one still expects quenching of the tryptophan when bound to acceptor-labeled membranes or nucleic acids.

- A3.2. A. The data in Figure 3.48 can be used to determine the value of F_0/F at each $[Cl^-]$, where $F_0 = 1.0$ is the SPQ fluorescence intensity in the absence of Cl^- , and F is the intensity at each Cl^- concentration. These values are plotted in Figure 3.49. Using Stern-Volmer eq. 1.6, one obtains $K = 124 M^{-1}$, which is in good agreement with the literature value¹⁸² of $118 M^{-1}$.
- B. The value of F_0/F and τ_0/τ for $0.103 M Cl^-$ can be found from eq. 1.6. Using $K = 118 M^{-1}$, one obtains $F_0/F = \tau_0/\tau = 13.15$. Hence the intensity of SPQ is $F = 0.076$, relative to the intensity in the absence of Cl^- , $F_0 = 1.0$. The

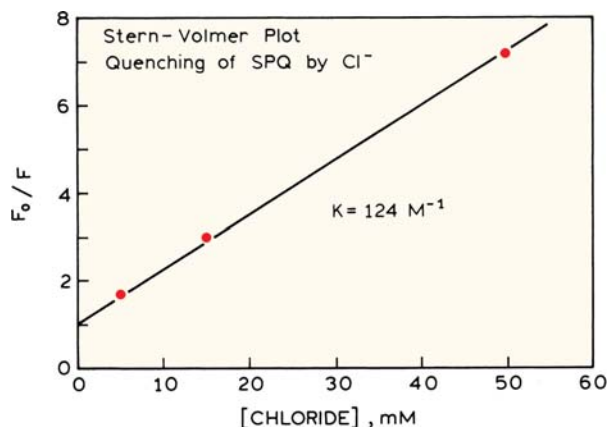


Figure 3.49. Stern-Volmer plot for the quenching of SPQ by chloride.

lifetime is expected to be $\tau = 26.3/13.15 = 2.0$ ns.

- C. At $[Cl^-] = 0.075 M$, $F = 0.102$ and $\tau = 2.67$.
- D. The Stern-Volmer quenching constant of SPQ was determined in the absence of macromolecules. It is possible that SPQ binds to proteins or membranes in blood serum. This could change the Stern-Volmer quenching constant by protecting SPQ from collisional quenching. Also, binding to macromolecules could alter τ_0 , the unquenched lifetime. Hence it is necessary to determine whether the quenching constant of SPQ is the same in blood serum as in protein-free solutions.

- A3.3. A. The dissociation reaction of the probe (P_B) and analyte (A) is given by



where B and F refer to the free and bound forms of the probe. The fraction of free and bound probe is related to the dissociation constant by

$$K_D = \frac{[P_F]}{[P_B]}[A] \quad (3.4)$$

For the non-ratiometric probe Calcium Green, the fluorescence intensity is given by

$$F = q_F C_F + q_B C_B, \quad (3.5)$$

where q_i are the relative quantum yields, C_i the molecular fraction in each form, and $C_F + C_B = 1.0$. The fluorescent intensities when all the probe is free is $F_{\min} = kq_F C$, and then all the probe is bound in $F_{\max} = kq_B C$, where k is an instrumental constant.

Equation 3.5 can be used to derive expressions for C_B and C_F in terms of the relative intensities:

$$F_B = \frac{F - F_{\min}}{F_{\max} - F_{\min}} \quad (3.6)$$

$$F_F = \frac{F_{\max} - F}{F_{\max} - F_{\min}} \quad (3.7)$$

The fractions C_B and C_F can be substituted for the probe concentration in (3.4), yielding

$$[A] = [\text{Ca}^{2+}] = K_D \frac{F - F_{\max}}{F_{\max} - F} \quad (3.8)$$

- B. The fluorescence intensity (F_1 or F_2) observed with each excitation wavelength (1 or 2) depends on the intensity and the concentrations (C_F and C_B) of the free (S_{f1} or S_{f2}), or bound (S_{b1} or S_{b2}), forms at each excitation wavelength:

$$F_1 = S_{f1}C_F + S_{b1}C_B, \quad (3.9)$$

$$F_2 = S_{f2}C_F + S_{b2}C_B. \quad (3.10)$$

The term S_i depends on the absorption coefficient and relative quantum yield of Fura-2 at each wavelength.

Let $R = F_1/F_2$ be the ratio of intensities. In the absence and presence of saturating Ca^{2+} ,

$$R_{\min} = S_{f1}/S_{f2}, \quad (3.11)$$

$$R_{\max} = S_{b1}/S_{b2}. \quad (3.12)$$

Using the definition of the dissociate constant,

$$[\text{Ca}^{2+}] = \frac{C_B}{C_F} K_D \quad (3.13)$$

one obtains

$$[\text{Ca}^{2+}] = K_D \frac{R - R_{\max}}{R_{\min} - R} \left(\frac{S_{f2}}{f_{b2}} \right) \quad (3.14)$$

Hence one can measure the $[\text{Ca}^{2+}]$ from these ratios of the emission intensities at two excitation wavelengths. However, one needs control measurements, which are the ratio of the intensities of the free and bound forms measured at one excitation wavelength, as well as measurements of R_{\min} and R_{\max} .¹⁸³

From Figure 4.2 the phase angle is seen to be about 60 degrees. Using $\omega = 2\pi \cdot 80$ MHz and $\tau_\phi = \omega^{-1} [\tan \phi]$ one finds $\tau = 3.4$ ns. The modulation of the emission relative to the excitation is near 0.37. Using eq. 4.6 one finds $\tau_m = 5.0$ ns. Since the phase and modulation lifetimes are not equal, and since $\tau_m > \tau_\phi$, the intensity decay is heterogeneous. Of course, it is difficult to read precise values from Figure 4.2.

A4.2. The fractional intensity of the 0.62-ns component can be calculated using eq. 4.28, and is found to be 0.042 or 4%.

A4.3. The short lifetime was assigned to the stacked conformation of FAD. For the open form the lifetime of the flavin is reduced from $\tau_0 = 4.89$ ns to $\tau = 3.38$ ns due to collisions with the adenine. The collision frequency is given by $k = \tau^{-1} - \tau_0^{-1} = 9 \times 10^7/\text{s}$.

A4.4. In the presence of quencher the intensity decay is given by

$$I(t) = 0.5 \exp(-t/0.5) + 0.5 \exp(-t/5) \quad (4.42)$$

The α_1 and α_2 values remain the same. The fact that the first tryptophan is quenched tenfold is accounted for by the $\alpha_i\tau_i$ products, $\alpha_1\tau_1 = 0.25$ and $\alpha_2\tau_2 = 2.5$. Using eq. 4.29 one can calculate $\bar{\tau} = 4.59$ ns and $\langle\tau\rangle = 2.75$ ns. The average lifetime is close to the unquenched value because the quenched residue ($\tau_1 = 0.5$ ns) contributes only $f_1 = 0.091$ to the steady-state or integrated intensity. If the sample contained two tryptophan residues with equal steady-state intensities, and lifetimes of 5.0 and 0.5 ns then $\bar{\tau} = 0.5(\tau_1) + 0.5(\tau_2) = 2.75$ ns. The fact that $\langle\tau\rangle$ reflects the relative quantum yield can be seen from noting that $\langle\tau\rangle/\tau_0 = 2.75/5.0 = 0.55$, which is the quantum yield of the quenched sample relative to the unquenched sample.

A4.5. The DAS can be calculated by multiplying the fractional intensities ($f_i(\lambda)$) by the steady-state intensity at each wavelength ($I(\lambda)$). For the global analysis these values (Figure 4.65) match the emission spectra of the individual components. However, for the single-wavelength data the DAS are poorly matched to the individual spectra. This is because the $\alpha_i(\lambda)$ values are not well determined by the data at a single wavelength.

A4.6. The total number of counts in Figure 4.45 can be calculated from the $\alpha\tau$ product. The value of α is the number of counts in the time zero channel or 10^4 counts. The total number of photons counted is thus 4

CHAPTER 4

- A4.1. Calculation of the lifetimes from intensity decay is straightforward. The initial intensity decreases to 0.37 (=1/3) of the initial value at $t = 5$ ns. Hence, the lifetime is 5 ns.

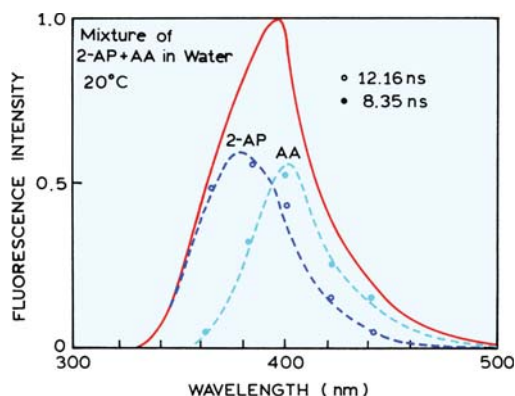


Figure 4.65. Emission spectra of a two-component mixture of anthranilic acid (AA) and 2-aminopurine (2-AP). The data show the fractional amplitudes associated with each decay time recovered from the global analysis. From [187].

$\times 10^6$. Assuming 1 photon is counted each 10^{-5} seconds the data acquisition time is 400 s or 6.7 minutes. If the data were collected by TCSPC with a 1% count rate the data acquisition time would be 670 minutes.

- A4.7. For a 4-ns lifetime the excitation pulses should be at least 16 ns apart, which corresponds to a pulse rate of 62.5 MHz. Using a 1% count rate yields a photon detection rate of 0.625 MHz. At this rate the time needed to count 4×10^6 photons is 6.4 seconds. Can the TAC convert photons at this rate? The 0.625 MHz count rate corresponds to 1.6 microsecond to store the data. Using a TAC with a 120-ns deadtime the TAC should be able to accept all the photons. A TAC with a $2 \mu\text{s}$ deadtime would be unable to accept the data and the counting would be inefficient.
- A4.8. The fractional intensity is proportional to the $\alpha\tau$ products. Using eq. 4.28, $f_1 = 0.9990$ and $f_2 = 0.001$.

CHAPTER 5

- A5.1. The decay times can be calculated from either the phase or modulation data at any frequency, using eqs. 5.3 and 5.4. These values are listed in Table 5.7. Since the decay times are approximately equal from phase and modulation, the decay is nearly a single exponential. One expects the decay to become non-exponential at high chloride concentrations due to transient effects in quenching. This effect is not yet visible in the FD data for SPQ.

Table 5.7. Apparent Phase and Modulation Lifetimes for the Chloride Probe SPQ

Chloride concentration	Frequency (MHz)	Apparent phase lifetime (τ_ϕ) (ns)	Apparent modulation lifetime (τ_m) (ns)
0	10	24.90	24.94
	100	24.62	26.49
10 mM	10	11.19	11.07
	100	11.62	11.18
30 mM	10	5.17	5.00
	100	5.24	5.36
70 mM	10	2.64	2.49
	100	2.66	2.27

- A5.2. The chloride concentration can be determined from the phase or modulation values of SPQ at any frequency where these values are sensitive to chloride concentration. Examination of Figure 5.15 indicates that this is a rather wide range from 5 to 100 MHz. One can prepare calibration curves of phase or modulation of SPQ versus chloride, as shown in Figure 5.56. An uncertainty of $\pm 0.2^\circ$ in phase or $\pm 0.5\%$ in modulation

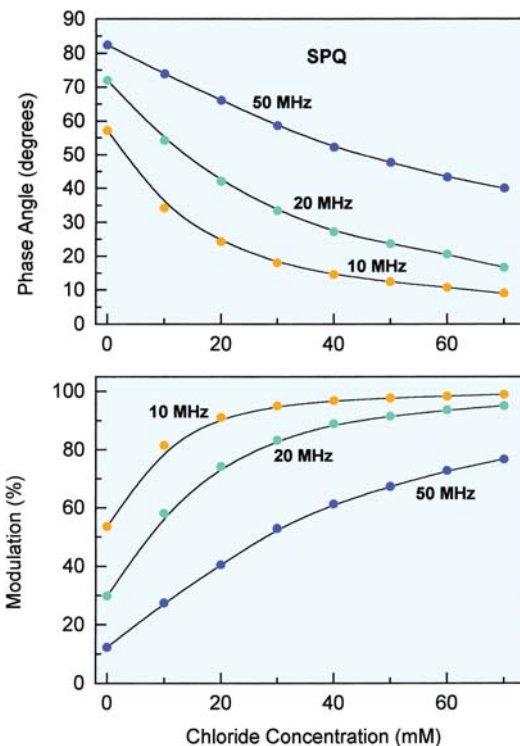


Figure 5.56. Dependence of the phase and modulation of SPQ on chloride concentration.

Table 5.8. Phase-Modulation Apparent Lifetimes for a Double-Exponential Decay^a

Frequency (MHz)	ϕ (deg)	m	τ_ϕ (ns)	τ_m (ns)
50 ($\alpha_1 = \alpha_2$)	50.5	0.552	3.86	4.81
50 ($f_1 = f_2$)	25.6	0.702	1.53	3.23
100 ($\alpha_1 = \alpha_2$)	60.1	0.333	2.76	4.51
100 ($f_1 = f_2$)	29.8	0.578	0.91	3.17

^aFor both decay laws the lifetimes are 0.5 and 5.0 ns.

results in chloride concentrations accurate to approximately ± 0.2 and 0.3 mM respectively, from 0 to 25 mM.

- A5.3. A list of the phase and modulation values for the two decay laws, as well as the apparent phase and modulation lifetimes, is given in Table 5.8. As expected, $\tau_\phi^{\text{app}} < \tau_m^{\text{app}}$. Both values decrease with higher modulation frequency. The phase angles are smaller, and the modulation is higher, when $f_1 = f_2$ than when $\alpha_1 = \alpha_2$. When $f_1 = f_2$, the α_i values are $\alpha_1 = 0.909$ and $\alpha_2 = 0.091$. The fractional contribution of the short-lifetime component is larger when $f_1 = f_2$.
- A5.4. The Raman peak at 410 nm is equivalent to $24,390$ cm^{-1} . The Raman peak of water is typically shifted $3,600$ cm^{-1} . Hence the excitation wavelength is at $27,990$ cm^{-1} , or 357 nm.
- A5.5. The scattered light has an effective lifetime of zero. Hence the scattered light can be suppressed with $\phi_D = 90^\circ$. The phase angle of quinine sulfate at 10 MHz can be calculated from $\phi = \tan(\omega\tau) = 51.5^\circ$. The maximum phase-sensitive intensity for quinine sulfate would be observed with $\phi_D = 51.5^\circ$. The scattered light is suppressed with $\phi_D = 90^\circ$. At this phase angle the phase-sensitive intensity is attenuated by a factor of $\cos(\phi_D - \phi) = \cos(90 - 51.5) = 0.78$ relative to the phase-sensitive intensity with $\phi_D = 51.5^\circ$.
- A5.6. The detector phases of $17.4 + 90^\circ$ and $32.1 - 90^\circ$ are out of phase with DNS-BSA and DNS, respectively. This is known because at $\phi_D = 32.1 - 90^\circ$ only free DNS is detected. In the equimolar DNS-BSA mixture the phase-sensitive intensity of DNS is decreased by 50% . Hence 50% of the DNS is bound to BSA. Similarly, at $\phi_D = 17.4 + 90^\circ$ only the fluorescence of the DNS-BSA complex is detected. Relative to the solution in which DNS is completely bound, the intensity is 50% . Hence 50% of the DNS is bound. The phase-sensitive intensities of the first two solutions may be

rationalized as follows. Upon addition of a saturating amount of BSA all the DNS is bound. Therefore its contribution to the signal at $\phi_D = 32.1 - 90^\circ$ is eliminated. The intensity increases twofold, and now is observed with $\phi_D = 17.4 + 90^\circ$. However, a twofold increase in intensity is not observed because the signal from the bound DNS is more demodulated than that of the free DNS. Specifically, these values are 0.954 and 0.847 for 5 and 10 ns, respectively. Hence the expected twofold increase in fluorescence intensity is decreased by a factor of $0.847/0.954 = 0.888$.

- A5.7. The viscosity of propylene glycol changes dramatically with temperature, which affects the rate of solvent relaxation. At an intermediate temperature of -10°C the relaxation time is comparable to the lifetime. Under these conditions the emission spectrum contains components of the unrelaxed initially excited state (F) and the relaxed excited state (R). Suppression on the red side of the emission (410 nm) results in recording the emission spectrum of the F state. Suppression of the blue side of the emission (310 nm) results in recording of the emission spectrum of the R state. Of course, these are only the approximate spectra of these states, but the phase-sensitive spectra appear to show the positions of the unrelaxed and relaxed emission spectra. At very low temperatures (-60°C) all the emission is from the unrelaxed state, and at high temperatures (40°C) all the emission is from the relaxed state. Since there is only one lifetime across the emission spectra, suppression on either side of the emission suppresses the entire emission spectrum.

CHAPTER 6

- A6.1. The Stokes shift in cm^{-1} can be calculated from the Lippert equation (eq. 6.17). Because it is easy to confuse the units, this calculation is shown explicitly:

$$\nu_A - \nu_F = \frac{2(0.3098)}{(6.6256 \times 10^{-27})(2.9979 \times 10^{10})} \frac{(14 \times 10^{-18})^2}{(4.0 \times 10^{-8})^3}$$

$$\bar{\nu}_A - \bar{\nu}_F = 9554 \text{ cm}^{-1} \quad (6.23)$$

The emission maximum in the absence of solvent effects is assumed to be 350 nm, which is $28,571$ cm^{-1} . The orientation polarizability of methanol is

expected to decrease the excited state energy by 9554 cm^{-1} , to 19,017 cm^{-1} , which corresponds to 525.8 nm.

The units for $\bar{\nu}_A - \bar{\nu}_F$ are as follows:

$$\frac{(\text{esu cm})^2}{(\text{ergs})(\text{cm/s}(\text{cm}^3))} \quad (6.24)$$

Recalling that $\text{erg} = \text{g cm}^2/\text{s}^2$ and $\text{esu} = \text{g}^{1/2} \text{cm}^{3/2}/\text{s}$, one obtains $\bar{\nu}_A - \bar{\nu}_F$ in cm^{-1} .

A6.2. The change in dipole moment can be estimated from the Lippert plot (Figure 6.53). This plot shows biphasic behavior. In low-polarity solvents the emission is probably due to the LE state, and in higher-polarity solvents the emission is due to the ICT state. The slopes for each region of the Lippert plot are

$$\begin{aligned} \text{slope (LE)} &= 7000 \text{ cm}^{-1} \\ \text{slope (ICT)} &= 33,000 \text{ cm}^{-1} \end{aligned}$$

The slope is equal to $2(\mu_E - \mu_G)^2/hca^3$. Assuming a radius of 4.2 Å used previously,⁴²

$$(\mu_E - \mu_G)^2 = \frac{7000}{2} hca^3 \quad (6.25)$$

$$= \frac{7000}{2} (6.626 \times 10^{-27}) (3 \times 10^{10}) (4.2 \times 10^{-8})^3 = 5.15 \times 10^{-35}$$

The units of $(\mu_E - \mu_G)^2$ are $(\text{cm}^{-1})(\text{erg s})(\text{cm/s})(\text{cm}^3)$. Using $\text{erg} = \text{g cm}^2/\text{s}^2$, one obtains the units $(\text{g cm}^3/\text{s}^2)(\text{cm}^2)$. Taking the square root yields

$$\frac{\text{g}^{1/2} \text{cm}^{3/2}}{\text{s}} \text{cm} \quad (6.26)$$

Since $\text{esu} = \text{g}^{1/2} \text{cm}^{3/2}/\text{s}$, the result $(\mu_E - \mu_G)$ is in esu cm. This yields $(\mu_E - \mu_G) = 7.1 \times 10^{-18} \text{ esu cm} = 7.1\text{D}$. The dipole moment of Prodan is estimated to change by 7.1 Debye units upon excitation. An electron separated from a unit positive charge by 1 Å has a dipole moment of 4.8D. Hence there is only partial charge separation in the LE state. It should be noted that this value is smaller than initially reported⁴² due to a trivial error during the calculations.⁵⁸

For the ICT state a similar calculation yields $(\mu_E - \mu_G)^2 = 2.42 \times 10^{-34}$ and $\Delta\mu = 1.56 \times 10^{-17} \text{ esu cm} =$

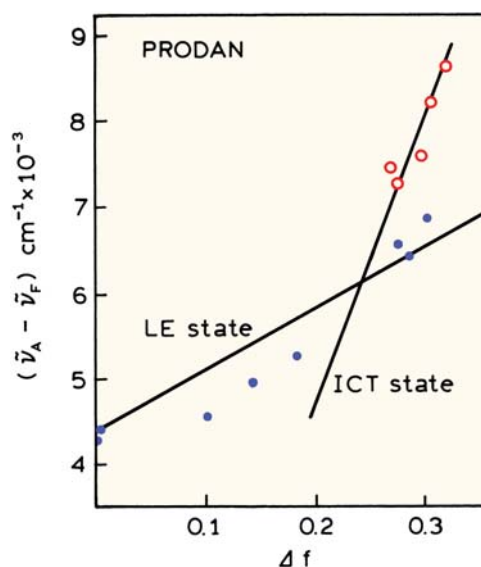


Figure 6.53. Lippert plot of the Stokes shift of Prodan. Data from [42].

15.6D. This change in dipole moment is equivalent to separation of a unit charge by 3.2 Å, which suggests nearly complete charge separation in the ICT state of Prodan.

CHAPTER 7

- A7.1. Assume the decay is a single exponential. Then the time where the intensity has decayed to 37% of its original intensity is the fluorescence lifetime. These values are $\tau_F = 1 \text{ ns}$ at 390 nm and $\tau = 5 \text{ ns}$ at 435 nm. The decay time of 5 ns at 435 nm is the decay time the F-state would display in the absence of relaxation. The lifetime of the F-state at 390 nm is given by $1/\tau_F = 1/\tau + 1/\tau_S$. This is equivalent to stating the decay time of the F-state (γ_F) is equal to the sum of the rates that depopulate the F-state, $\gamma_F = 1/\tau + k_S$. Hence $\tau_S = 1.25 \text{ ns}$.
- A7.2. In the fluid solvents ethanol or dioxane the apparent lifetimes of TNS are independent of wavelength, indicating spectral relaxation is complete in these solvents. In glycerol or DOPC vesicles the apparent lifetimes increase with wavelength, suggesting time-dependent spectral relaxation. The observation of $\tau^\phi > \tau^m$ at long wavelength is equivalent to observing a negative pre-exponential factor, and proves that relax-

ation is occurring at a rate comparable to the intensity decay rate.

- A7.3. The lifetime of the R state (τ_{OR}) can be calculated from the phase angle difference $\Delta\phi = \phi_R - \phi_F$. At 100 MHz this difference is 58° , which corresponds to a lifetime of 16 ns.
- A7.4. A. Acridine and acridinium may be reasonably expected to display distinct absorption spectra. The emission spectrum in 0.2 M NH_4NO_3 (Figure 7.49) shows evidence for emission from both acridine and acridinium. Hence if both species were present in ground state, the absorption spectrum should be a composite of the absorption spectra of acridine and acridinium. In contrast, if the acridinium is formed only in the excited state, then the absorption spectrum in 0.2 M NH_4NO_3 should be almost identical to that of neutral acridine.
- B. Examination of the data (Table 7.6) reveals two decay times that are independent of emission wavelength. This indicates that there are two emitting species and that their decay rates are independent of emission wavelength. On the short-wavelength side of the emission the decay is a single exponential. This result indicates the reaction is irreversible and that the measured decay times at other wavelengths contain contributions from both acridine and acridinium. Proof of an excited-state reaction is provided by observation of negative pre-exponential factors. As the observation wavelength is increased this term becomes more predominant. At the longest observation wavelengths one finds that the pre-exponential factors are nearly equal in magnitude and opposite in sign. This near equality of the pre-exponential factors indicates that at 560 nm the emission is predominantly from the relaxed species. The fact that α_2 is slightly larger than α_1 indicates that there is still some emission from neutral acridine at 560 nm.
- A7.5. Red-edge excitation selects for fluorophores that are most strongly interacting with the solvent. The solvent configuration around these selected fluorophores is similar to that in a solvent-relaxed state. The TRES with 416-nm excitation do not show a time-dependent

shift because the fluorophore is already in the relaxed state.

CHAPTER 8

- A8.1. The apparent bimolecular quenching of 2-AP by Cu^{2+} can be found by noting that $F_0/F = 1.10$ at 2×10^{-6} M Cu^{2+} . Hence $K = 50,000 \text{ M}^{-1}$ and $k_q = 5 \times 10^{12} \text{ M}^{-1} \text{ s}^{-1}$. Similarly, $F_0/F = 1.7$ at 0.001 M DMA, yielding $K = 700 \text{ M}^{-1}$ and $k_q = 7 \times 10^{10} \text{ M}^{-1} \text{ s}^{-1}$. Both values are larger than the maximum value possible for diffusive quenching in water, near $1 \times 10^{10} \text{ M}^{-1} \text{ s}^{-1}$. This implies some binding or localization of the quenchers near the fluorophores.
- A8.2. The data in Figure 8.72 can be used to calculate the lifetimes of pyrene, which are 200, 119, and 56 ns in the presence of N_2 , air or O_2 , respectively. Assuming the oxygen solubility in DMPC vesicles is fivefold larger than in water (0.001275 M/atm in water), the oxygen bimolecular quenching constant is $k_q = 2 \times 10^9 \text{ M}^{-1} \text{ s}^{-1}$. This value is about 20% of the value expected for a fluorophore dissolved in water.
- A8.3. The data in the absence of benzyl alcohol (Figure 8.73) can be used to calculate a bimolecular quenching constant of $6 \times 10^9 \text{ M}^{-1} \text{ s}^{-1}$. This indicates that the naphthalene is mostly accessible to iodide and probably not bound to the cyclodextrin. This conclusion is supported by the data in the presence of benzyl alcohol. In the presence of benzyl alcohol the Stern-Volmer plots curve downward in the presence of β -CD (Figure 8.74). This suggests the presence of two naphthalene populations, one of which is less accessible to iodide quenching. In the presence of benzyl alcohol and 5.1 mM β -CD the Stern-Volmer plot is still curved, and the apparent value of k_q decreases, which indicates shielding from iodide quenching. Under these conditions it seems that naphthalene binds to β -CD only in the presence of benzyl alcohol.
- A8.4. Figure 8.77 shows a plot of F_0/F versus $[I^-]$. From the upward curvature of this plot it is apparent that both static and dynamic quenching occur for the same population of fluorophores. The dynamic (K_D) and static (K_S) quenching constants can be calculated by a plot of the apparent quenching constant (K_{app}) versus the

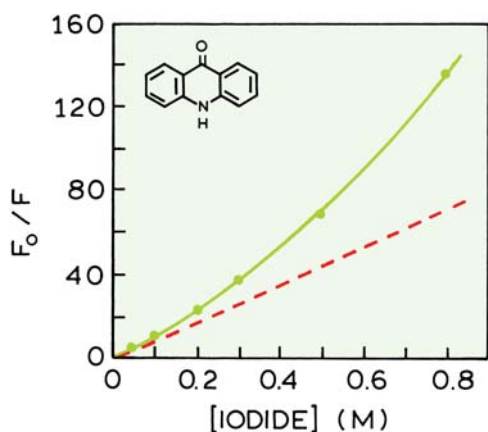


Figure 8.77. Iodide quenching of acridone. Data from [175].

concentration of quencher $[I^-]$. The apparent quenching constant is given by $(F_0/F - 1)/[I^-] = K_{app}$.

M KI	K_{app}
0	—
0.04	91.0
0.10	96.0
0.20	110.0
0.30	121.0
0.5	135.0
0.8	170.0

These results are plotted in Figure 8.78. In the plot the y-intercept is $K_D + K_S = 89 \text{ M}^{-1}$, and the slope is $K_D K_S = 101 \text{ M}^{-2}$. The quadratic equation can be solved to find K_D and K_S . Assuming the larger value is K_D we obtain $K_D = 87.8 \text{ M}^{-1}$ and $K_S = 1.15 \text{ M}^{-1}$. The bimolecular quenching constant is given by $K_D/\tau_0 = k_q = 4.99 \times 10^9 \text{ M}^{-1} \text{ s}^{-1}$. The collisional frequency can be calculated independently from the Smoluchowski equation. Assuming a collision radius of 4 \AA , and the diffusion of the quencher to be dominant, one obtains

$$\begin{aligned}
 k_0 &= 4\pi RDN/10^3 \\
 &= [(4\pi(4 \times 10^{-8} \text{ cm})(2.065 \times 10^{-5} \text{ cm}^2/\text{sec}) \\
 &\quad (6.02 \times 10^{23} \text{ mole}^{-1}))]/(10^3 \text{ cm}^3 \text{ l}^{-1})] \\
 &= 0.625 \times 10^{10} \text{ M}^{-1} \text{ sec}^{-1} \quad (8.51)
 \end{aligned}$$

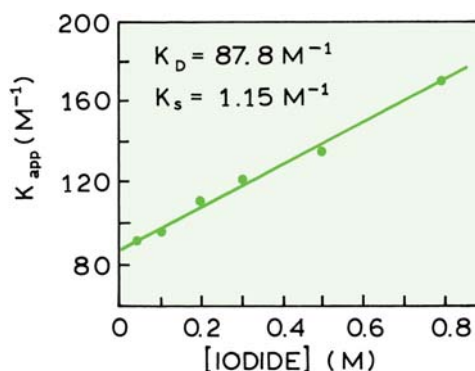


Figure 8.78. Static and dynamic quenching constants of acridone. Data from [175].

This value describes the quenching constant expected if 100% of the collisional encounters are effective in quenching. Hence the quenching efficiency $\gamma = k_q/k_0 = 0.80$.

The radius of the sphere of action can be calculated using any of the F_0/F values for which there is excess quenching. At 0.8 M iodide the expected value of F_0/F due only to dynamic quenching is

$$\left(\frac{F_0}{F}\right)_D = 1 + 87.8(0.8) = 71.24 \quad (8.52)$$

This is indicated by the dashed line in Figure 8.77. The observed value of F_0/F is 137. Using

$$F_0/F = (1 + K_D[Q]) \exp([Q]NV/1000) \quad (8.53)$$

we obtain $\exp([Q]NV/1000) = 1.92$ or $[Q]NV/1000 = 0.653$. From these results one can calculate that the volume of the sphere of action is $V = 1.36 \times 10^{-21} \text{ cm}^3$. Using $V = 4/3 \pi r^3$, where r is the radius, one finds $r = 6.9 \text{ \AA}$. According to this calculation, whenever an iodide ion is within 6.9 \AA of an excited acridone molecule the probability of quenching is unity.

The static quenching constant is quite small, as is the radius of the sphere of action. It seems that no actual complex is formed in this case. Rather, the static component is due simply to the probability that a fluorophore is adjacent to a quencher at the moment of excitation.

A8.5. Using the data in Problem 8.5 one may calculate the following:

[AMP] (mM)	τ_0/τ	F_0/F	$(F_0/F)/(\tau_0/\tau)$
0.0	1.0	1.0	1.0
1.75	1.265	1.40	1.107
3.50	1.502	1.80	1.198
5.25	1.741	2.35	1.35
7.0	1.935	3.00	1.55

The collisional or dynamic quenching constant can be calculated from a plot of τ_0/τ versus [AMP] (Figure 8.79). The dynamic quenching constant is 136 M^{-1} . Using the lifetime in the absence of quencher one finds $k_q = K_D/\tau_0 = 4.1 \times 10^9 \text{ M}^{-1} \text{ s}^{-1}$, which is typical for a diffusion-controlled reaction which occurs with high efficiency.

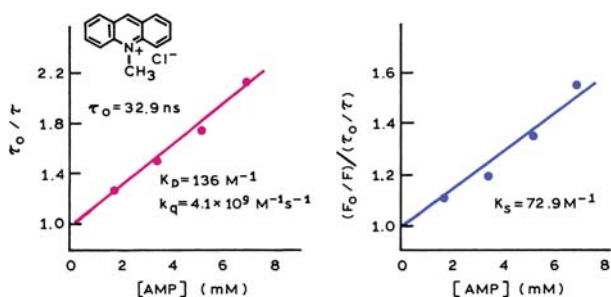


Figure 8.79. Quenching of methylacridinium chloride by AMP. From [18].

In the previous problem we obtained K_S and K_D from a plot of the apparent quenching constant versus quencher concentration (Figure 8.78). In this case both the lifetime and yield data are given, and a simpler procedure is possible. We calculated the quantity $(F_0/F)/(\tau_0/\tau)$. From eqs. 8.8, and 8.19 this quantity is seen to reflect only the static component of the quenching:

$$\frac{F_0/F}{\tau_0/\tau} = 1 + K_S[\text{AMP}] \quad (8.54)$$

A plot of $(F_0/F)/(\tau_0/\tau)$ versus [AMP] yields the association constant as the slope (Figure 8.79).

In contrast to the apparent association constant for the "acridone-iodide complex," this value (72.9 M^{-1}) is much larger. An actual ground-state complex is likely in this case. This was demonstrated experimentally by examination of the absorption spectrum of MAC, which was found to be changed in the presence of AMP. If the MAC-AMP complex is nonfluorescent, then the only emission observed is that from the

uncomplexed MAC. Since these molecules are not complexed, the excitation spectrum of MAC in the presence of AMP will be that of MAC alone.

A8.6. The susceptibility of a fluorophore to quenching is proportional to its fluorescence lifetime. Fluorophores with longer lifetimes are more susceptible to quenching. To decide on the upper limit of lifetimes, above which oxygen quenching is significant, we need to consider dissolved oxygen from the air. Based on the assumed accuracy of 3% we can use $F_0/F = \tau_0/\tau = 1.03$. Since the atmosphere is 20% oxygen, the oxygen concentrations due to atmospheric oxygen are one-fifth the total solubility. For aqueous solutions

$$\frac{F_0}{F} = \frac{\tau_0}{\tau} = 1.03 = 1 + k_q\tau_0[\text{O}_2] \quad (8.55)$$

Using the information provided for aqueous solutions

$$\tau_0 = \frac{0.03}{k_q[\text{O}_2]} = \frac{0.03(5)}{(1 \times 10^{10})(.001275)} = 11.8 \text{ ns} \quad (8.56)$$

For the ethanol solution

$$\tau_0 = \frac{0.03(5)}{(2 \times 10^{10})(.001275)(5)} = 1.2 \text{ ns} \quad (8.57)$$

If the unquenched lifetimes are longer than 1.2 ns in ethanol, or 11.8 ns in water, then dissolved oxygen from the air can result in significant quenching (greater than 3%). If desired this quenching can be minimized by purging with an inert gas, such as nitrogen or argon.

A8.7. The rate of collisional deactivation can be calculated from the decrease in lifetime due to collisions with the adenine ring. The lifetimes in the absence (τ_0) and presence of (τ) of the adenine moiety are $\tau_0 = \gamma^{-1}$ and $\tau = (\gamma + k)^{-1}$. Therefore,

$$k = \frac{1}{\tau} - \frac{1}{\tau_0} = 2.0 \times 10^8 \text{ s}^{-1} \quad (8.58)$$

The quantum yield of FAD is decreased by both static and dynamic quenching:

$$\frac{F}{F_0} = \frac{Q(\text{FAD})}{Q(\text{FMN})} = f \frac{\tau}{\tau_0} \quad (8.59)$$

where f is the fraction not complexed. Hence

$$f = \frac{\tau_0 Q(\text{FAD})}{\tau Q(\text{FMN})} = \frac{(4.6)(0.09)}{(2.4)(1.0)} = 0.17 \quad (8.60)$$

83% of the FAD exists as a nonfluorescent complex.

- A8.8. Using the data provided one can calculate the following quantities needed for the Stern-Volmer plots:

$[I^-]$, M	F_0/F	ΔF	$F_0/\Delta F$	$[I^-]^{-1}$, M ⁻¹
0.0	1.000	0	—	—
0.01	1.080	0.074	13.51	100
0.03	1.208	0.172	5.814	33.3
0.05	1.304	0.233	4.292	20.0
0.10	1.466	0.318	3.145	10.0
0.20	1.637	0.389	2.571	5.0
0.40	1.776	0.437	2.288	2.5

The downward curvature of the Stern-Volmer plot indicates an inaccessible fraction (Figure 8.80). From the intercept on the modified Stern-Volmer plot one finds $f_a = 0.5$. Hence one tryptophan residue per subunit is accessible to iodide quenching. The slope on the modified Stern-Volmer plot is equal to $(f_a K)^{-1}$. Thus $K = 17.4 \text{ M}^{-1}$. By assumption, the quenching constant of the inaccessible fraction is zero using these results one can predict the quenching plots for each tryptophan residue.

$[I^-]$, M	$[I^-]^{-1}$, M ⁻¹	$(F_0/F)_b$	$(F_0/F)_a^+$	$(F_0/\Delta F)_b$	$(F_0/\Delta F)_a^{++}$
0.0	0	1.0	1.0	—	—
0.01	100	"	1.174	"	6.747
0.03	33.3	"	1.522	"	2.916
0.05	20.0	"	1.870	"	2.149
0.10	10.0	"	2.740	"	1.575
0.20	5.0	"	4.480	"	1.287
0.40	2.5	"	7.96	"	1.144

+Calculated from $F_0/F = 1 + 17.4 [I^-]$.

++Calculated from $F_0/\Delta F = 1/K[Q] + 1$.

For the accessible fraction the Stern-Volmer plot is linear and the apparent value of $f_a = 1$ (Figure 8.81). Hence if the quenching data were obtained using 300-nm excitation, where only the accessible residue was excited, all the fluorescence would appear to be accessible. Since the inaccessible fraction is not quenched, $F_0/F = 1$ for this fraction. One cannot construct a modified Stern-Volmer plot since $\Delta F = 0$ for this fraction. The bimolecular quenching constant can be calculated using $K = 17.4 \text{ M}^{-1}$ and $\tau = 5 \text{ ns}$, yielding a bimolecular quenching constant $k_q = 0.35 \times 10^{10} \text{ M}^{-1} \text{ s}^{-1}$.

- A8.9. Quenching of Endo III by poly(dAdT) displays saturation near $20 \mu\text{M}$, which indicates specific binding of

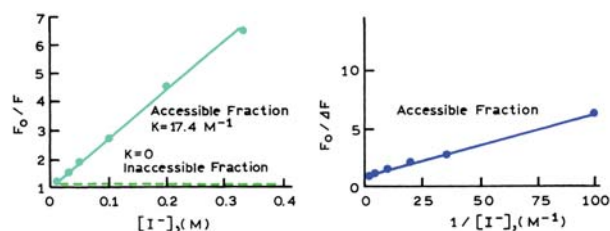


Figure 8.80. Predicted Stern-Volmer plots for the accessible and inaccessible tryptophan residues.

poly(dAdT) to Endo III. Assume the quenching is dynamic. Then K_D is near 10^5 M^{-1} , resulting in an apparent value of $k_q = 2 \times 10^{13} \text{ M}^{-1} \text{ s}^{-1}$. This is much larger than the diffusion controlled limit, so there must be some specific binding.

About 50% of the fluorescence is quenched. In Section 8.9.1 we saw that both residues were equally fluorescent. Hence the titration data (Figure 8.75) suggests that one residue, probably 132, is completely quenched when poly(dAdT) binds to Endo III.

- A8.10. The structure of wild-type tet repressor is shown in Figure 8.39. The W75F mutant contains a phenylalanine in place of Trp 75, and thus only one Trp at position 43. This tryptophan is immediately adjacent to bound DNA, which quenches the Trp 43 emission. The extent of quenching is over 50% because there is only one type of tryptophan. The wild-type protein would be expected to show less quenching because Trp 75 will probably not be quenched by DNA.

- A8.11. The relative intensities can be calculated from the Stern-Volmer equation:

$$\frac{F_0}{F} = \frac{\tau_0}{\tau} = 1 + k_q \tau_0 \quad (8.61)$$

For DBO with a lifetime of 120 ns, and $k_q = 9 \times 10^6 \text{ s}^{-1}$, the relative intensity is $F/F_0 = 0.48$. The DBO is about 50% quenched. For $\tau_0 = 2 \text{ ns}$, $F/F_0 = 0.98$ and the quenching would probably not be detectable. For $\tau_0 = 2 \text{ ms}$, $F/F_0 = 5.6 \times 10^{-5}$ and the fluorophore would be completely quenched.

CHAPTER 9

- A9.1. In order for PET to occur $\Delta G < 0$. We can use the Rehm-Weller equation to estimate the oxidation

potential of donor fluorophore if the other quantities are known. The $S_0 \otimes S_1$ wavelength of 365 nm corresponds to 3.4 eV (eqs. 9.11 and 9.12). Using $\Delta G < 0$ and eq. 9.10 yields $E(D^+/D) \otimes 3$ V. Hence it requires more than 69.2 kcal/mole to oxidize the fluorophore. If more than 3 volts were required to remove an electron from the fluorophore then PET would not occur. It is difficult to intuitively understand the sign of $E(D^+/D)$ because of the convention that $\Delta E > 0$ corresponds to $\Delta G < 0$.

- A9.2. Methylation of the pyridine results in a greater affinity for electrons. Hence PET from the fluorophore occurs to the pyridinium group but not to the more electron-rich pyridine group.

CHAPTER 10

- A10.1. At 430, 290, and 270 nm the r_0 values of perylene are near 0.38, 0.10, and 0.0, respectively. The angle β between the absorption and emission moments can be calculated using eq. 10.22. These calculations yield $\beta = 16.8, 45, \text{ and } 54.7^\circ$, respectively.
- A10.2. If the sample is weakly scattering, the scattered component will be completely polarized ($r = 1.0$). The measured anisotropy can be obtained using eq. 10.6

$$r_{\text{obs}} = 0.30(0.80) + 1.0(0.20) = 0.44 \quad (10.53)$$

The anisotropy above 0.40 should be an immediate warning that the measured value was not due only to fluorescence.

- A10.3. The corrected ratio, $I_{\text{VV}}/I_{\text{HV}}$, is given by 1.33/0.45 = 2.96. Therefore $r_0 = 0.395$ and $P_0 = 0.495$. The angle between the absorption and emission dipoles can be calculated using eq. 10.22. Substitution of $r_0 = 0.395$ yields $\beta = 5.2^\circ$.
- A10.4. The denominator in eq. 10.43 is given by

$$\int_0^\infty I(t) dt = I_0 \int_0^\infty \exp(-t/\tau) dt = I_0 \tau \quad (10.54)$$

The numerator in eq. 10.43 is given by

$$\int_0^\infty I(t) r(t) dt = \int_0^\infty \exp\left[-t\left(\frac{1}{\tau} + \frac{1}{\theta}\right)\right] dt = I_0 r_0 \frac{\tau \theta}{\tau + \theta} \quad (10.55)$$

Division of eq. 10.55 by 10.54 yields eq. 10.44.

- A10.5. The rotational correlation time of perylene can be calculated using eq. 10.46:

$$\theta = \frac{\eta V}{RT} = \frac{(0.01194 \text{ P})(252 \text{ g/mole})(0.74 \text{ ml/g})}{(293^\circ\text{K})(8.314 \times 10^7 \text{ erg/mole } ^\circ\text{K})} \quad (10.56)$$

$$\theta = 91 \text{ ps} \quad (10.57)$$

The anisotropy can be calculated using eq. 10.44:

$$r = \frac{0.36}{1 + 6/0.091} = 0.005 \quad (10.58)$$

A similar calculation for propylene glycol at 25°C yields $\theta = 2.4$ ns and $r = 0.103$.

- A10.6. Equation 10.51 can be derived by reasoning an expression for the average anisotropy. Suppose the quantum yield of the free and bound forms are q_F and q_B , respectively. Then the measured anisotropy is

$$r = \frac{f_F q_F r_F + f_B q_B r_B}{f_F q_F + f_B q_B} \quad (10.59)$$

The correctness of this expression can be seen by noting the numerator is simply a revised form of the additivity law for anisotropies, and the products $f_F q_F$ and $f_B q_B$ represent the intensities of each form of the probe. The denominator normalizes these values to fractional fluorescence intensities. Equation 10.59 can be rearranged to eq. 10.51 by noting $f_F + f_B = 1.0$ and $R = q_B/q_F$. Setting $R = 1$ yields eq. 10.50.

- A10.7. A. The observed polarizations may be converted into anisotropies using $r = 2P/(3 - P)$. The latter are more convenient since

$$\bar{r} = f_F r_F + f_B r_B \quad (10.60)$$

where the subscripts F and B represent the free and bound forms of the fluorophore, and f_i is the fraction of fluorescence due to each form of the probe. When $[\text{BSA}] = 0$ one observes r_F , and when $[\text{BSA}] \gg K_d$ one observes r_B . These considerations are summarized below:

[BSA]	Observable	r
0	r_F	0.010
$2 \times 10^{-5} \text{ M}$	r	0.200
$\gg K_d$	r_B	0.300

Using eq. 10.59 one obtains

$$0.20 = f_F(0.01) + (1 - f_F)(0.30) \quad (10.61)$$

and hence $f_F = 0.345$ and $f_B = 0.655$. Since the concentration of DNS is much less than that of BSA, we can assume that the concentration of unliganded BSA is not depleted by the binding of DNS. The ratio of free to bound DNS is given by $0.345/0.655$. Hence from eq. 10.52:

$$K_d = \frac{(2 \times 10^{-5} \text{ M})(0.345)}{(0.655)} = 1.05 \times 10^{-5} \text{ M} \quad (10.62)$$

B. In the use of eq. 10.60 we assumed that the calculated fractional intensity of each species represented the fraction of the DNS which was bound and free. However, if the relative quantum yield of the bound probe is twofold larger than the free probe, then clearly the concentration of the bound form is twofold lower. Therefore:

$$K_d = \frac{(2 \times 10^{-5} \text{ M})(0.345)}{(0.655)/2} = 2.1 \times 10^{-5} \text{ M} \quad (10.63)$$

C. A change in quantum yield could be readily detected by comparing the intensity of the DNS solution, with and without added BSA. Since the DNS concentrations are identical the relative intensities represent the relative quantum yields.

D. Using the data provided, the calculated rotational correlation time of BSA is 20 ns. The anisotropy of free DNS will decay too rapidly for measurement with most currently available instruments. For the solution containing a concentration of BSA adequate to bind all the DNS one expects

$$r(t) = 0.20e^{-t/20} \quad (10.64)$$

For the $2 \times 10^{-5} \text{ M}$ solution

$$r(t) = f_B r_0 e^{-t/20} = 0.131 e^{-t/20} \quad (10.65)$$

CHAPTER 11

- A.11.1. The angle can be calculated using eq. 11.51. Using an apparent time of 0, an anisotropy of 0.22, as r_∞ , one finds $\langle \cos^2 \theta \rangle = 0.924$ and $\theta = 16^\circ$.
- A.11.2. The most direct approach is to use the amplitudes from the intensity decay. The radiative rate of a fluorophore is usually not affected by its environment. Hence, the relative values of α_i represent the fraction of the FMN free or bound to YFP. The dissociation constant is given by

$$K_d = \frac{[\text{FMN}][\text{YFP}]}{[\text{FMN} \cdot \text{YFP}]} \quad (11.52)$$

This equation can be rewritten in terms of the total YFP concentration and the fraction of FMN bound (f_B):

$$K_d = \frac{[\text{YFP}]_T (1 - f_B)^2}{f_B} \quad (11.53)$$

where $[\text{YFP}]_T = [\text{YFP}] + [\text{FMN} \cdot \text{YFP}]$ is the total concentration of YFP. This expression can be understood by noticing that the concentrations of free YFP and FMN are both given by $[\text{YFP}]_T(1 - f_B)$, and that the concentration of $[\text{FMN} \cdot \text{YFP}] = [\text{YFP}]_T f_B$. At $[\text{YFP}] = 0.18 \mu\text{M}$ the fraction bound is given by

$$f_B = \frac{\alpha_2}{\alpha_1 + \alpha_2} = 0.31 \quad (11.54)$$

Hence, $K_d = 0.28 \times 10^{-6} \text{ M}$.

CHAPTER 12

- A12.1. The anisotropy of any time can be calculated using eq. 12.1. These values are listed in Table 12.3. The

Table 12.3. Associated Anisotropy Decay

t (ns)	$f_1(t)$	$f_2(t)$	$r_1(t)$	$r_2(t)$	$r(t)$
0	0.5	0.5	0.3	0.3	0.30
1	0.45	0.55	0.0	0.29	0.16
5	0.25	0.75	0.0	0.27	0.20

anisotropy values for the non-associated decay can be calculated using

$$r(t) = r_0[0.5 \exp(-t/0.05) + 0.5 \exp(-t/40)] \quad (12.51)$$

For $t = 0, 1,$ and 5 ns these values are 0.30, 0.146, and 0.132, respectively.

The presence of an associated anisotropy decay can be seen from the increase in anisotropy at 5 ns as compared to 1 ns. For the non-associated decay the anisotropy decreases monotonically with time.

A12.2. For a non-associative model the anisotropy decay is given by

$$r(t) = r_0[g_1 \exp(-t/\theta_1) + g_2 \exp(-t/\theta_2)] \quad (12.52)$$

where subscripts 1 and 2 refer to components in the decay, not the location of the fluorophore. From Figure 12.5 the time-zero anisotropy appears to be about 0.32. Using the parameter values in this figure,

$$r(t) = 0.32[0.7 \exp(-t/0.30) + 0.3 \exp(-t/685)] \quad (12.53)$$

A plot of $r(t)$ would show a rapid decrease to 30% of the time-zero value followed by a long tail where the anisotropy does not decay during the lifetime of the fluorophore.

A12.3. The anisotropy can be calculated using eqs. 10.6 and 10.22. The anisotropy from the three transitions can be calculated using $\beta = 0^\circ$ and $\pm 120^\circ$. Hence, $r = 0.33(0.40) + 0.33(-0.05) + 0.33(-0.05) = 0.10$.

A12.4. The apparent $r(0)$ values of melittin are near 0.16, which is considerably less than $r_0 = 0.26$. This indicates that the tryptophan residue in melittin displays fast motions that are not resolved with the available range of lifetimes (0.6 to 2.4 ns).

The apparent correlation times from melittin can be calculated from the slopes in Figure 12.41. For example, in the absence of NaCl the slope is near 5.8×10^9 ,

which is equal to $(r(0)\theta)^{-1}$. Hence the apparent correlation time is 1.08 ns.

CHAPTER 13

A13.1. The D–A distance can be calculated using eq. 13.12. The transfer efficiency is 90%. Hence the D–A distance is $r = (0.11)^{1/6}R_0 = 0.69R_0 = 17.9 \text{ \AA}$. The donor lifetime in the D–A pair can be calculated from eq. 13.14, which can be rearranged to $\tau_{DA} = (1 - E)\tau_D = 0.68 \text{ ns}$.

A13.2. The equations relating the donor intensity to the transfer efficiency can be derived by recalling the expressions for relative quantum yields and lifetimes. The relative intensities and lifetimes are given by

$$F_D = \frac{\Gamma_D}{\Gamma_D + k_{nr}}, \quad \tau_D = \frac{1}{\Gamma_D + k_{nr}} \quad (13.34)$$

$$F_{DA} = \frac{\Gamma_D}{\Gamma_D + k_{nr} + k_T}, \quad \tau_{DA} = \frac{1}{\Gamma_D + k_{nr} + k_T} \quad (13.35)$$

where Γ_D is the emission rate of the donor and k_{nr} is the non-radiative decay rate. The ratio of intensities is given by

$$\frac{F_{DA}}{F_D} = \frac{\Gamma_D + k_{nr}}{\Gamma_D + k_{nr} + k_T} = \frac{\tau_D^{-1}}{\tau_{DA}^{-1} + k_T} \quad (13.36)$$

Hence

$$1 - \frac{F_{DA}}{F_D} = \frac{k_T}{\tau_D^{-1} + k_T} = E \quad (13.37)$$

One can derive a similar expression for the transfer efficiency E based on lifetime using the right-hand side of eqs. 13.34 and 13.35.

It should be noted that k_T was assumed to be a single value, which is equivalent to assuming a single distance. We also assumed that the donor population was homogeneous, so that each donor had a nearby acceptor, that is, labeling by acceptor is 100%.

A13.3. The excitation spectra reveal the efficiency of energy transfer by showing the extent to which the excitation of the naphthyl donor at 290 nm results in dansyl

emission. The transfer efficiency can be calculated from the emission intensity at 450 nm for 290-nm excitation, which reflects acceptor emission due to excitation of the donor and direct excitation of the acceptor. Dansyl-L-propyl-hydrazide does not contain a donor, and hence this excitation spectrum defines that expected for 0% transfer. For dansyl-L-propyl- α -naphthyl, in which the donor and acceptor are closely spaced, energy transfer is 100% efficient. For this donor-acceptor pair the greatest sensitivity of the excitation spectrum to energy transfer is seen near 290 nm, the absorption maximum of the naphthyl donor. For the other derivatives the intensity is intermediate and dependent upon the length of the spacer. For 290-nm excitation the transfer efficiency can be calculated from the relative intensity between 0 and 100% transfer. The efficiency of energy transfer decreases as the length of the spacer is increased.

The object of these experiments was to determine the distance dependence of radiationless energy transfer. Hence we assume that the efficiency of energy transfer depends on distance according to

$$E = \frac{(R_0/r)^j}{(R_0/r)^j + 1} \quad (13.38)$$

where R_0 and r have their usual meanings, and j is an exponent to be determined from the observed dependence of E on r . Rearrangement of eq. 13.38 yields

$$\ln(E^{-1} - 1) = j \ln r - j \ln R_0 \quad (13.39)$$

Hence a plot of $\ln(E^{-1} - 1)$ versus $\ln r$ has a slope of j . These data are shown in Figure 13.41. The slope was found to be 5.9 ± 0.3 .¹⁸ From this agreement with the

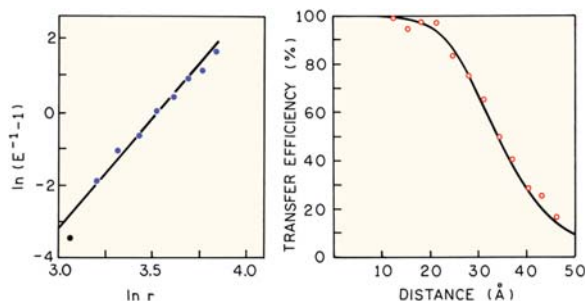


Figure 13.41. Distance dependence of the energy transfer efficiencies in dansyl-(L-propyl)_n- α -naphthyl; $n = 1-12$. Revised from [18].

predicted value of $j = 6$ these workers concluded that energy transfer followed the predictions of Förster. See [18] for additional details.

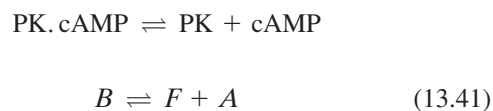
The value of R_0 can be found from the distance at which the transfer efficiency is 50%. From Figure 13.41 (right) R_0 is seen to be near 33 Å.

- A13.4. The lifetime of compound I is τ_{DA} and the lifetime of compound II is τ_D . Compound II serves as a control for the effect of solvent on the lifetime of the indole moiety, in the absence of energy transfer. The rate of energy transfer is given by $k_T = \tau_{DA}^{-1} - \tau_D^{-1}$.

$$k_T = CJ \quad (13.40)$$

where C is a constant. Hence a plot of k_T versus J should be linear. The plot of k_T vs. J is shown in Figure 13.42. The slope is 1.10. These data confirm the expected dependence of k_T on the overlap integral. See [20] for additional details.

- A13.5. If the wavelength (λ) is expressed in nm, the overlap integral for Figure 13.9 can be calculated using eq. 13.3 and is found to be $4.4 \times 10^{13} \text{ M}^{-1} \text{ cm}^{-1} (\text{nm})^4$. Using eq. 13.5, with $n = 1.33$ and $Q_D = 0.21$, one finds $R_0 = 23.6 \text{ Å}$. If λ is expressed in cm then $J(\lambda) = 4.4 \times 10^{-15} \text{ M}^{-1} \text{ cm}^3$, and using eq. 13.8 yields $R_0 = 23.6 \text{ Å}$.
- A13.6. The disassociation reaction of cAMP (A) from protein kinase (PK) is described by



where B represents PK with bound cAMP, F the PK without bound cAMP, and A the concentration of

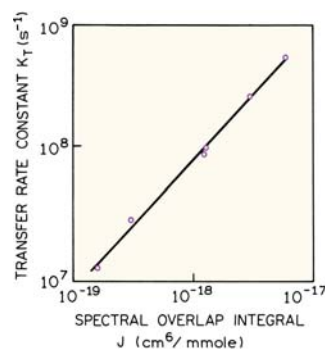


Figure 13.42. Dependence of the rate of energy transfer on the magnitude of the overlap integral. Revised from [20].

cAMP. The dissociation constant for cAMP is defined by

$$K_D = \frac{[F][A]}{[B]} \quad (13.42)$$

Using conservation of mass, $[F] + [B] = [T]$ is the total protein kinase concentration, and one can show the bound and free fractions of PK are given by

$$f_B = \frac{[B]}{[T]} = \frac{[A]}{K_D + [A]}, \quad f_F = \frac{[F]}{[T]} = \frac{K_D}{K_D + [A]} \quad (13.43)$$

Let R_B and R_F represent the intensity ratio of each species. At any given cAMP concentration the observed ratio R is

$$R = f_B R_B + f_F R_F \quad (13.44)$$

Assuming that $f_B + f_F = 1.0$, one obtains

$$[A] = [\text{cAMP}] = K_D \left(\frac{R - R_F}{R_B - R} \right) \quad (13.45)$$

A ratio of intensities is independent of the total PK concentration, and independent of sample-to-sample variations in PK concentration. Hence intensity ratio-metric measurements are convenient and accurate. See [99] for additional details.

- A13.7. A. The efficiency of energy transfer can be calculated from eq. 13.13:

$$E = 1 - \frac{4.1}{20.5} = 0.80 \quad (13.46)$$

- B. The expected lifetime in the presence of DNP can be calculated using eq. 13.14 with $\tau_D = 5.0$ ns and $E = 0.8$:

$$\tau_{DA} = \tau_D(1-E) = 1 \text{ ns} \quad (13.47)$$

- C. The rate of energy transfer (k_T) can be calculated using eq. 13.11 with $E = 0.8$ and $\tau_D = 5$ ns:

$$k_T = \frac{E\tau_D^{-1}}{1-E} = 8 \times 10^8 \text{ s}^{-1} \quad (13.48)$$

- D. The distance can be calculated using eq. 13.12. Substitution and rearrangement yields, $r^6 = 0.20 R_0^6$, and therefore $r = 38.2 \text{ \AA}$.
- E. The efficiency can be calculated using eq. 13.12 with $r = 20 \text{ \AA}$. The efficiency is 0.9959. Once the efficiency is known the intensity can be calculated using eq. 13.13. The fluorescence intensity (F_{DA}) is expected to be 0.0041 $F_D = 0.0841$.
- F. The 1% impurity would contribute 1% of 20.5, or 0.205 to the total intensity. The contribution from this minor component would be $(0.205/0.0841) = 2.44$ -fold more intense than the signal from the DNP-binding protein, and would invalidate any interpretation of the intensity in the presence of DNP.
- G. The lifetime of the sample would be dominated by the impurity and thus would be near 5 ns. Such a result is indicative of an impurity. Specifically, the yield is decreased to 0.0041 of the original value, but the lifetime is relatively unchanged. When this result is found one should consider the presence of a fluorescent impurity.

- A13.8. In order to calculate the possible effects of κ^2 on distance we need to determine the depolarization factors due to segmental motion of the donor and acceptor. Knowledge of the rotational correlation time of the protein (θ) allows us to account for this component in the steady state anisotropy. The depolarization factors due to overall rotation (d_{pi}) can be calculated from the Perrin equation. For the donor ($\tau_D = 5$ ns) and acceptor ($\tau_A = 15$ ns) these factors are

$$d_{PD} = \frac{1}{1 + \tau_D/\theta} = 0.5 \quad (13.49)$$

$$d_{PA} = \frac{1}{1 + \tau_A/\theta} = 0.25 \quad (13.50)$$

Recall that the overall depolarization is given by Soleillet's rule (Chapter 10), $r = r_0 d_{pi} d_{si}$, where d_{si} is the factor due to segmental motions of the donor or acceptor. Hence we can use the steady-state anisotropies and calculate the depolarization factors due to rapid segmental probe motions:

$$d_D^* = \left(\frac{r_D}{r_0 d_{PD}} \right)^{1/2} = 0.71 \quad (13.51)$$

$$d_A^x = \left(\frac{r_A}{r_0 d_{pA}} \right)^{1/2} = 0.71 \quad (13.52)$$

Hence the maximum and minimum values of κ^2 are 0.19 and 2.62 (eqs. 13.18 and 13.19). According to eqs. 13.23 and 13.24, the D–A distance can range from $0.81R_0$ to $1.26R_0$, or from 20.3 to 31.5 Å.

A13.9. If $f_A = 1.0$ then the transfer efficiency is given by eq. 13.13:

$$E = 1 - \frac{0.5}{1.0} = 0.5 \quad (13.53)$$

and the D–A distance is thus equal to R_0 . If $f_A = 0.5$ the transfer efficiency is given by eq. 13.17:

$$E = 1 - \frac{0.5 - 1.0(0.5)}{1.0(0.5)} = 1.0 \quad (13.54)$$

If $f_A = 0.5$ then the transfer efficiency for the actual D–A pair is 100%, and thus the D–A distance is less than $0.5R_0$. The presence of acceptor underlabeling results in a higher intensity for the presumed D–A pair and an overestimation of the true D–A distance.

A13.10. Equation 13.25 can be easily derived by writing expression for the acceptor intensity. In the absence (F_A) and presence of donor (F_{AD}) the intensities are given by

$$F_A(\lambda_A^{em}) = \varepsilon_A(\lambda_D^{ex}) C_A(\lambda_A^{em}) \quad (13.55)$$

$$F_{AD}(\lambda_A^{em}) = [\varepsilon_A(\lambda_D^{ex}) + E\varepsilon_D(\lambda_D^{ex})] C_A(\lambda_A^{em}) \quad (13.56)$$

where excitation is at λ_D , intensities are measured at λ_A , and E is the transfer efficiency. $C_A(\lambda_A^{em})$ is a constant relating the intensity at λ_A to the acceptor concentration. Dividing 13.55 by 13.56, followed by rearrangement, yields eq. 13.25.

If the extent of donor labeling is less than 1.0, then the acceptor intensities are given by

$$F_A(\lambda_A^{em}) = \varepsilon_A(\lambda_D^{ex}) C_A(\lambda_A^{em}) \quad (13.57)$$

$$F_A(\lambda_A^{em}) = [\varepsilon_A(\lambda_D^{ex}) + f_D E \varepsilon_D(\lambda_D^{ex})] C_A(\lambda_A^{em}) \quad (13.58)$$

where f_D is the fractional labeling with the donor. These expressions can be understood by recognizing that the directly excited acceptor intensity is independent of f_D , but the acceptor intensity due to energy transfer depends on f_D . Rearrangement of eqs. 13.57 and 13.58 yields 13.25.

A13.11. Let $C_A(\lambda_A)$ and $C_D(\lambda_A)$ be the constants relating the intensities at λ_A to the acceptor and donor concentrations, respectively, when both are excited at λ_D . Since the donor is assumed to emit at λ_A , eqs. 13.55 and 13.56 become

$$F_A(\lambda_A) = \varepsilon_A(\lambda_D) C_A(\lambda_A) \quad (13.59)$$

$$F_{AD}(\lambda_A) = [\varepsilon_A(\lambda_D) + E\varepsilon_D(\lambda_D)] C_A(\lambda_A) + \varepsilon_D(\lambda_D) C_{DA}(\lambda_A) \quad (13.60)$$

In eq. 13.58 we considered the contribution of the donor in the D–A pair to the intensity at λ_A . In general $C_{DA}(\lambda_A)$ will be smaller than $C_D(\lambda_A)$ due to FRET quenching of the donor. However, $C_D(\lambda_A)$ can be measured with the donor-alone sample. $C_{DA}(\lambda_A)$ can be estimated using the shape of the donor emission to estimate the donor contribution at λ_A in the doubly labeled sample. Eqs. 13.59 and 13.60 can be rearranged to

$$\frac{F_{AD}(\lambda_A)}{F_D(\lambda_D)} - 1 = \frac{E\varepsilon_D(\lambda_D)}{\varepsilon_A(\lambda_D)} + \frac{\varepsilon_D(\lambda_D) C_{DA}(\lambda_A)}{\varepsilon_A(\lambda_D) C_A(\lambda_A)} \quad (13.61)$$

The transfer efficiency as seen from the acceptor emission is given by eq. 13.25, which assumes that the donor does not emit at the acceptor wavelength. Hence the acceptor emission increases the apparent efficiency to

$$E_{app} = E + \frac{C_{DA}(\lambda_A)}{C_A(\lambda_A)} \quad (13.62)$$

and would thus be larger than the actual efficiency. If the donor does not contribute at λ_A , then $C_{DA}(\lambda_A) = 0$

and E_{app} becomes the true efficiency. See [83] for additional details.

A13.12. The true transfer efficiency is defined by the proportion of donors that transfer energy to the acceptor, and is given by

$$E = \frac{k_T}{\tau_D^{-1} + k_q + k_T} \quad (13.63)$$

The apparent efficiency seen for the donor fluorescence is given by

$$E_D = \frac{k_T + k_q}{\tau_D^{-1} + k_q + k_T} \quad (13.64)$$

The apparent efficiency (E_D) is larger than the true efficiency (E) because the additional quenching pathway decreases the donor emission more than would have occurred by FRET alone. See [56] for additional details.

CHAPTER 14

A14.1. The intensity decays of A and C would both be single exponential, but the intensity decay of B would be a triple exponential. For sample A the donors are at a unique distance from acceptors at 15, 20, and 25 Å. The transfer rate is given by

$$k_T = \frac{1}{\tau_D} \left(\frac{20}{15} \right)^6 + \frac{1}{\tau_D} \left(\frac{20}{20} \right)^6 + \frac{1}{\tau_D} \left(\frac{20}{25} \right)^6 \quad (14.27)$$

Calculation of the transfer rate yields $k_T = 6.88\tau_D^{-1}$. Hence the decay of sample A is given by eq. 14.1 and is a single exponential with

$$I_{DA}(t) = \exp\left[-\frac{t}{\tau_D} - \frac{t6.88}{\tau_D}\right] = \exp\left(-\frac{t}{0.63}\right) \quad (14.28)$$

The intensity decay of sample C would be the same single exponential with the same decay time of 0.63 ns.

The intensity decay of sample B would be a triple exponential. There would be three different decay times, which can be calculated from the three transfer

rates in eq. 14.28. The decay times are 0.76, 2.5, and 3.96 ns.

A14.2. Since the unquenched lifetime and quantum yields of the three proteins in sample B are the same, the radiative decay rates are the same and the relative amplitude of the three proteins would be the same. Hence the intensity decay would be given by

$$I(t) = \sum_i \alpha_i e^{-t/\tau_D} \quad (14.29)$$

with $\alpha_1 = \alpha_2 = \alpha_3 = 0.33$ and $\tau_1 = 0.76$, $\tau_2 = 2.5$ and $\tau_3 = 3.96$ ns.

In contrast to the α_i values, the fractional intensities will be very different for each protein in sample B. These values are given by

$$f_i = \frac{\alpha_i \tau_i}{\sum_j \alpha_j \tau_j} \quad (14.30)$$

Hence the fractional intensities of the three proteins are 0.105, 0.346, and 0.549.

A14.3. The presence of three acceptors could not be detected in sample A. This is because the only observable would be the decreased donor quantum yield or lifetime. The only way the three acceptors could be detected is from the absorption spectrum, assuming one knows the extinction coefficient for a single acceptor.

A14.4. The apparent distance for an assumed single acceptor can be found from eq. 14.2. Numerically we found $k_T = 6.88 \tau_D^{-1}$, which can be equated to an apparent distance:

$$k_T = \frac{6.88}{\tau_D} = \frac{1}{\tau_D} \left(\frac{R_0}{r_{\text{app}}} \right)^6 \quad (14.31)$$

Solving for r_{app} yields $R_0/r_{\text{app}} = 1.38$, so $r_{\text{app}} = 14.5$ Å. The extent of energy transfer is thus seen to be dominated by the closest acceptor at 15 Å. The presence of two more acceptors at 20 and 25 Å only decreases the apparent distance by 0.5 Å.

A.14.5. A. One acceptor per 60-Å cube corresponds to an acceptor concentration of 8 mM. Use of eq. 13.33 with $R_0 = 30$ Å yields a critical concentration of 17 mM.

- B. A covalently linked acceptor is somewhat equivalent to one acceptor per sphere of 30 Å, or 8.84×10^{18} acceptors/cm³. This is equivalent to an acceptor concentration of 15 mM. Covalent attachment of an acceptor results in a high effective acceptor concentration.

CHAPTER 15

- A.15.1. Using the data provided in Figure 15.28 one can calculate the following values:

Mole% Rh-PE	Rh-PE/Å ²	Rh-PE/R ₀ ²	F _{DA} /F _D
0.0	0.0	0.0	1.0
0.2	2.8×10^{-5}	0.071	0.62
0.4	5.7×10^{-5}	0.143	0.40
0.8	11.4×10^{-5}	0.286	0.21
1.2	17.1×10^{-5}	0.429	0.15

The distance of closest approach can be estimated by plotting the last two columns of this table on the simulations shown in Figure 15.17. The observed energy transfer quenching is greater than predicted for no excluded area, $r_c = 0$, or much less than R_0 . This suggests that the donors and acceptors are fully accessible and probably clustered in the PE vesicles. The R_0 value was not reported in [64].

- A15.2. The decay times can be used with eq. 15.20 to obtain the transfer rate $k_T = 1.81 \times 10^3 \text{ s}^{-1}$. Dividing by the EB concentration ($2.77 \text{ } \mu\text{M}$) yields $k_T^b = 6.5 \times 10^8 \text{ M}^{-1} \text{ s}^{-1}$.

Using eq. 15.25 and the values of R_0 and r_c , the maximum bimolecular rate constant is $1.1 \times 10^6 \text{ M}^{-1} \text{ s}^{-1}$. The measured values could be larger than the theoretical values for two reasons. The positively charged donors may localize around the negatively charged DNA. This results in a larger apparent concentration of EB. Given the small value of r_c we cannot exclude the possibility of an exchange contribution to k_T^b .

- A15.3. To a first approximation the donor intensity is about 50% quenched when $C/C_0 = 0.5$. This value of C/C_0 can be used to calculate the acceptor concentration in any desired units, as listed in Table 15.3.

Acceptor concentrations near 2 mM are needed in homogeneous solution. This is generally not practical for proteins because the absorbance due the acceptor would not allow excitation of the protein. Also, such high concentrations of acceptors are likely to perturb the protein structure.

Table 15.3. Approximate Concentrations for 50% Quenching in One, Two, and Three Dimensions

Equation	Concentrations for 50% energy transfer
$C_0 = (4/3\pi R_0^3)^{-1}$	9.55×10^{17} acceptors/cm ³ = 1.59 mM
$C_0 = (\pi R_0^2)^{-1}$	6.4×10^{11} acceptors/cm ² = 4.5×10^{-3} acceptors/lipid
$C_0 = (2R_0)^{-1}$	5×10^5 acceptors/cm = 1.7×10^{-2} acceptors/base pair

The situation is much better in proteins and nucleic acids. In this case the acceptors need only to be about one per 222 lipids or one per 59 base pairs. This favorable situation is the result of a locally high concentration of acceptors due to their localization in the lipid or nucleic acid. The bulk concentration of acceptors can be low and is determined by the bulk concentration of membrane or nucleic acid.

- A15.4. The simulations in Figure 15.31 determine the R_0 value because the two-dimensional concentration of acceptors is known from the area/lipid and the fractional acceptor concentrations. Any point on these curves can be used to calculate R_0 . For an acceptor density of 0.05 and $t = \tau_D$ the value of $I_{DA}(t)/I_D^0$ is about 0.003. The value of β can be found from eq. 15.9, yielding $\beta = 2.41$. For A/PL = 0.05 the area per acceptor molecule is $C_0 = 1400 \text{ } \text{Å}^2/\text{acceptor}$. Using eq. 15.10 and 15.11 yields $R_0 = 39.8 \text{ } \text{Å}$, which agrees with the value of 40 Å given in [50].

CHAPTER 16

- A16.1. A. Without experimentation, it is not possible to predict how the fluorescence properties of the protein will vary when it is unfolded. In general, one can expect the extent of tyrosine fluorescence to increase when the protein is unfolded. This could be detected by excitation at 280 nm. The tyrosine emission would appear near 308 nm. It is also probable that the fluorescent intensity or the emission maxima of the single-tryptophan residue would change as the protein is unfolded. Once the spectral characteristics of the native and unfolded states are determined, the data can be used to quantify the unfolding process. It is important to remember that anisotropy or lifetime measurements may not

- accurately reflect the fractional populations of the folded and unfolded states. This is particularly true if the quantum yields of the fluorescent residues in the protein change upon unfolding.
- B. The extent of exposure to the aqueous phase could be studied by measuring the Stern-Volmer bimolecular quenching constant (k_q) and comparison of the measured values with those observed for an N-acetyl-L-tryptophanamide in the same solvent. One should choose the neutral tryptophan analogue to avoid electrostatic effects on the quenching process. The extent of exposure to the aqueous phase can be estimated by comparing the measured quenching constant for the protein with that found for the model compounds.
 - C. If the protein associates to form a dimer, it is possible that the tryptophan residue becomes shielded from the aqueous phase. In this case one can expect a change in the intensity or emission maximum of the protein. If the tryptophan residue remains exposed to the aqueous phase upon dimer formation, then it is probable that the emission spectrum and intensity will remain the same. In this case the extent of the association should still be detectable by changes in the steady-state anisotropy.
 - D. In order to measure the distance of the tryptophan to the reactive site it is necessary to select an appropriate acceptor and to covalently label the protein. It is critical for the protein to be completely labeled with acceptor, because the unlabeled fraction will contribute a large amount to the measured intensity, resulting in an underestimation of the distance. Following calculation of the Förster distance, R_0 , from the spectral properties of the donor and acceptor, the distance can be measured from the decrease in the donor quantum yield due to the presence of acceptor.
 - E. While not immediately obvious, the extent of energy transfer from a tryptophan donor to an acceptor is expected to change upon association of the acceptor-labeled monomers. This is because, upon dimerization, each tryptophan residue will be brought into proximity of the acceptor on the other subunit. Hence each tryptophan will transfer to two acceptors, resulting

- A16.2. A. Dimerization could be detected from the steady-state intensity or the intensity decay. Upon dimer formation one will observe a twofold increase in the relative quantum yield. If the dimerization occurs due to a change in protein concentration, then it is necessary to normalize the measured intensities to the same protein concentration. If dimerization occurs as a result of a change in solution conditions, then the intensity change may be observed at a constant protein concentration.
- B. Dimer formation could be detected by an increase in the mean lifetime. When dimerization is partially complete one expects the decay to be a double exponential.
- C. Dimerization could not be detected from the steady-state anisotropy. The anisotropy (r) of the monomer and dimer can be calculated using the Perrin equation:

$$r = \frac{r_0}{1 + \tau/\theta} \quad (16.6)$$

where τ is the lifetime and θ is the rotational correlation time. The steady-state anisotropy of the monomer (r_M) and dimer (r_D) are equal: $r_M = r_D = 0.10$.

- D. Dimerization could be detected by measuring the anisotropy decay, which will display a longer mean correlation time as dimers are formed.
- E. When 50% of the monomers have formed dimers, these dimers contribute twice as much as the monomers to steady-state intensity. Hence the fractional intensities are $f_M = 0.33$ and $f_D = 0.66$. The steady-state anisotropy is given by

$$r = 0.33r_M + 0.66r_D = 0.10 \quad (16.7)$$

and is unchanged during dimerization.

For the intensity decay we need to calculate the values of α_M and α_D . The relative values are given by $\alpha_M = 0.33/2.5 = 0.13$ and $\alpha_D = 0.66/5.0 = 0.13$. Hence the intensity decay is given by

$$I(t) = 0.5 \exp(-t/\tau_M) + 0.5 \exp(-t/\tau_D) \quad (16.8)$$

The α_i values are equivalent because we assumed that the intensities and lifetimes both increased by the same amount, meaning that the radiative decay rate stayed the same.

For a mixture of monomers and dimers the anisotropy decay follows the associated model, where each decay time is associated with one of the correlation times. At any time t the fractional intensity of the monomer or dimer is given by

$$f_M(t) = \frac{0.5e^{-t/\tau_M}}{I(t)} \quad (16.9)$$

$$f_D(t) = \frac{0.5e^{-t/\tau_D}}{I(t)} \quad (16.10)$$

where $I(t)$ is given by eq. 16.8. The anisotropy decay is given by

$$r(t) = f_M(t)r_M(t) + f_D(t)r_D(t) \quad (16.11)$$

Hence this mixture of monomers and dimers displays an associated anisotropy decay.

- A16.3. There are two possible explanations for the CRABPI emission spectra in Figure 16.74. Figure 16.6 shows that the absorption spectra of indole shift to longer wavelengths with increasing solvent polarity and/or hydrogen bonding. CRABPI contains three tryptophan residues in different environments, which probably results in slightly different absorption spectra. An increase in excitation wavelength could result in selective excitation of the tryptophan residues in a more polar environment, which have longer-wavelength emission maxima.

A second possible explanation is a real-edge excitation shift (REES). A solution of indole or tryptophan in a viscous polar solution will show a shift to longer-wavelength emission as the excitation wavelength is increased. This effect is due to selective excitation of those fluorophores that are surrounded by solvent molecules that have orientations similar to the relaxed excited state. In the case of CRABPI the dominant cause of the emission spectral shifts is probably the different environments of the three tryptophan residues.

- A16.4. The emission spectra in Figure 16.75 show that the region of MRP near W93 binds to calmodulin. The N-terminal region of MRP does not appear to interact with calmodulin, or at least interaction does not result in a spectral shift. The presence or absence of interaction of W4 with calmodulin could be further studied by steady-state anisotropy measurements. If W4 does not interact with calmodulin, then there should be no change in the anisotropy of W4 upon addition of calmodulin.

- A16.5. Figure 16.76 shows the steady-state intensities of WT-LADH and the W314L mutant. For both acrylamide and iodide the amount of quenching is higher for W15 in the mutant protein than for the WT protein containing both W15 and W314. The Stern-Volmer plots in Figure 16.77 show a higher quenching constant for W15 in W314L than for the WT protein. The data in Figure 16.76 and 16.71 thus indicate that W15 in LADH is more accessible to water-soluble quenchers than is W314, which contributes part of the observed intensity in the WT protein. The modified Stern-

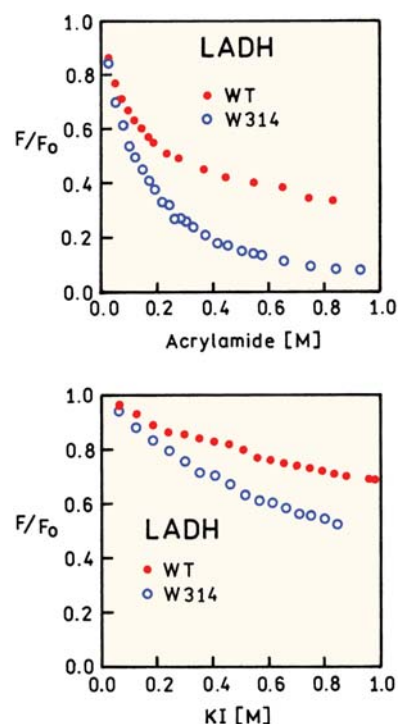


Figure 16.76. Fluorescence intensity of WT-LADH and the W314L tryptophan mutant in the presence of acrylamide and iodide. Revised from [201].

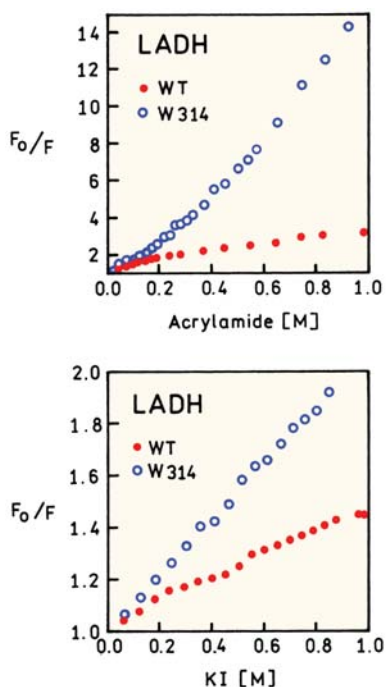


Figure 16.77. Stern-Volmer plots for acrylamide and iodide quenching of WT-LADH and the W314L tryptophan mutant.

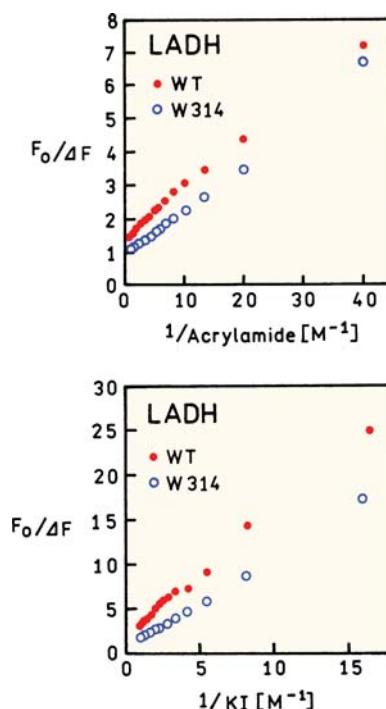


Figure 16.78. Modified Stern-Volmer plots for iodide and acrylamide quenching of WT-LADH and the W314L tryptophan mutant.

Volmer plots in Figure 16.78 suggest a somewhat higher y-axis intercept for the WT protein than for W314L. A higher y-axis intercept indicates a larger fraction of fluorescence that is not accessible to quenchers, which in the case of the WT protein is W15.

CHAPTER 17

A17.1. The activation energy for any process can be calculated by plotting the logarithm of the rate constant (k) versus the inverse of the temperature in degrees Kelvin. For an anisotropy decay the rotational rate (R) is related to the rotational correlation time (θ) by $\theta = (6R)^{-1}$. The plot of $\ln(6R)$ versus $(EK)^{-1}$ is shown in Figure 17.49. The activation energy can be calculated from the Arrhenius equation:¹⁴⁸

$$\ln(k) = \ln(6R) = -\frac{E_A}{R_g} + \ln A \quad (17.4)$$

where A is a constant of integration and R_g is the gas constant. This equation is simply an expression that

the rate of a process depends on a frequency factor and the energy needed to pass over an energy barrier:

$$k = A \exp(-E_A/RT) \quad (17.5)$$

From this analysis (Figure 17.49) one finds $E_A = 6.178$ kcal/mole, which is typical for rotational diffusion of proteins in water. Also, this value is comparable to the activation energy for the temperature-dependent viscosity of water, $E_A = 4.18$ kcal/mole.

The steady-state anisotropy for RNase T₁ at each temperature can be calculated from the Perrin equation

$$r = \frac{r_0}{1 + \tau/\theta} \quad (17.6)$$

Hence the values are expected to be 0.151, 0.137, 0.128, 0.114, and 0.104, in order of increasing temperature from -1.5 to 44.4°C in Table 17.7.

A17.2. The cone angle for tryptophan rotational freedom can be calculated from the ratio of the anisotropy amplitude associated with the long correlation time, to the

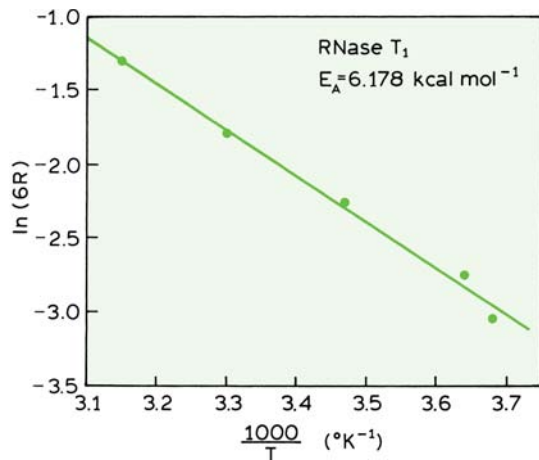


Figure 17.49. Arrhenius plot for the rotational correlation times of RNase T₁. Data from [54].

total anisotropy. The fractional contribution of the long correlation time (t_L) is given by

$$f_L = \frac{r_{01}}{r_{01} + r_{02}} \quad (17.7)$$

This fraction can be related to the displacement of the transition dipole according to the definition of anisotropy:

$$\cos^2 \beta = \frac{2f_L + 1}{3} \quad (17.8)$$

Alternatively, this fraction can be related to the angle (θ_c) through which the tryptophan rotates before striking an energy barrier:

$$f_L = \left[\frac{1}{2} \cos \theta_c (1 + \cos \theta_c) \right]^2 \quad (17.9)$$

Application of these expressions to the data in Table 17.4 yields the following results in Table 17.9.

- A17.3. The time-zero anisotropy, $r(0)$, for RNase T₁ in Table 17.7 is derived from the time-domain data and is lower than from other reports. One possible origin of the difference is the shorter excitation wavelength (295 nm) for the time-domain data and the possibility of a small error in the reported excitation wavelength. Another difference is that $r(0)$ was a variable parameter in the analysis of the time-domain data. It is possible that a short component in the anisotropy decay was missed by limited time resolution, as suggested by molecular dynamics simulations or RNase T₁.¹⁴⁹
- A17.4. A. The intensity decays more slowly at longer emission wavelengths. This indicates that the mean decay time is increasing. In this case the effect is due to an increasing fractional contribution of the long-lived component (9.8 ns).
- B. The decay-associated spectra are calculated using the data in Table 17.8 and eq. 17.3, resulting in the DAS shown in Figure 17.50. In order to interpret the DAS one has to assume that each decay time (3.8 or 9.8 ns) is associated with one of the tryptophan residues. Using this assumption the 3.8 ns decay time is associated with a blue-shifted emission and a lower quantum yield than the red-shifted 9.8 ns residue.
- C. The most rigorous way to confirm assignment of the DAS is to create the single tryptophan mutants. Each mutant should display one of the calculated DAS. One could also use quenching by iodide or acrylamide with the two tryptophan

Table 17.9. Angular Freedom of NATA and Tryptophan Residues in Single-Tryptophan Peptides and Proteins at 20°C

Proteins	$r_0 = r_{01} + r_{02}$	f_L	β (deg)	θ_c (deg)
RNase T ₁ , 20°C	0.310	1.00	0.0	0.0
Staph. nuclease	0.321	0.944	11.1	11.2
Monellin	0.315	0.768	23.2	23.8
ACTH	0.308	0.386	39.8	43.8
Gly-trp-gly	0.325	0.323	42.2	47.3
NATA	0.323	1.00	0.00	0.00
Melittin monomer	0.323	0.421	38.4	41.9
Melittin tetramer	0.326	0.638	29.4	30.8

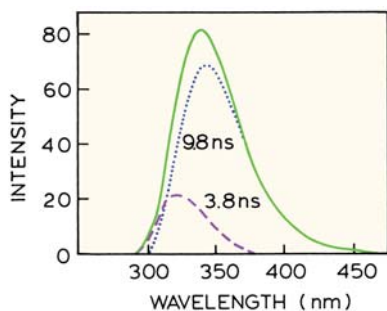


Figure 17.50. Decay-associated spectra calculated from Table 17.7. Data from [147].

wild type protein. In this case one expects the 9.8-ns emission to be more sensitive to quenching given its longer lifetime and higher exposure to the aqueous phase. The emission spectra could also be resolved by the quenching-resolved method.

- A17.5. The Förster distance for any given value of κ^2 can be calculated using

$$R_0(\text{in } \text{Å}) = 9.78 \times 10^3 [\kappa^2 n^{-4} Q_D J(\lambda)]^{1/6} \quad (17.10)$$

Using this expression the Förster distance is 35.1 Å for $\kappa^2 = 2/3$ and 42.2 Å for $\kappa^2 = 2$. Since the crystal structure shows $\kappa^2 = 2$, the R_0 value of 42.2 Å should be used to calculate the tryptophan-to-heme distance. This distance r can be calculated using the transfer efficiency (E) and R_0 values from

$$E = \frac{R_0^6}{R_0^6 + r^6} \quad (17.11)$$

For a transfer efficiency of 97% the distance is $r = 23.6$ Å using $R_0 = 42.2$ Å. If the value of $R_0 = 35.1$ Å is used, then $r = 19.7$ Å. The trp-to-heme distance¹⁰⁶ from the crystal structure is 17.2 Å. Even though the crystal structure shows $\kappa^2 = 2$, the calculated distance is in better agreement with the structure using $\kappa^2 = 2/3$.

CHAPTER 18

- A18.1. The anisotropy of DPPS is higher for two-photon excitation because of $\cos^4 \theta$ photoselection. The ratio of the two- to one-photon anisotropies is near 1.39,

which is close to the predicted values for parallel transitions: 1.425 (Section 18.5).

The anisotropy is independent of temperature because the lifetime decreases with increasing temperature. The decrease in lifetime offsets the decrease in correlation time, resulting in a constant anisotropy.

- A18.2. The output of mode-locked dye lasers is usually cavity dumped by a device inside the laser cavity. During the time periods between dumping, power builds up in the optical cavity and the average power does not decrease much as the repetition rate is decreased. The repetition rate of a Ti:sapphire laser is usually reduced using a pulse picker that is outside the cavity. The extra pulses are discarded and there is no buildup of power in the cavity between picking. The average power drop is proportional to the decreased repetition rate. For this reason Ti:sapphire lasers are usually used without pulse pickers with an 80-MHz repetition rate. The FD data in Figure 18.17 were obtained using the harmonic content of the 80-MHz pulse train so that only a limited number of frequencies were measured (Chapter 5).

- A18.3. Release of calcium in the cell results in increased energy transfer in the cameleon. When energy transfer increases the donor intensity at the shorter wavelength (480 nm) decreases relative to the acceptor intensity at 535 nm. Hence the ratio becomes larger, which is shown on the scale as the red color.

CHAPTER 19

- A19.1. The lifetimes can be calculated using $\tan \phi = \omega \tau$. From Figure 19.13 the phase angles at 0 and 20.55% oxygen are 48 and 15°, respectively. Recalling the frequency $\omega = 2\pi\nu$, the respective lifetimes are 45.2 and 10.9 μs.
- A19.2. The data in Figure 19.80 can be used to determine the lifetimes of camphorquinone in PMMA at various partial pressures of oxygen. These values can be used to construct a lifetime Stern-Volmer plot (Figure 19.83). The oxygen bimolecular quenching constant is near $2.8 \times 10^6 \text{ M}^{-1} \text{ s}^{-1}$, which is nearly 10^4 smaller than that for oxygen in water. This suggests a low diffusion coefficient of oxygen in PMMA of about $7 \times 10^{-9} \text{ cm}^2/\text{s}$. Of course, the accuracy of these values depends on the assumed oxygen solubility in PMMA.
- A19.3. Careful examination of Figure 19.9 reveals that $[\text{Ru}(\text{Ph}_2\text{phen})_3]^{2+}$ is quenched tenfold at 30 torr oxy-

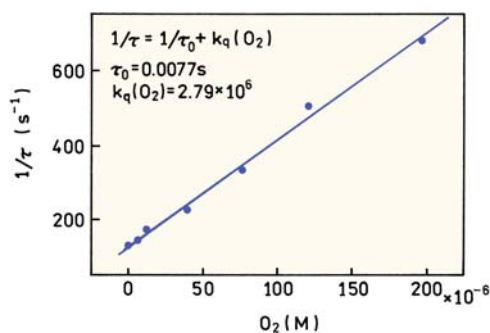


Figure 19.83. Stern-Volmer plot for oxygen quenching of camphorquinone in PMMA. Data from [308].

gen. The Stern-Volmer quenching constant is proportional to the lifetime, which is near 5 μ s. Hence for the 5-ns probe $F_0/F = 1.009$ at this same oxygen pressure. At the highest oxygen pressure of 80 torr, the short-lifetime probe will be quenched less than 3%. This extent of quenching is negligible, so the 5-ns probe can serve as an intensity reference.

- A19.4. The spectra in Figure 19.81 show that the absorption of TB decreases with decreasing pH. The high-pH form of TB is the acceptor for SR101. As the percentage of CO_2 increases the pH of the polymer matrix decreases. This results in a decreased absorbance of TB, less RET from SR101 to TB, and an increase in the apparent lifetime. The increases in apparent lifetime result in the larger phase angle with 2% CO_2 . The apparent lifetimes of 0 and 2% CO_2 are 0.35 and 1.24 ns, respectively.
- A19.5. A. The range of anisotropies can be calculated from the Perrin equation

$$r = \frac{r_0}{1 + (\tau/\theta)} \quad (19.15)$$

The anisotropy of the free peptide will be 0.080, and the anisotropy of Ab-FI-P will be 0.385.

- B. The anisotropies are additive (e.g., 19.14). Hence the anisotropy with 10% free FI-P is given by

$$r = 0.10(0.08) + 0.90(0.385) = 0.355 \quad (19.16)$$

- C. Displacement of FI-P from Rh-Ab will result in a tenfold increase in the intensity of FI-P due to elimination of RET. For such cases, the fraction-

al intensity of the free and bound forms are given by

$$f_F = \frac{m_F q_F}{m_F q_F + m_B q_B} \quad (19.17)$$

$$f_B = \frac{m_B q_B}{m_F q_F + m_B q_B} \quad (19.18)$$

where m_i are the molecular fractions in the free or bound state, and q_i are the quantum yields. If $q_F = 10q_B$, then

$$f_F = \frac{10m_F}{10m_F + m_B} \quad (19.19)$$

For a molecular fraction of 10%, $f_F = 0.53$. Hence 10% displacement of FI-P results in over 50% of the emission from the free peptide. The anisotropy is

$$r = 0.53(0.08) + 0.47(0.40) = 0.230 \quad (19.20)$$

and is seen to decrease more rapidly with displacement of FI-P. We used 0.40 for the anisotropy of the bound form because RET will decrease the lifetime of the fluorescein to 0.40 ns.

CHAPTER 20

- A20.1. A. The decay time can be calculated from the slope of the long-lifetime component using any two points. For instance, extrapolating the long decay time to zero, the intensities of this component at $t = 0$ and $t = 500$ ns in Figure 20.50 are near 2000 and 600, respectively. For a single-exponential decay the intensities at two points in time are related by $\ln I(t_1) - \ln I(t_2) = -t_1/\tau + t_2/\tau$. Insertion of the values at $t = 0$ and $t = 500$ ns yields $\tau = 415$ ns.
- B. $\alpha_1 = 0.962$, $\alpha_2 = 0.038$. These values are from Figure 20.50, following normalization of α_1 and $\alpha_2 = 1.0$.
- C. $f_1 = 0.296$, $f_2 = 0.704$.

- D. $f_1 = 0.0004$, $f_2 = 0.9996$. This result shows that off-gating essentially eliminates the short-lived component, decreasing its fractional contribution from 0.296 to 0.0004.
- A20.2. The oxygen bimolecular quenching constant can be calculated using the decay times in the absence and in the presence of 100% oxygen. The value of $\tau_o/\tau = 16.3 = 1 + k_q\tau_o[\text{O}_2]$. Using $[\text{O}_2] = 0.001275 \text{ M}$ and $\tau_o = 3.7 \mu\text{s}$ one obtains $k_q = 3.24 \times 10^9 \text{ M}^{-1} \text{ s}^{-1}$. This value is reasonably close to the diffusion-controlled limit and indicates that the quenching by oxygen is highly efficient.

CHAPTER 21

- A21.1. To answer this question we need to design quenching or anisotropy measurements that could potentially be used for sequencing. Consider sequencing with four fluorescent ddNTPs. The Stern-Volmer quenching constants could be different due to either different lifetimes or different accessibilities to the collisional quencher. Then the sequence could be determined by the quenching constant for each fluorescent band on the gel. Determination of the quenching constant requires a minimum of two intensity measurements: in the absence of quencher and in the presence of a known concentration of quencher. Although such measurements are possible, the use of two samples to measure a single base is too complicated for large-scale sequencing of DNA.

Suppose that the sequencing reaction is performed with a single fluorescent primer. Because anisotropy measurements depend on molecular weight, in principle each oligonucleotide will display a different anisotropy. In practice the anisotropies for DNA oligomers, differing by a single base pair, are likely to be too similar in magnitude for useful distinction between oligomers. If the adjacent base pair changes the lifetime of the labeled oligomer, then the anisotropy measurements may be able to identify the base.

Consider the use of four fluorescent ddNTPs, each with a different lifetime. In this case the anisotropy would be different for each base pair, and the anisotropy measurement could be used to identify the base. This approach is more likely to succeed for longer oligomers, where the anisotropy will become

mostly independent of molecular weight. For shorter oligomers the anisotropy will depend on the fragment length.

CHAPTER 22

- A22.1. In Figure 22.15 it is clear that the F-actin is red and the green color is where the mitochondria are expected to be localized. In Figure 22.19 the colors are reversed: F-actin is green and mitochondria are red. At first glance it appears that the legend for one of the figures is incorrect, or that the cells in Figure 22.15 were labeled with fluorophores that stained actin red and mitochondria green. The legends are correct. Both images are created using pseudocolors. Figure 22.19 was created by an overlay of three intensity images. The color of each image was assigned to be similar to the emission maxima of the probes: DAPI is blue, Bodipy-FL is green, and MitoTracker is red. These assignments give the impression that Figure 22.19 is a real color image. In Figure 22.15 the colors were assigned according to lifetime. The lifetime in the nucleus was assigned a blue color, which agrees with Figure 22.19. However, in Figure 22.15 the lifetime of F-actin was assigned to be red, and the lifetime of MitoTracker was assigned to be green. The pseudocolor assignments of the red- and green-emitting fluorophores are opposite in Figures 22.15 and 22.19.

CHAPTER 23

- A23.1. The intensity needed to excite the fluorophore can be calculated using eq. 23.5. If there is no intersystem crossing than $S_1 = \tau\sigma I_e S_T$. The intensity required is given by $S_1/S_T = 0.5 \tau\sigma I_e$. The cross-section for absorption can be calculated using eq 23.1, yielding $\sigma = 4 \times 10^{-16} = 4 \text{ \AA}^2$. In performing this calculation it is important to use a conversion factor of $10^3 \text{ cm}^2/\text{liter}$.

The number of photons per cm^2 per second can be calculated from $I_e = 0.5 (\tau\sigma)^{-1} = 3.1 \times 10^{23}/\text{cm}^2 \text{ s}$. The power can be calculated from the number of photons per second per cm^2 and the energy per photon $= h\nu/\lambda$, yielding $103 \text{ kW}/\text{cm}^2$, and an area of $1 \mu\text{m}^2 = 10^{-8} \text{ cm}^2$, so the power needed to saturate the fluorophore is $0.001 \text{ watts}/\text{cm}^2$.

CHAPTER 24

A24.1. Figure 24.8 gives the concentration of R6G and the inverses of the $\tau = 0$ intercept give the apparent number of fluorophores. Using $G(0) = 0.12$ at 1.25 nM yields $N = 8.3$ molecules. The volume can be calculated from

$$V_{\text{eff}} = N/\bar{C}N_A$$

where N_A is Avogadro's number, yielding $V_{\text{eff}} = 11.0$ fl. The effective volume is related to the dimensions by $V_{\text{eff}} = \pi^{3/2} s^2 u$, which becomes $V_{\text{eff}} = 4\pi^{3/2} s^3$ for the assumed u/s ratio. Recalling that 10^3 liters = 1 cubic meter, one finds $s = 0.79$ μm and $u = 3.16$ μm .

A24.2. The ratio of the diffusion times can be read off the graph. Taking the maximum difference near $G(\tau) = 0.35$, one finds $\tau_D(\text{GroEL})/\tau_D(\alpha\text{-LA}) = 0.4/0.15 = 2.7$, which indicates a $3^3 = 19.7$ -fold increase in molecular weight. This is somewhat less than the expected value of 49.4 from the ratio of the molecular weight. One possible explanation is the diffusion coefficient of denatured $\alpha\text{-LA}$ is lower than for the native protein, causing the τ_D ratio to be lower than expected.

24.3. If we know the diffusion coefficient the time can be calculated without knowing the beam diameter. The time required to diffuse 10 μm can be calculated using $\Delta x^2 = 2D\tau$, where Δx is the distance. Using $D = 3 \times 10^{-8}$ cm^2/s and recalling that 10^4 $\text{cm}^2 = 1$ m^2 , one finds $\tau = 16.7$ s. The time required to diffuse 10 μm does not depend on the beam diameter, so τ is the same for a 1- or 2- μm diameter beam.

A24.4. The autocorrelation function yields the relaxation time for the opening-closing reaction, which is $\tau_R = (k_1 + k_2)^{-1}$. The equilibrium constant is given by $K = k_1/k_2$. The values of K can be determined by examining the fluorescence intensity of the beacon as a function of temperature. The fractional intensity between the low- and high-temperature intensities yields the fraction of the beacon that is open at the temperature used to collect $G(\tau)$. This fraction yields the equilibrium constant K , allowing k_1 and k_2 to be calculated.

A24.5. The volume in the TIR FCS experiment can be estimated using $V = \pi s^2 d$. The volume is 1.96 fl. The concentration needed is given by

$$\bar{C} = N/VN_A$$

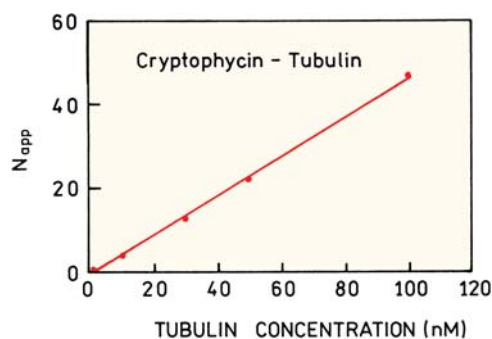


Figure 24.51. Effect of sample dilution on the apparent number of diffusing tubulin particles. Revised and reprinted with permission from [38]. Copyright © 2003, American Chemical Society.

where N_A is Avogadro's number, and

$$\bar{C} = 8.5 \text{ nM}$$

The area occupied by a single lipid molecule is 0.7 nm^2 . The area of the illuminated membrane is 19.6 $\mu\text{m}^2 = 19.6 \times 10^6$ nm^2 . Hence to obtain 10 fluorophores in the illuminated area the fraction of labeled fluorophores should be 7.3×10^{-7} , or approximately 1 labeled lipid per 1,372,000 unlabeled lipid molecules.

A24.6. The effect of dilution on the self-association of tubulin can be determined in two ways. If the tubulin complex dissociates upon dilution then the diffusion coefficient will decrease and the autocorrelation curves shift to shorter times. Because of the change in amplitude the presence or absence of a shift cannot be seen in Figure 24.50.

Another way to determine if the complex dissociates is from the apparent number of diffusing molecules. If all the substrates are labeled, dissociation will result in a higher value of N_{app} . Figure 24.51 shows a plot of N_{app} versus total tubulin concentration. N_{app} scales linearly with concentration, showing the complexes do not dissociate. This approach is only valid if all the tubulin is labeled. If there was only one labeled tubulin per complex then dissociation would not increase N_{app} but the diffusion coefficient would change.

CHAPTER 25

A25.1. The radiative decay rate in the absence of SIF can be calculated from the quantum yield and natural lifetime

τ_N . Since $\Gamma = \tau_N^{-1}$, then $\Gamma = 2.5 \times 10^8 \text{ s}^{-1}$. Using the definition of the quantum yield in eq. 25.1 the non-radiative decay rate is given by

$$k_{nr} = \frac{\Gamma - Q_O \Gamma}{Q_O} = 122.5 \times 10^8 \text{ s}^{-1} \quad (25.5)$$

This value of k_{nr} is reasonable because k_{nr} must be significantly larger than Γ to account for the low value of $Q_O = 0.02$.

In the presence of SIF the quantum yield increases 4.8-fold to $Q_m = 0.096$. This quantum yield is related to the total decay rate by

$$Q_m = \frac{\Gamma_T}{\Gamma_T + k_{nr}} \quad (25.6)$$

so that

$$\Gamma_T = \frac{Q_m k_{nr}}{1 - Q_m} = 1.3 \times 10^9 \text{ s}^{-1} \quad (25.7)$$

The radiative decay rate due to the metal is given by $\Gamma_m = \Gamma_T - \Gamma = 1.05 \times 10^9 \text{ s}^{-1}$. Hence $\Gamma_m/\Gamma = 4.7$.

If only 10% of the Rose Bengal is affected, then the apparent quantum yield (Q_A) is related to the quantum yield near the SIF and in solution as

$$Q_A = 0.90Q_O + 0.10Q_m \quad (25.8)$$

Using $Q_A = 0.096$, then $Q_m = 0.78$. The value of Γ_T can be calculated from eq. 25.7, so that $\Gamma_T = 4.34 \times 10^{10} \text{ s}^{-1}$, and then $\Gamma_m = 4.32 \times 10^{10} \text{ s}^{-1}$. If only 10% of the RB population is affected by the SIF, then $\Gamma_m/\Gamma = 173$.

Index

A

- Absorption spectroscopy, 12
- Acetate quenching, 535
- Acetoxymethyl esters, 647, 648
- 2-Acetylanthracene (2-AA), 214–215
- N-Acetyl-L-tryptophanamide. *See* NATA (N-acetyl-L-tryptophanamide)
- N-Acetyl-L-tyrosinamide (NATyrA). *See* NATyrA
- N-Acetyl tryptamine, 314
- Acoustooptic (AO) crystal, 110, 112
- Acoustooptic (AO) modulators, 165
- Acoustooptic deflector, laser, 111–112
- Acridine
 - DNA technology, 716–717
 - excited-state reactions, 260, 267–268
- Acridine orange, 2, 3, 514–515
- Acriflavine, 190, 191
- Acrylamide quenching, 278–279, 284–286, 287, 290, 292–293, 313, 336
 - absorption spectra, 301
 - bimolecular quenching constants, 281–282
 - covalent adduct formation, 314
 - intensity decays, 346
 - NATA, 285, 346, 347
 - proteins, 547
 - DNA β helicase hexamer, 313
 - metalloprotease, 550–551
 - single-tryptophan, 547, 548
 - tryptophan position and, 550
 - quenching efficiency, 281
 - quenching-resolved spectra, 302
 - structural motifs and tryptophan spectral properties, 561–562, 563
 - transient effects, 346–347
- Acrylodan, 70, 217, 226
- Actin, 784
- 1-Adamantanol, 228
- Adduct formation, intramolecular quenching, 314
- Adenine and derivatives, 16, 278, 287–288
 - Förster distances, 468
- Adenosine monophosphate, 16
- Adenylate kinase, 823
- ADMAN, 230
- ϵ -ADP, 313
- Adrenocorticotropin (ACTH), 536, 547
- Adrenodoxin (AD), 561
- Aequorea victoria*, 81, 82
- Aladan-GB1, 245
- Alcohol dehydrogenase, 395, 584
- Alcohols, dielectric relaxation times, 250–251
- Alexa 488
- Alexa 546, 459
- Alexa Fluor, 69, 70–71
- Alkaline phosphatase, 318
- Alkylaminoanthracene derivatives, phosphate sensors, 643
- N-Alkyl pyridinium, 278
- Allophycocyanin, 84, 468
- Alpha helices, 561–562, 563
- Aluminum, 868
- Alzheimer's disease, 827
 - aggregation of β -amyloid peptides, 515–516
 - fluorescence-lifetime imaging microscopy, 750
 - time-resolved RET imaging, 498
- Amines, 316
 - fluorogenic probes, 79
 - quenching, 278, 279, 314, 642
- Amino acids
 - genetically inserted, 565–566
 - phosphorescence quenching, 318
 - time-resolved emission spectra (TRES), 244–245
- 9-Aminoacridine, 434
- Aminoacyl-tRNA synthetase, 565
- 3-Aminofluoranthene (AFA), 190, 191
- 3-Amino-N-methylphthalimide, 257
- 4-Aminophthalimide (4-AP), 240
- 2-Aminopurine, 75, 76
 - frequency-domain lifetime measurements, 180–185
 - mixture lifetime resolution, 138–141
 - time-domain lifetime measurements, 137–138
- Ammonium group, 579
- Amphiphilic starlike macromolecules (ASM), 253
- Amplifiers, 115
- Amplitude-weighted lifetime, 142
- β -Amyloid peptides, energy transfer, 515–516
- Amyloid plaques, fluorescence-lifetime imaging microscopy, 750
- Amyloid proteins, 827
- Analog-to-digital converter (ADC), 105, 115, 122
- Analyte recognition probes, 78–79, 643–650. *See also* specific elements
 - calcium and magnesium, 647–650
 - cation probe specificity, 644
 - intracellular zinc, 650
 - sodium and potassium, 645–647
 - theory of, 644–645
- 2-Anilinoanthracene (2-AN), 213–214, 216, 242
- 1-Anilinoanthracene-8-sulfonic acid. *See* ANS (1,8-anilinoanthracene-8-sulfonic acid)
- 8-Anilinoanthracene-1-sulfonic acid (8-ANS). *See* 8,1-ANS
- Anion indicators, 16–17
- Anion sensors, 641–643. *See also* Chloride probes
 - chloride, 631–632
 - oxygen, 627–630

- Anisotropy, 353–378
- applications, 20–21
 - biochemical applications, 372–374
 - helicase-catalyzed DNA unwinding, 373–374
 - melittin association detected from homotransfer, 374
 - peptide binding to calmodulin, 372–373
 - trp repressor binding to DNA, 373
 - definition, 353–355
 - electronic state resolution from polarization spectra, 360–361
 - emission wavelength and, 437–438
 - energy transfer, 453
 - excitation anisotropy spectra, 358–361, 531–533
 - excitation photoselection of fluorophores, 357–358
 - instrumentation, 36–37
 - lifetime-resolved, 435–436
 - measurement, 361–366
 - comparison of methods, 363–364
 - depolarization, trivial causes, 365–366
 - factors affecting anisotropy, 366
 - L-format or single channel method, 361–363
 - magic-angle polarizer conditions, 364
 - polarizer alignment, 364
 - resonance energy-transfer effects, 364–365
 - T-format or two-channel method, 363–364
 - total intensity, 364
 - membranes and membrane-bound proteins, 374–377
 - distribution, 375–377
 - membrane microviscosity, 374–375
 - metal–ligand complexes, 685, 688–689
 - multiphoton excitation, 612–613, 615
 - excitation photoselection for two-photon excitation, 612
 - two-photon anisotropy for DPH, 612–613
 - Perrin equation, rotational diffusion effects, 366–370
 - examples of Perrin plots, 369–370
 - rotational motions of proteins, 367–369
 - Perrin plots
 - of proteins, 370–372
 - segmental motion effects, 436
 - photoselection, 357–358
 - polarization, molecular information from fluorescence, 19
 - principles, 12–13
 - proteins
 - association reactions, 372–374
 - Perrin plots, 370–372
 - rotational motion, 102–103
 - segmented motions, 436
 - single-molecule detection, 775–776
 - Soleillet's rule, depolarization factor multiplication, 436–437
 - theory, 355–358
 - transition moments, 377–378
 - tryptophan, 531–532
- Anisotropy, advanced concepts, 413–438
- associated anisotropy decay, 413–417
 - theory, 414–415
 - time-domain measurements, 415–417
 - biochemical examples, 417–419
 - frequency-domain measurements, 417–418
 - time-domain studies of DNA binding to Klenow fragment, 417
 - DNA, 432–433
 - ellipsoids, anisotropy decay, 419–420
 - ellipsoids of revolution, 420–425
 - oblate, intuitive description of, 422–423
 - rotational correction times, 423–425
 - simplified, 421–422
 - stick vs. slip rotational diffusion, 425
 - global anisotropy decay analysis, 429–432
 - with collisional quenching, 430–431
 - with multi-wavelength excitation, 429–430
 - quenching application to protein anisotropy decays, 431–432
 - planar fluorophores with high symmetry, 435
 - rotational diffusion
 - of ellipsoids, theory, 425–426
 - frequency-domain studies of, 427–429
 - of non-spherical molecules, 418–419
 - time-domain studies, 426–427
 - transition moments, 433–435
- Anisotropy decay laws, 390–394
- associated delays, 393
 - correlation time distributions, 393
 - hindered rotors, 391–392
 - non-spherical fluorophores, 391
 - segmental mobility of biopolymer-bound fluorophore, 392–393
- Anisotropy decays, 14, 102–103, 413–417
- energy transfer, 453
 - in frequency domain, 588–589
 - melittin, 590–591
 - proteins, 587–588, 589–591
 - ribonuclease T₁, 584–585
- Anisotropy decays, time-dependent, 383–409
- analysis, 387–389
 - frequency-domain decays, 390
 - r_0 value, 389
 - time-domain decays, 387–389
 - correlation time imaging, 406–408
 - laws governing, 390–394
 - associated decays, 393
 - correlation time distributions, 393
 - decays of rhodamine green and rhodamine green-dextran, 394
 - hindered rotors, 391–392
 - non-spherical fluorophores, 391
 - segmental mobility of biopolymer-bound fluorophore, 392–393
 - membrane probe, characterization of, 401–402
 - membranes, hindered rotational diffusion in, 399–402
 - microsecond, 408–409
 - long-lifetime metal–ligand complexes, 408–409
 - phosphorescence, 408
 - nucleic acids, 402–406
 - DNA binding to HIV integrase, 404–406
 - DNA oligomer hydrodynamics, 403
 - intracellular DNA dynamics, 403–404
 - proteins, frequency-domain decays of, 383–387, 397–399
 - apomyoglobin, rigid rotor, 397–398
 - melittin, 398
 - oxytocin, picosecond rotational diffusion, 399
 - proteins, time-domain decays of, 383–387, 394–397
 - alcohol dehydrogenase, 395
 - domain motions of immunoglobulins, 396–397
 - free probe, effects of, 397
 - phospholipase A₂, 395
 - Subtilisin Carlsberg, 395–396
- Anisotropy fluorescence correlation spectroscopy, 829
- Anisotropy polarization, 624–625
- molecular information from fluorescence, 19
- Anisotropy spectra, excitation, 358–361, 531–533
- Annexins, 148
- Annexin V, 148, 585–587

- ANS
 time-resolved fluorescence correlation spectroscopy, 819
- 8,1-ANS (8-anilino-1-naphthalenesulfonate), 226–227, 258
- ANS (1-anilino-naphthalene-6-sulfonic acid), 71–72
- ANS (1-anilino-naphthalene-8-sulfonic acid)
 anisotropy decay, 417–418
 red-edge excitation, 258
 solvent effects, 212
- 6-ANS (6-anilino-naphthalene-2-sulfonic acid), 230
 Förster distances, 468
- ANS derivatives, solvent effects, 212
- Anthracene, 3, 56, 59, 316, 632
 emission spectrum, 9, 199
 frequency-domain lifetime measurements, 170–171
 orientation factor, 465
 quenchers of, 278, 279
 TRES and DAS comparison, 255
- Anthranilic acid
 frequency-domain lifetime measurements, 180–185
 mixture lifetime resolution, 138–141
 time-domain lifetime measurements, 137–138
- 9-Anthroxycholine (9-AC), 226–227
- Anthroyl fatty acid, 72
- Anthroyloxy fatty acids, 279
 9-AS, 359–360
 12-AS, 360, 375
 Förster distances, 468
 solvent relaxation, 248–249
 TRES, 248–249
- 12-Anthroyloxy stearate, 375
- 9-Anthroyloxy stearic acid, 359–360, 369
- Anthroylxanthy cations, quenchers of, 279
- Antibody labeling, 69
- APC (allophycocyanin)
 Förster distances, 468
- Apoazurin, 546–547, 583–584
- Apo E3, 454–455
- Apo E4, 454–455
- Apolipoproteins, 454
- Apomyoglobin, 17, 368, 417–418, 549
 anisotropy decay, 397–398
 protein folding, 560
 time-resolved emission spectra (TRES), 243–244
- Apoperoxidase, 368
- Apparent distance distributions, 478–480
- Apparent phase and modulation lifetimes, 191–192, 266–267
- Aptamers, 724–726
- APTRA, 644, 649
- Archaeobacterial histone-like protein (HTa), 544–545
- Arc lamps, 28, 31, 33
- Argon-hydrogen flashlamps, 113–114
- Argon-ion lasers, 39, 109, 110–111, 715–716
- Aromatic amino acids, 314. *See also* Phenylalanine; Tryptophan;
 Tyrosine
 fluorescence parameters of, 64
 intensity decays, 578
 quantum yield standards, 54
 spectral properties, 530–535
- Arrays
 DNA, 732–734
 multiplexed microbead:suspension, 726–728
- Arsine ligand, 693
- 9-Arylxanthy cations, 279
- 9-AS, 359–360
- 12-AS, 360, 375
- Asparaginase, 548
- Associated anisotropy decays, 393, 413–417
- Association constant, 282
- Association reactions
 anisotropy, 372–374
 helicase-catalyzed DNA unwinding, 373–374
 melittin association detected from homotransfer, 374
 peptide-calmodulin binding, 372–373
 Tip repressor-DNA binding, 373
 calmodulin, tryptophan mutants, calcium binding site resolution, 552
 energy transfer, 455–456
 literature references, 837
 orientation of bound peptide, 456–457
 Prodan effects on emission spectra, 217–219
 quenching, 304–305
 accessibility to quenchers, 312–313
 substrate binding to ribozymes, 311–312
 specific binding reactions, 304–305
- Asymptotic standard errors (ASEs), 134–135, 163, 180
- ATP, 455
- ATPase, single-molecule activity, 770–771
- Autocorrelation function, 132–133
- Autocorrelation function of fluorescence fluctuations, 800–802,
 804–805, 810–811, 813
- Avalanche photodiodes (APDs), 114
- Avidin, 450, 676
- 7AW, 564, 565
- Azacrown, 79
- Azacrown ethers, 644
- Azide, 348
- Azurin, 536, 546, 547, 583, 588
 emission spectra of molecules with one or two tryptophan, 539
 fluorescence studies of, 538
 site-directed mutagenesis of single-tryptophan, 538–539
- ## B
- BABAPH, 253–255
- BABP, 253–255
- Background signal, 366
- Bandpass filters, 39
- BAPTA, 79, 644, 647–648
- BAPTA-based probes, 648–649
- Barnase, 556–557
 decay-associated spectra, 591–592
- β -Barrel, 538
- BCECF, 751
- Bead sensors, 656
- Beam splitter, 29, 777
- Beer-Lambert law, deviation from, 58–59
- Beer's law, deviation from, 59
- Benzene, 230
 quenching of indole, 537
- Benzobenzofluoranthene, 632
- Benzodiazepines, 23
- 5,6-Benzoquinoline, 279
- Bialkali photocathode, 45–46
- Bilins, 84
- Bimolecular quenching, 281–282, 294, 304, 547–549
- Bimolecular quenching constant, 339
- Binding. *See* Association reactions

- Bioaffinity reactions, 807–810
- Biomembranes
- fluorescence correlation spectroscopy, 810–815
 - binding to membrane-bound receptors, 813–815
 - lateral diffusion, 812–813
 - literature references, 838
- Biomolecules
- anisotropy, 372–374
 - peptide binding to calmodulin, 372–373
 - co-localization of, literature references, 791
 - diffusion of, literature references, 791–792
 - energy transfer (*See* Energy transfer)
 - fluorophores, principles, 15–17, 20–21 (*See also* Fluorophores)
 - frequency-domain lifetime measurements, 177, 186–189
 - DNA, DAPI-labeled, 186–187
 - fluorescence microscopy with LED light source, 189
 - gigahertz data, 177–178
 - green fluorescent protein, one- and two-photon excitation, 171
 - Mag-Quin-2, magnesium probe, 187–188
 - melittin lifetime distributions, cross fitting of models, 188–189
 - NADH intensity decay, 172
 - recovery of lifetime distributions from data, 188
 - SPQ, collisional quenching, 171–172
 - staphylococcal nuclease and melittin multi-exponential decay, 171
 - laser scanning microscopy, 750
 - photoinduced electron transfer quenching, 341–342
 - polarization, literature references, 794
 - quenching
 - effects of quenchers on proteins, 292
 - ethenoadenine derivatives, 287–288
 - substrate binding to ribozymes, 311–312
 - Tet repressor, 302–304
 - single-molecule detection, 757–788
 - ATPase activity, 770–771
 - calcium sensor, 784
 - chaperonin protein, 771–773
 - conformational dynamics of Holliday junction, 782–783
 - enzyme kinetics, 770
 - molecular beacons, 782
 - motions of molecular motors, 784
 - turnover of single enzyme molecules, 780–782
 - single-molecule detection, time-resolved studies, 779–780
 - solvent effects on emission spectra
 - calmodulin, hydrophobic surface exposure, 226–227
 - cyclodextrin binding using dansyl probe, 227–228
 - membrane binding site polarity, 206–207
 - with Prodan, 217–219
 - with solvent-sensitive probes, 226–229
 - structural analogs as fluorophores, 80
 - time-domain lifetime measurements
 - chlorophyll, 146–147
 - FAD intensity decay, 147–148
 - multi-exponential or heterogeneous decays of, 101–103
 - single-tryptophan protein, 145
 - time-resolved emission spectra (TRES)
 - analysis, 246–248
 - apomyoglobin, 243–244
 - labeled membranes, 245–249
 - proteins, spectral relaxation in, 242–243
- Biopolymers
- bound fluorophore segmental mobility, 392–393
 - diffusion in, 501
- Biotin, 310
- 2,2'-Bipyridine, 684
- Bis DNA stains, 713–715
- Bis-MSB, 610
- Blood gas sensors
 - energy-transfer mechanisms, 633–634
 - two-state, optical detection of, 637
- Blue-shifted spectra, 538–539, 551
- BODIPY, 69–70, 221
- DNA technology, 710
 - Förster distances, 468
 - homotransfer, 450
- Bodipy-PC, 812–813
- Bodipy TR, 24
- Bombesin, 590
- Boron-containing fluorophores, 651
- Boundary lipid, membranes, 298
- Bound fluorophore segmental mobility, 392–393
- Bovine cardiac troponin I, 589
- Bovine pancreatic trypsin inhibitor (BPTI), 482
- Bovine serum albumin, 71, 584, 589, 678
 - metal-enhanced fluorescence, 851–853
- Bovine spongiform encephalopathy, 827
- BPE (β -phycoerythrin), 468
 - Förster distances, 468
- Brightness of fluorophores, 802–803, 817–819
- Bromate, quenching by, 278–279
- Bromide, 278, 295–296, 631
- Brominated phosphatidylcholines, 295
- Bromine, 5
- Bromobenzene, 278–279
- Bromo-phosphatidylcholine, 295–296, 298, 301
- Brownian rotation, 365
- Butanol, Stokes shift, 210
- C**
- Ca²⁺-ATPase
 - anisotropy decay, 408
 - boundary lipid quenching, 298
- Cadmium, 278
- Cadmium selenide, 675
- Caffeine, 304
- Calcite, 51
- Calcium
 - calmodulin binding using phenylalanine and tyrosine, 545–546
 - calmodulin binding using tryptophan-containing mutants, 552
 - concentration from lifetime, 744–745
 - induced changes in troponin C conformation, 490–493
 - intensity decay, 585–587
 - lanthanides, 679
 - multiphoton microscopy, 616–617
 - single-molecule sensor, 784
- Calcium-binding proteins, 679
- Calcium Green, 79, 616, 645, 648–649, 656
- Calcium sensors, 17, 617, 647–650
 - chelators, 644
 - green fluorescent protein mutant-based, 455–456, 654–655
 - QUIN-2, fluorescence lifetime imaging microscopy, 744–745
- Calibration of monochromators, 38
- Calmodulin, 20, 88–89
 - binding to target protein, 551–552
 - calcium binding site resolution, 552

- calcium binding using phenylalanine and tyrosine, 545–546
- calcium sensors, 617
- energy transfer
 - MLCK binding and, 456–457
 - melittin binding, 485
 - peptide binding anisotropy, 372–373
 - single-molecule calcium sensor, 784
 - solvent effects on emission spectra, 226–227
- Camphorquinones, 672
- Capillary gel electrophoresis, 712
- Carbazole, 632
 - quenchers of, 278–279
- Carbocyanine, 72
- β -Carboline, 53
- Carbon dioxide
 - blood gas measurement, 637
 - energy-transfer mechanisms, 633–634
- Carbon disulfide, 279
- Carbonic anhydrase, 368
- Carboxyfluorescein, 638
- Carboxy groups, quenching by, 279
- Carboxynaphthofluorescein, 641
- Cascade Blue, 727–729
- Cascade Yellow, 70
- Cavity dumper, 111–112
- CCD detectors, 49
- CCVJ, 224
- CD 220, 174
- CD 222, 647
- CDKN1A gene, 733
- Cells
 - labeling with quantum dots, 677–678
 - three-dimensional imaging of, 618–619
- Cellular retinoic acid binding protein I (CRABPI), 560
- Cesium, 278, 279
- C-fos protein, 461
- Chaperonin, 771–773, 806
- Chaperonin GroEL, protein binding, 807
- Charged-coupled device (CCD), 766
- Charge effects, quenching, 286–288
- Charge transfer
 - quenching, 306
 - solvent effects, 219–221
- Charge-transfer complex, 9, 337
- Chelators, 644, 659
 - for lanthanides, 679
- Chemical sensing probes. *See* Analyte recognition probes; specific ions
- Chicken pepsinogen, 597
- Chloride
 - green fluorescent protein, 307–309
 - imaging of, 306–307
 - quenching by, 171–172, 279, 306
- Chloride probes, 17, 67, 306–307, 631–632
- Chlorinated compounds, quenching by, 278–279
- Chlorinated hydrocarbons, 632
- Chloroform, Stokes shift, 210
- Chlorophyll, intensity decay of, 146–147
- Cholesterol, 293–294, 297, 400
 - analogs, 80
- Cholesterol oxidase (Cox), 780, 781
- Chromatin, 403
- Chromophores, 84
- Chymotrypsin, 368
- Clinical chemistry, 19
 - sensors, 623–624
- Coaxial flashlamps, 112–113
- Cobalt, quenching by, 279
- Cocaine, 724
- Cofactors
 - intrinsic fluorescence, 63–64
 - protein binding of NADH, 65–66
 - time-domain lifetime measurement, 147
- Colicin E1 folding, 292–293
- Collection efficiency function, 801
- Collisional frequency, fluorophore-quencher, 281
- Collisional quenching, 11, 277–278, 546
 - anisotropy decay, time-dependent, 430–431
 - combined with static quenching, 282–283
 - DNA probes, 286
 - ethenoadenine–DNA- β helicase hexamer, 313
 - examples, 283–284
 - frequency-domain lifetime measurements, 171
 - relaxation dynamics, 256
 - as sensor mechanisms, 306–309, 627–633
 - chloride, 306–309, 631–632
 - oxygen, 627–630
 - sensors, 626
 - simulated intensity decay, 101–102
 - theory of, 278–282
 - bimolecular quenching constant, interpretation of, 281–282
 - Stern-Volmer equation, derivation of, 280–281
- Colloids
 - interactions with fluorophores, 846–848
 - metal, 845–846
 - in metal-enhanced fluorescence, 856
- Colored-glass filters, 38–39
- Color effects
 - frequency-domain lifetime measurements, 168–169
 - in photomultiplier tubes, 47
 - time-domain lifetime measurements, 119–121
- Combination filters, 40
- Compact PMTs, 118
- Concanavalin A, 634–635
- Confidence intervals
 - frequency-domain lifetime measurements, 179–180
 - resolution of two closed spaced lifetimes, 182
 - time-domain lifetime measurements, 134–135, 136
 - of two widely spaced lifetimes, 179–180
- Confocal detection optics, 761–763
- Conformation, 436, 529
 - changes of, 291–293
 - heterogeneity
 - ribonuclease T_1 , 584–585
 - rotational (*See* Rotamers)
- Conformational distance. *See* Energy transfer, time-resolved
- Conformational dynamics in macromolecules, 820–821
- Constant function discriminator (CFD), 104–106
- Continuous relaxation model, 237
- Continuous spectral relaxation, 237–241, 247–248
- Continuous wave, laser, 112
- Convolution integral, 106–107, 193, 487
- COPA, 401–402
- Copper, 278
- Coronene, 86, 287
- Corrected emissions spectra, 51–54

- Correlation time distributions, 386–387, 393
 DNA binding to HIV integrase, 404–406
- Correlation time imaging, 406–408
- Correlation times, 353–354, 367–371, 422
- Cortisol, 661–662
- Cos cells
 fluorescence-lifetime imaging microscopy, 745–746
- Cosyntropin, 590
- Coumarin, 57–58, 73
 Förster distances, 468
- Coumarin 108, 151–152, 222
- Coumarin-based potassium probe, 646–648
- Coumarin derivatives
 fluorescence-lifetime imaging microscopy, 748
 photoinduced electron transfer quenching, 338–340
 quenching, 284
 solvent relaxation, 249–250, 253
- Coum-Eu, 189–190
- Covalent adduct formation, intramolecular quenching, 314
- C-peptide, 813–814
- CRABPI (retinal binding protein), 560
- Crambin, 535
- Cramer's rule, 198
- Creatine kinase, 662–663
- Cresyl violet, 54
- Creutzfeldt-Jakob disease, 827
- Critical concentration, 466
- Cross-correlation in flow measurements, 831
- Cross-correlation method, 164–167, 177, 194
- Crown ethers, 17, 643–645, 647, 649
- C-Snaffl 2, 127–128
- Cy3, metal-enhanced fluorescence, 848–851
- Cy3.5, 746–747
- Cy5.5, 657–658, 660–661
- Cyan fluorescent protein (CFP), 458, 497, 654
- Cyanine dyes, 74–75, 512–513
 immunoassays, 641
 potassium sensors, 635
- 9-Cyanoanthracene, 185–186, 255, 279, 364, 744
 frequency-domain lifetime measurements, 170–171
- 3-Cyanoperylene (PeCN), 129
- Cy5 (carboxymethylindocyanine-N-hydroxysuccinimidyl ester),
 780, 787, 824
 acceptor, 680
 Förster distances, 468
 metal-enhanced fluorescence, 848–851
- Cyclic AMP receptor protein (CRP), 291–292
- Cyclodextrins
 phosphorescence of bound probes, 317
 quenching, 286
 solvent effects, 227–228
- Cyclohexane, indole emission spectra in cyclohexane-ethanol
 mixture, 533–534
- Cysteine, 278, 651
- Cytotoxin II, 535
- D**
- Dabyl, 721–722
- Dabyl acceptor, 724
- Danca, 243–244
- Dansylamide
 RET in three dimensions, 509–510
- Dansyl chloride, 16–17
- Dansyl groups, 16, 67–68
 anisotropy decay, 396–397
 creatine kinase immunoassay, 663
 energy transfer, 447–449, 451
 ethylenediamine, 495
 Förster distances, 447, 468
 solvent effects, 227–228
- DANZA, 662–663
- DAPI, 15, 16, 41, 75, 186–187, 359
 fluorescence-lifetime imaging microscopy, 750
 multiphoton excitation, 610–612
- Dapoxyl probes, 229
- Dapoxyl SEDA, 229–230
- DAS. *See* Decay-associated spectra (DAS)
- Data analysis, 129–130
 cross-fitting
 distance distribution, 481–482
 melittin lifetime distributions, 188–189
 frequency-domain lifetime measurements, 162–163
 literature references, 837
 time-domain lifetime measurement, 129–133
 maximum entropy method, 148–149
- DBO, 314
- DCM, 112
- DCVJ, 225
- d-d state, 685
- Dead time, 124
 time-to-amplitude converter (TAC), 115
- Debye-Sears modulator, 163
- Decay, 170–173. *See also* Intensity decay
- Decay-associated spectra (DAS), 581, 596–598
 barnase, 591
 frequency-domain data for calculation of, 269–270
 TRES and DAS comparison, 255
 two-state model, 263
- Decay time. *See* Lifetime (decay time)
- Deconvolution, 131
- Dehydroergosterol, 80
- Delay lines, 116
- Demodulation, 98
- Denaturation, 588
- Denatured pepsin, 806
- Denatured proteins, emission spectra for, 538
- Dendrimers and polymers
 literature references, 791
- DENS, 26. *See also* Dansyl groups
- Deoxycytidine quenching, 284
- Deoxynucleotide triphosphates (dNTPs), 729
- Depolarization, trivial causes, 365–366
- Depolarization factor multiplication, 436–437
- Depth-dependent quenching, 296–298
- Detection profile, 802–803
- Detectors
 CCD, 49
 charged-coupled device, 766
 higher-frequency measurements, 176–177
 laser scanning microscopy, 749–750
 optical phase-sensitive, 743
 for single-molecule detection, 765–766
 single-photon-counting avalanche photodiode, 765
 time-correlated single-photon counting, 117–121
 color effects in, 119–121

- compact PMTs, 118
- DNA sequencing, 123–124
- dynode chain PMTs, 118
- microchannel plate PMTs, 117–118
- multi-detector and multidimensional, 121–124
- photodiodes as, 118–119
- time effects of monochromators, 121
- Deuterium pulse lamps, 113
- Dexter interaction, 335
- Dextran, 394, 634–635
- 1,2-bis(9,10-Dibromooleyl)phosphatidylcholine, 298
- Dicarboxy derivatives, 685
- Dichloroacetamide, 278
- Dichroic beam splitter, 41
- Dichroic filter, 761
- 4-(Dicyanomethylene)-2-methyl-6-(4-dimethylaminostyryl)-4H-pyran (DCM), 112
- Dideoxynucleotide triphosphate (ddNTP), 705, 706, 708
- Dielectric constant, 210, 211
- Dielectric properties of solvents, 250
- Dielectric relaxation times, 250–251
- 4,4'-Diethylaminomethyl-2,2'-bipyridine, 694
- Diethylaniline, 129, 196, 197, 199, 278
- Diffusion
 - of intracellular kinase, 823
 - lateral in membranes, 812–813
 - representative literature references, 504
 - rotational, 828–830
 - of single molecules, literature references, 791–792
 - translational, fluorescence correlation spectroscopy, 802–804
- Diffusion, rotational. *See* Rotational diffusion
- Diffusion coefficients, 277, 498–501, 803–804
 - effect of molecular weight, 806–807
- Diffusion effects
 - anisotropy decay, non-spherical molecules, 418–419
 - for linked D–A pairs, 498–501
 - apparent distance distributions, 478–480
 - experimental measurement, 500–501
 - RET and diffusive motions in biopolymers, 501
 - simulations of RET for flexible pair, 499–500
 - oxytocin, 399
 - RET in rapid-diffusion limit, 520–524
 - acceptor location in lipid vesicles, 521–522
 - retinal location in rhodopsin disk membranes, 522–524
 - RET with unlinked donors and acceptors, 508–509
- Diffusion-enhanced energy transfer in solution, 467
- Diffusion in membranes
 - lateral, 300–301
 - rotational, 399–402 (*See also* Rotational diffusion)
- Diffusion-limited quenching, 281–282
- Diffusive motions in biopolymers, 501
- Dihexadecyl phosphate, 514
- Dihydro-4,4-diisothiocyanostilbene-2,2-disulfonic acid (H2DIDS), 631
- Dihydroequilenin (DHE), 270, 284, 285–286
- Dihydrolipoic acid, 675
- Dihyronicotinamide, 278
- Dihydroorotate dehydrogenase (DHOD), 781–782
- Dihydroxyacetone phosphate, 555
- DiI₁₂, 766–767
- DiI-C₂₀, 812–813
- DiI₁, 512–513
- Dilauroyl phosphatidylcholine (DLPC), 812–813
- Dimensionality effect, experimental RET, 511–515
 - one dimension, 514–515
 - two dimensions, 512–514
- Dimethoxynaphthalene, 336
- 4-Dimethylamino-4-bromostilbene, 177
- 7-(Dimethylamino)coumarin-4-acetate, 251
- 5-Dimethylamino-1-naphthalenesulfonic acid (Dansyl). *See* Dansyl groups
- 4-Dimethylamino-4'-nitrostillbene (DNS), 206
- trans-4-Dimethylamino-4'-(1-oxobutyl) stilbene (DOS), 206–207
- Dimethylaniline (DMA), 336
- N,N-Dimethylaniline sulfonate (DMAS), 286
- 9,10-Dimethylanthracene (DMA), 426
- Dimethyldiazaperopyrenium (DMPP), 514, 515
- Dimethylformamide, 278–279
- Dimethylnaphthalene, 279
- Dimyristoyl-L- α -phosphatidylcholine. *See* DMPC (dimyristoyl-L- α -phosphatidylcholine)
- Dinitrobenzenesulfonyl (DNBS)
 - Förster distances, 468
- Dioleoyl-L- α -phosphatidylcholine. *See* DOPC
- Dipalmitoyl-L- α -phosphatidylcholine (DPPC), 207, 293–294, 812–813
- Dipalmitoyl-L- α -phosphatidylglycerol (DPPG)
 - metal–ligand complexes, 691
- Dipeptides, 542
- 9,10-Diphenylanthracene (DPA), 54, 172–173
- 1,6-Diphenyl-1,3,5-hexatriene. *See* DPH (1,6-diphenyl-1,3,5-hexatriene)
- 2,5-Diphenyl-1,3,4-oxadiazole (PPD), 105
- 2,5-Diphenyloxazole (DPO), 228–229
- Dipicolinate, 523
- Dipicolinic acid, 522
- Dipole moments, solvent effects in emission spectra, 210–211
- Dipoles
 - imaging of radiation patterns, 778–779
 - single-molecule detection, 776–777
- Dirac delta-function, 120
- Direct recording, TRES, 240–241
- Distance-dependent quenching (DDQ) model, 344–346
- Distance distribution functions, 487
- Distance distributions, 477–479. *See also* Energy transfer; time-resolved
 - calcium-induced changes in troponin C conformation, 490–493
 - DNA, four-way Holliday junction in, 493–494
 - in glycopeptide, 495–496
 - in peptides, 479–481
 - concentration of D–A pairs and, 482
 - cross-fitting data to exclude alternative models, 481–482
 - donor decay with acceptor, 482
 - rigid vs. flexible hexapeptide, 479–481
 - in proteins, 485–489
 - distance distribution functions, 487
 - melittin, 483–485
 - from time-domain measurements, 487
- of proteins
 - analysis with frequency domain data, 485–487
 - representative literature references, 504
 - unfolding of yeast phosphoglycerate kinase, 494–495
- Distance measurements, resonance energy transfer, 451–453
 - melittin, α helical, 451–452
 - orientation factor effects on possible range of distances, 452–453
 - protein folding measured by RET, 453–454
- Disulfide oxidoreductase DsbA, 591–592
- Disulfides, quenching by, 279

- DM-Nerf, 639
- DMPC (dimyristoyl-L- α -phosphatidylcholine), 18, 216, 400
cholesterol membranes, 256–257, 293–294
- DMPP (dimethyldiazaperopyrenium), 514–515
- DMQ (2,2'-dimethyl-p-quaterphenyl), 23
- DMSS, 744
- DNA
- anisotropy decay
 - time-domain studies of DNA binding to Klenow fragment, 417
 - anisotropy decay, time-dependent, 402–406, 432–433
 - DNA binding to HIV integrase, 404–406
 - intracellular DNA dynamics, 403–404
 - oligomer hydrodynamics, 403
 - distance distributions
 - double-helical, 507–508
 - four-way Holliday junction in, 493–494
 - dynamics with metal–ligand probes, 688–690
 - energy transfer, 507
 - in one dimension, 514–515
 - frequency-domain lifetime measurements, 186–187
 - helicase-catalyzed unwinding, 373–374
 - hybridization, 20
 - using metal-enhanced fluorescence, 853
 - interaction with proteins, 552–554
 - metal-enhanced fluorescence, 848–851
 - quenching, 341–342
 - intramolecular, 314–315
 - representative literature references, 504
 - Tri ρ repressor binding anisotropy, 373
 - two-photon excitation of DNA bound fluorophore, 610–612
- DNA base analogs, 75–78
- DNA- β helicase, 313
- DNA-bound probe accessibility, quenching, 286–287
- DNA polymerase, 417
- DNA probes, 75–80
- DNA sequencing, 705–712
- DNA technology, 705–734
- aptamers, 724–726
 - DNAzymes, 726
 - cleavage, 810
 - by restriction enzyme, 826
 - conformational dynamics of Holliday junction, 782–783
 - distance-dependence of metal-enhanced fluorescence, 851–853
 - DNA arrays, 732–734
 - light-generated, 734
 - spotted microarrays, 732–734
 - fluorescence correlation spectroscopy
 - bioaffinity reactions, 808–810
 - fluorescence in-situ hybridization, 727–730
 - applications of, 729–730
 - preparation of probe DNA, 728–729
 - hybridization, 715–720
 - excimer formation, 225, 718–719
 - one donor- and acceptor-labeled probe, 717–718
 - polarization assays, 719
 - polymerase chain reaction, 720
 - lanthanides, 681
 - molecular beacons, 720–724
 - based on quenching by gold, 723–724
 - with fluorescent acceptors, 722
 - hybridization proximity beacons, 722–723
 - intracellular detection of mRNA, 724
 - with nonfluorescent acceptors, 720–722
 - multicolor FISH and spectral karyotyping, 730–732
 - multiplexed microbead arrays: suspension arrays, 726–728
 - oligomers, 809–810
 - RET applications, 493–494
 - sequencing, 705–712
 - energy-transfer dyes, 709–710
 - examples of, 706–707, 708–709
 - lifetime-based, 712
 - multidimensional time-correlated single-photon counting (TCSPC), 123–124
 - NIR probes, 710–711
 - nucleotide labeling methods, 707–708
 - principle of, 705–706
 - single-molecule detection
 - literature references, 792
 - stains, high-sensitivity, 712–715
 - energy-transfer stains, 715
 - fragment sizing by flow cytometry, 715
 - high-affinity bis, 713–715
- DNAzymes, 726
- DNBS (dinitrobenzenesulfonyl)
 - Förster distances, 468
- Docking, energy transfer, 460
- Domain motion, 396–397, 501
- Domain-to-domain motions in proteins, 690
- Donor–acceptor pairs. *See also* Energy transfer
 - acceptor decays, 489
 - and distance distributions in peptides, 477–478
 - DNA hybridization, one donor- and acceptor-labeled probe, 717–718
 - effect of concentration on, 482
 - energy-transfer mechanisms, 13–14
 - fluorescence-lifetime imaging microscopy, 742
 - Förster distance, 443–444, 468
 - linked, 340–341
 - linked, diffusion effects, 498–501
 - experimental measurement, 500–501
 - RET and diffusive motions in biopolymers, 501
 - simulations of RET for flexible pair, 499–500
 - molecular beacons, 720
 - single-molecule detection, 773–775
 - theory of, 445–448
 - unlinked, effect of diffusion, 508–509
- Donor decay without acceptor in peptides, 482
- DOPC (dioleoyl-L- α -phosphatidylcholine), 275
 - quenching, 294–295
- DOS (trans-4-dimethylamino-4'-(1-oxybutyl)-stilbene), 206–207
- DOTCI, 174
- 10-Doxylnonadecane (10-DN), 295
- 5-Doxylstearate (5-NS), 299
- DPA (diphenylanthracene), 54, 172–173, 301–302
- DPH (1,6-diphenyl-1,3,5-hexatriene), 11, 15–16, 72, 355, 375
 - anisotropic rotational diffusion, 428
 - anisotropy decays, time-dependent, 399–401
 - ellipsoids of revolution, 421
 - in film, 433–434
 - Förster distances, 468
 - hindered rotors, 391
 - quenching-resolved spectra, 301–302
 - two-photon anisotropy of, 612–613
- DPO (2,5-diphenyloxazole), 228–229
- DPPC (dipalmitoyl-i-a-phosphatidylcholine) systems, 206–207, 293–294
 - energy transfer in two dimensions, 512–513
 - Patman-labeled, TRES, 245–247

- DPPG vesicles, 408, 691
DsRed, 82
DTAC micelles, 286
Dual-color cross fluorescence correlation spectroscopy, 823–828
Dye lasers, 110–112
Dyes. *See also* specific dyes
 energy-transfer, 709–710
 red and near-IR, 74–75
 solvent relaxation, 253
Dynamic quenching. *See* Collisional quenching; Quenching
Dynamics of relaxation. *See* Relaxation dynamics
Dynode chains, 44–45, 46–47
Dynorphin, 590
- E**
- EcoRI, 826
EDANS, 721
Efficiency, quenching, 281, 333–334, 542
EGFP (excited green fluorescent protein)
 fluorescence correlation spectroscopy, 816–817
EIA 5-(iodoacetamido)eosin
 Förster distances, 468
Einstein equation, 12
Electrical bias, 166
Electron-exchange quenching, 335
Electronics
 frequency-domain fluorometers, 164–165
 photomultiplier tube, 44–45
 time-correlated single-photon counting, 114–117
Electronic state resolution from polarization spectra, 360–361
Electronic states, 1, 5
 of metal–ligand complexes, 684–685
Electron scavengers, quenching by, 278
Electron transfer
 photoinduced (PET), 335–336, 627
 quenching in flavoprotein, 315–317
Electrooptic modulators, 165–166
ELISA, 659
Ellipsoids, 418–419
 anisotropy decay, 419–420
 of revolution, 420–425
 rotational diffusion of, 425–426
Elongation factor (Ta-GDP), 548
Emission center of gravity, 246–247
Emission filter, 41
Emission spectra, 3–4, 7–8
 decay-associated, 591–592, 596–598
 instrumentation, 27–31
 distortions in, 30–31
 for high throughput, 29–30
 ideal spectrofluorometer, 30
 molecular information from fluorescence, 17–18
 phase-sensitive, 194–197
 solvent effects, 219–221
 through optical filters, 43–44
 tryptophan decay-associated, 581
Emission spectra, corrected
 instrumentation, 52–54
 comparison with known emission spectra, 52–53
 conversion between wavelength and wavenumber, 53–54
 correction factors obtained with standard lamp, 53
 quantum counter and scatterer use, 53
Emission spectra, quenching-resolved, 301–304
 fluorophore mixtures, 301–302
 Tet repressor, 302–304
Emission wavelength, and anisotropy, 437–438
Encounter complexes, 333–334
Endonuclease, 290–291
Energy gap law, 687–688
Energy transfer, 443–468
 biochemical applications, 453–458
 intracellular protein folding, 454–455
 orientation of protein-bound peptide, 456–457
 protein binding to semiconductor nanoparticles, 457–458
 protein folding measured by RET, 453–454
 RET and association reactions, 455–456
 data analysis, 485–487
 diffusion-enhanced, 467
 distance distributions, 477–479
 distance measurements
 melittin, α helical, 451–452
 distance measurements using RET, 451–453
 incomplete labeling effects, 452
 orientation factor effects on possible range of distances,
 448–449, 452–453
DNA hybridization, one donor- and acceptor-labeled probe, 717–718
effect of colloids, 847
energy-transfer efficiency from enhanced fluorescence, 461–462
Förster distances, 443–444, 445–446, 468
GFP sensors, 654–655
homotransfer, 450
incomplete labeling effects, 452
lanthanides, 680–681
long-wavelength long-lifetime fluorophores, 696
in membranes, 462–465
 lipid distributions around Gramicidin, 463–465
 membrane fusion and lipid exchange, 465
nucleic acids, 459–461
 imaging of intracellular RNA, 460–461
orientation factor, 465
protein kinase C activation, fluorescence-lifetime imaging
 microscopy, 746–747
proteins, 539–545
 anisotropy decreases, detection of ET by, 531–532
 interferon- γ , tyrosine-to-tryptophan energy transfer in, 540–541
 phenylalanine-to-tyrosine, 543–545
 RET efficiency quantitation, 541–543
proteins as sensors, 652–654
quantum dots, 678
radiationless, anisotropy measurement, 365
red-edge excitation shifts, 259
representative R_0 values, 467–468
RET sensors, 458–459
 imaging of intracellular protein phosphorylation, 459
 intracellular RET indicator for estrogens, 458
 Rac activation in cells, 459
sensor mechanisms, 633–637
 glucose, 634–635
 ion, 635–636
 pH and CO₂, 633–634
 theory for, 636–637
silver particles effect, 854–855
single-molecule detection, 773–775
 literature references, 794
in solution, 466–467

- Energy transfer [cont'd]
 theory of, 445–451
 for donor–acceptor pair, 445–448
 homotransfer and heterotransfer, 450–451
 orientation factor, 448–449
 transfer rate dependence on distance, overlap integral, and orientation factor, 449–450
- Energy transfer, time-resolved, 477–501
 acceptor decays, 489
 advanced topics
 single-protein-molecule distance distribution, 496–497
 biochemical applications of distance distributions, 490–496
 calcium-induced changes in troponin C conformation, 490–493
 DNA, four-way Holliday junction in, 493–494
 hairpin ribozyme, 493
 unfolding of yeast phosphoglycerate kinase, 494–495
 diffusion effects for linked D–A pairs, 498–501
 experimental measurement, 500–501
 RET and diffusive motions in biopolymers, 501
 simulations of RET for flexible pair, 499–500
 distance distribution data analysis, 485–489
 frequency-domain analysis, 485–487
 time-domain analysis, 487
 distance distribution in proteins
 analysis with frequency domain data, 485–487
 distance distribution functions, 487
 from time-domain measurements, 487
 distance distributions from steady-state data, 443
 D–A pairs with different R_0 values, 445–446
 quenching, changing R_0 by, 447
 distance distributions in glycopeptide, 495–496
 distance distributions in peptides, 479–482
 concentration of D–A pairs and, 482
 cross-fitting data to exclude alternative models, 481–482
 donor decay without acceptor, 482
 rigid vs. flexible hexapeptide, 479–481
 distance distributions in proteins, 482–485
 domain motion in, 501
 melittin, 483–485
 incomplete labeling effects, 487–489
 orientation factor effects, 489
 representative literature references, 504
 RET imaging, 497–498
- Energy-transfer efficiency from enhanced fluorescence, 461–462
- Energy-transfer immunoassay, 660–661
- Energy-transfer stains and dyes, DNA, 715
- Energy transfer to multiple acceptors in one, two, or three dimensions, 507–524
 dimensionality effect on RET, 511–515
 one dimension, 514–515
 two dimensions, 512–514
 with multiple acceptors, 515–516
 aggregation of β -amyloid peptides, 515–516
 RET imaging of fibronectin, 516
 in presence of diffusion, 519–524
 restricted geometries, 516–519
 effect of excluded area, 518–519
 RET in rapid-diffusion limit, 520–524
 acceptor location in lipid vesicles, 521–522
 retinal location in rhodopsin disk membranes, 522–524
 three dimensions, 507–511
 diffusion effects on RET with unlinked donors and acceptors, 508–509
 experimental studies, 509–511
- Enzyme cofactors
 intrinsic fluorescence, 63–65
 time-domain lifetime measurement, 147
- Enzyme kinetics, 770
- Enzymes
 DNA, degradation, 808
 turnover of, 780–781, 782
- Eosin, 10, 633
- Eosin-labeled ethanolamine, 448
- Eosin-labeled lipid, 447
- Epifluorescence, 41
- Epi-illumination, 761
- Erbium, 682, 683
- Erythrosin, 408
- Erythrosin B, 10
- Escherichia coli* maltose-binding protein, 653
- Escherichia coli* Tet repressor, 302–304
- Estradiol, 80
- Estrogens, intracellular RET indicator for, 458
- 1,2-Ethanedithiol (EDT), 86
- Ethanol
 indole emission spectra in cyclohexane-ethanol mixture, 533–534
 indole lifetime in, 533–534
 polarizability properties, 207
 rotational diffusion in, 367
 specific solvent effects, 213, 214
 tryptophan anisotropy spectra in, 533
- Ethnoadenine derivatives, 287–288
 Förster distances, 468
- Ethers, 209, 279
- Ethidium bromide, 75, 286
 anisotropy decay, 402, 403–404, 432–433
 DNA technology, 713, 714
 energy transfer in one dimension, 514, 515
 metal–ligand probes, 688
- Ethidium homodimer, 75
- Ethoxycoumarin, 230
- Ethyl acetate, 206–207
- Ethylaniline, 338
- Ethylcellulose, 634
- Ethylenediamine, dansylated, 229, 230
- 1-Ethylpyrene, 286
- Europium, 3
 as fluorophores, 679
 Förster distances, 468
 immunoassays, 659
 metal-enhanced fluorescence, 843, 844
- Excimers, 9, 269–270
 DNA hybridization, 225, 718–719
- Exciplex formation, 9, 278
- Excitation, polarized, 778
- Excitation anisotropy, two-photon and multiphoton, 21–22, 612–613
- Excitation anisotropy spectra, 358–361, 531–533
- Excitation filter, 41
- Excitation photoselection of fluorophores, 357–358
- Excitation spectra
 anisotropy, 358–360, 531–533
 instrumentation, 27–31

- corrected spectra, 51–52
 - distortions in, 30–31
 - ideal spectrofluorometer, 30
 - spectrofluorometer for high throughput, 29–30
 - polarization, tyrosine and tryptophan, 531–533
 - Excitation wavelength independence of fluorescence, 7–8
 - Excited charge-transfer complex (exciplex), 9, 278
 - Excited-state intramolecular photon transfer (ESIPT), 221–222
 - Excited-state reactions
 - analysis by phase-modulation fluorometry, 265–270
 - apparent phase and modulation lifetimes, effects on, 266–267
 - wavelength-dependent phase and modulation values, 267–269
 - differential wavelength methods, 264
 - frequency-domain measurement of excimer formation, 196–197
 - naphthol dissociation, time-domain studies of, 264–265
 - naphthol ionization, 260–262
 - overview, 237–240
 - phase modulation, 265–270
 - phase-sensitive detection, 196–197
 - relaxation dynamics, 259–262
 - reversible two-state model, 262–264
 - steady-state fluorescence, 262–263
 - time-resolved decays for, 263–264
 - two-photon, 822–823
 - Exponential decays, frequency-domain lifetime measurements, 170–171
 - Extinction coefficients, 677
 - Extrinsic fluorophores, 15, 67
- F**
- FAD (flavin adenine dinucleotide), 64
 - imaging of, multiphoton microscopy, 617–618
 - quenching by adenine moiety, 278
 - time-domain lifetime measurement, 147–148
 - turnover of cholesterol oxidase, 780, 781
 - Fatty acid binding proteins, 226
 - Fatty acids. *See also* specific fatty acids
 - fluorenyl, 295–296
 - membrane probes, 72
 - FCVJ, 225
 - Femtosecond titanium:sapphire lasers, 108–109
 - Ferredoxin, 584
 - Fibronectin, 516
 - Film polarizers, 51, 366
 - Films, 433–434
 - laser scanning TCSPC film, 748–750
 - surface-plasmon resonance, 863
 - wide-field frequency-domain, 746–747
 - Filters. *See also* Optical filters
 - double dichroic, 824
 - holographic, 766
 - Rugate notch, 766
 - for single-molecule detection, 766–768
 - Fingerprint detection, 683
 - FITC. *See* Fluorescein isothiocyanate (FITC)
 - Fitted function, 106
 - FKBP5901, 149, 592–593
 - Flash-EDT₂, 86
 - Flashlamps, 32
 - time-correlated single-photon counting, 112–114
 - Flavin adenine dinucleotide. *See* FAD
 - Flavin mononucleotide, 16, 64, 316, 317, 397, 398
 - Flavoprotein, electron transfer, 315–316, 317
 - Flavoproteins, 65
 - Flexible D–A pairs, 499–500
 - Flexible hexapeptide, distance distributions, 479–481
 - Flow cytometry, 85
 - DNA fragment sizing, 715
 - Flow measurements using fluorescence correlation spectroscopy, 830–832
 - Fluid flow, 225
 - Fluorenyl fatty acids, 295–296, 299
 - Fluorenyl-PC, 72
 - Fluorescein, 2, 3, 20, 69, 70, 122, 695
 - anisotropic rotational diffusion, 428
 - brightness, 818
 - DNA energy-transfer reaction, 454
 - DNA technology, 707, 717, 719, 726
 - filters, 38
 - melittin labeled with, 374
 - metal–ligand complexes, 691
 - methionyl-tRNA synthetase labeled with, 370–371
 - as pH sensor, 637–639
 - quantum yield standards, 52
 - quenching, 310–312
 - resonance energy transfer, 365
 - time-resolved RET imaging, 498
 - Fluorescein isothiocyanate (FITC), 16, 17, 68
 - FITC-dextran, 635
 - Förster distances, 468
 - Fluorescence
 - energy-transfer efficiency, 461–462
 - intensity fluctuations, 798–799, 800
 - metal-enhanced, 841
 - Fluorescence anisotropy. *See* Anisotropy
 - Fluorescence correlation spectroscopy, 22–23, 757, 797–832
 - applications to bioaffinity reactions, 807–810
 - association of tubulin subunits, 807–808
 - DNA applications, 808–810
 - protein binding to chaperonin GroEL, 807
 - detection of conformational dynamics in macromolecules, 820–821
 - dual-color, 823–828
 - applications of, 826–828
 - DNA cleavage by restriction enzyme, 826
 - instrumentation for, 824
 - literature references, 837
 - theory of, 824–826
 - effects of chemical reactions, 816–817
 - examples of experiments, 805–807
 - effect of fluorophore concentration, 805–806
 - effect of molecular weight on diffusion coefficients, 806–807
 - flow measurements, 830–832
 - fluorescence intensity distribution analysis, 817–819
 - intersystem crossing, 815–816
 - theory for, 816
 - literature references, 837–839
 - in membranes, 810–815
 - binding to membrane-bound receptors, 813–815
 - lateral diffusion, 812–813
 - principles of, 798–799
 - rotational diffusion and photon antibunching, 828–830
 - theory of, 800–805
 - multiple diffusing species, 804–805
 - occupation numbers and volumes, 804
 - translational diffusion, 802–804
 - time-resolved, 819–820

- Fluorescence correlation spectroscopy [cont'd]
 total internal reflection, 821–822
 with two-photon excitation, 822–823
 diffusion of intracellular kinase, 823
- Fluorescence in-situ hybridization (FISH), 727–730
 applications of, 729–730
 preparation of probe DNA, 728–729
 spectral karyotyping, 730–732
- Fluorescence intensity distribution analysis, 817–819
- Fluorescence lifetime imaging microscopy (FLM), 97–98, 630, 741–752
 calcium concentration from lifetime, 744–745
 cos cells images, 745–746
 early methods for, 743–744
 frequency-domain laser scanning microscopy, 750–751
 literature references, 754
 laser scanning TCSPC film, 748–750
 images of amyloid plaques, 750
 literature references, 754
 literature references, 753–755
 using gated-image intensifier, 747–748
 wide-field frequency-domain film, 746–747
 imaging cells containing GFPs, 747
 laser scanning TCSPC film of cellular biomolecules, 750
 protein kinase C activation, 746–747
- Fluorescence microscopy, filters for, 41
- Fluorescence polarization. *See* Polarization
- Fluorescence-polarization immunoassays (FPIs), 661–663, 691–692
- Fluorescence quenching. *See* Quenching
- Fluorescence recovery after photobleaching, 814–815
- Fluorescence resonance energy transfer (FRET), 443. *See also*
 Energy transfer
- Fluorescence scanning spectroscopy
 theory of, 839
- Fluorescence standards. *See* Standards
- Fluorogenic probes, 79–80
- Fluorophore blinking, 767, 768, 769
- Fluorophores, 1, 63–95
 anisotropy decay, time-dependent, 391
 anisotropy of planar fluorophores with high symmetry, 435
 biochemical, 15–16
 blinking of, 815
 brightness, 817–819
 chemical sensing probes, 78–79
 colloid interactions, 846–848
 concentration, 805–806
 DNA probes, 15, 75–78
 dual color, 824–826
 excitation of multiple, 618
 excitation photoselection of, 357–358
 extrinsic, 15, 67–74
 membrane potential probes, 72–74
 membrane probes, 72
 photostability, 70–71
 protein labeling, role of Stokes shift in, 69–70
 protein-labeling probes, non-covalent, 71–72
 protein-labeling reagents, 67–69
- fluorescent proteins, 81–86
 green fluorescent protein, 81–83
 phycobiliproteins, 84–86
 phytofluors, 83–84
- fluorescence-lifetime imaging microscopy, 744
 glucose-sensitive, 650–651
 intercalated, 432–433
- intracellular proteins
 specific labeling of, 86
- intrinsic or natural, 15, 63–67
 enzyme cofactors, 63–65
 protein binding of NADH, 65–67
- lanthanides, 679–683
 fingerprint detection, 683
 nanoparticles, 682
 near-infrared emitting, 682, 683
 resonance energy transfer, 680–681
 sensors, 681–682
- long-lifetime metal–ligand complexes, 683–695
- long-lifetime probes, 86–88
 lanthanides, 87–88
 transition metal–ligand complexes, 88
- long-wavelength long-lifetime, 695–697
- mixtures, quenching-resolved emission spectra, 301–302
- multiphoton excitation for membrane-bound, 613
- photobleaching, 769
- photostability, 769–770, 849–850
- polarization, surface-bound, 786–787
- polarization of single immobilized, 786
- probe–probe interactions, 225–226
- proteins as sensors, 88–89
- quenchers of, 278, 279
- red and near-IR dyes, 74–75
- semiconductor nanoparticles, 675–678
 quantum dots, labeling cells with, 677–678
 quantum dots, resonance energy transfer, 678
 quantum dots, spectral properties, 676–677
- single-molecule detection, 23
- solvent effects on emission spectra, 226–228
- special probes
 fluorogenic, 79–80
 structural analogs of biomolecules, 80
 viscosity probes, 80–81
- two-photon excitation of, 610–612
- 4-Fluorotryptophan (4FW), 565
- FluoSphereJ, 635–636
- Fluro-3, 645
- FMN, enzyme turnover, 781–782
- Focused-ion-beam (FIB), 778
- Folate receptor, 375–376
- Förster, Theodor, 448
- Förster cycle, 261–262
- Förster distance (R_0), 14, 19, 332–333, 366, 468
 anisotropy decay, time-dependent, 389
 distance distribution from steady-state, 499, 500
 donor–acceptor pairs, 443–444, 468
 homotransfer, 450
 indole acceptor pair, 500
 proteins, 540
 representative, 467–468
 RET in three dimensions, 511
- Fractal dimensions, 514
- Fractional accessibility, 288–290, 290–291, 549
- Fractional intensity, 413
- Franck-Condon principle, 5, 8, 12, 211
- Franck-Condon state, 237
- Frequency-domain decays
 anisotropy, time-dependent, 383–387, 390
- Frequency-domain films, wide-field, 746–747

- Frequency-domain lifetime measurements, 157–204
 - apparent phase and modulation lifetime, 191–192
 - background correction, 169–170
 - biochemical examples, 186–189
 - DNA, DAPI-labeled, 186–187
 - fluorescence microscopy with LED light source, 189
 - Mag-Quin-2, magnesium probe, 187–188
 - melittin lifetime distributions, cross fitting of models, 188–189
 - recovery of lifetime distributions from data, 188
 - color effects, 168–169
 - gigahertz fluorometry, 175–178
 - biochemical examples, 177–178
 - measurements, 177
 - instrumentation, 163–168
 - cross-correlation detection, 166
 - frequency synthesizers, 167
 - history, 163–164
 - light modulators, 165–166
 - 200-MHz fluorometers, 164–165
 - photomultiplier tubes, 167–168
 - principles of measurement, 168
 - radio-frequency amplifiers, 167
 - multi-exponential data analysis, 178–186
 - global analysis of two-component mixture, 182–183
 - two closely spaced lifetimes, 180–182
 - two widely spaced lifetimes, 178–180
 - multi-exponential decay analysis
 - maximum entropy analysis, 185–186
 - three-component mixture, limits of resolution, 183–185
 - three-component mixture, resolution of 10-fold range of decay times, 185
 - phase angle and modulation spectra, 189–191
 - phase modulation fluorescence equations, derivation of, 192–194
 - cross-correlation detection, 194
 - lifetime relationship to phase angle and modulation, 192–194
 - phase-modulation resolution of emission spectra, 197–199
 - phase-sensitive emission spectra, 194–197
 - examples of PSDF and phase suppression, 196–197
 - representative decays, 170–173
 - collisional quenching of chloride sensor, 171–172
 - exponential, 170–171
 - green fluorescent protein, one- and two-photon excitation, 171
 - intensity decay of NADH, 172
 - multi-exponential decays of staphylococcal nuclease and melittin, 171
 - SPQ, collisional quenching, 171–172
 - scattered light, 172–173
 - simple frequency-domain instruments, 173–175
 - laser diode excitation, 174
 - LED excitation, 174–175
 - theory, 158–163
 - global analysis of data, 162–163
 - least-squares analysis of intensity decays, 161–162
 - Frequency-domain measurements
 - anisotropy decay, 417–418, 428–429, 588–589
 - excimer formation, 269–270
 - laser scanning microscopy, 750–751
 - protein distance distributions from, 485–487
 - time-domain lifetime measurements, 98–100
 - lifetime or decay time, meaning of, 99
 - phase modulation lifetimes, 99–100
 - Frequency doubling, 112
 - Frequency response, 160
 - Frequency synthesizers, 167
 - FRET. *See* Energy transfer
 - FR-GPI, 375–377
 - Front-face illumination, 55
 - FR-TM, 375–377
 - Fructose, 651
 - F-statistic, 133–134, 135, 136, 180
 - Fumarate, 278
 - Fura-2, 79, 648
 - Fusion proteins, 86
- G**
- β -Galactosidase, 79
 - Gastrin, 590
 - Gated detection, 124–125
 - Gated-image intensifier, 747–748
 - Gating, 819
 - Gaussian distributions, 487
 - correlation time, 393
 - Gaussian lifetime distributions, 143
 - Gauss-Newton algorithms, 131
 - Gaviola, 163
 - GB1, 244–245
 - Generalized polarization, 218
 - Genetically engineered proteins
 - azurins, 538–539
 - for ribonuclease protein folding studies, 558–559
 - in sensors, 651–652
 - spectral properties, 554–557
 - barnase, 556–557
 - tyrosine proteins, 557
 - G-factor, 36, 362, 389
 - GFP, 86
 - anisotropy, 377–378
 - fluorescence-lifetime imaging microscopy, 747
 - GFP5, 747
 - GFP sensors, 654–655
 - Giant unilamellar vesicles (GUVs), 219, 465, 466
 - fluorescence correlation spectroscopy, 812
 - Gigahertz fluorometry, 175–178
 - Glan-Thompson polarizer, 50, 51
 - Global analysis
 - anisotropy decay
 - with multi-wavelength excitation, 429–430
 - frequency-domain lifetime measurements, 162–163, 182–183
 - time-domain lifetime measurements, 138, 144–145
 - Glucagon, 547, 548, 583
 - Glucose-galactose binding protein (GGBP), 652
 - Glucose sensors, 650–651
 - energy-transfer mechanisms, 634–635
 - Glutamate, 551
 - Glyceraldehyde phosphate, 555
 - Glyceraldehyde-3-phosphate dehydrogenase (GPD), 292, 600
 - Glycerol, 250, 359
 - Glycopeptides, 495–496
 - β -Glycosidase, 594
 - gly-trp-gly, 588
 - Gold
 - quenching, 313–315
 - molecular beacons, 723–724
 - surface plasmon-coupled emission, 867
 - Gold colloids, 845–846

Gonadotropin, 548
 Goodness of fit (χ_R^2), 134–135, 136
 diffusion of D–A pairs, 500
 frequency-domain lifetime measurements, 162, 179–182
 mixture lifetime resolution, 140–141
 three-decay time model, 183–184
 time-domain lifetime measurements, 131–132, 133–134, 146
 Goppert-Mayer, Maria, 609
 Goppert-Mayer units, 609
 Gramicidin, 463–465
 Gratings
 in monochromators, 34–35, 36
 in spectrofluorometer, 28, 29
 surface plasmon-coupled emission, 868–869
 Green fluorescent protein, 307–309, 360
 fluorescence correlation spectroscopy, 811
 fluorophores, 81–83
 frequency-domain lifetime measurements, 171
 indicator for estrogens, 458
 single-molecule detection, 762–763, 778
 time-domain lifetime measurement, 145–146
 GroEL, 455–456, 771–773, 807
 GroES, 455–456, 772–773
 Ground-state complex
 quenching mechanisms, 278
 tyrosine, 534–535
 Guanidine hydrochloride, 555, 556
 Guanine, 311, 341, 342
 Guanosine-containing substrate-binding strand (G-SBS), 312
 Guanosine nucleotides, 311–312

H

Hairpin ribozyme, 493
 Half-wave voltage, 166
 Halides, 335
 Halocarbons, 335–336
 Halogenated anesthetics, 632
 Halogens, 11, 278, 279
 quenching by, 334
 Halothane, 304–305
 Hand-over-hand motion, 784
 Head-on photomultiplier tubes, 47
 Heat filter, 32
 α -Helical structure, 561–562, 563
 Helicase, 313
 Helicase-catalyzed DNA unwinding, 373–374
 Helium-cadmium laser, 173
 Heme proteins
 Förster distances, 468
 intrinsic fluorescence, 594–596
 solvent relaxation, 243–244
 Hemicyanine dyes, 254
 Her2 marker, labeling of, 678
 Herschel, John Frederick William, 2–3, 3
 Heterogeneous decays, time-domain lifetime measurements, 101–103
 Heterotransfer, 450–451
 Hexane, 214
 chlorophyll aggregates, 146–147
 polarizability, 209
 Stokes shift, 209, 210
 Hexokinase, 690
 High throughput, spectrofluorometer for, 29–30
 Hindered rotational diffusion, membranes, 399–402

Hindered rotors, 391–392
 Histidine, 341
 quenching, 278, 279
 Histocompatibility protein, 589
 HITEC, 52
 HIV integrase, 78, 404–406
 HIV protease, 80
 Hoechst 33258, 286–287
 Hoechst 33342, 75
 Hoechst 33358, 75
 Holliday junction
 in distance distributions, 493–494
 in single-molecule detection, 782–783
 Holographic filters, 766
 Holographic gratings, 37
 Homotransfer, 374, 450–451
 HPLC, 175
 HPTS (8-hydroxypyrene-1,3,6,8-trisulfonate)
 blood gas measurement, 637
 mirror-image rule exceptions, 8
 pH sensors, 639–640
 HTa (histone-like protein), 544–545
 Human antithrombin (AT), 560–561
 β -Human chorionic gonadotropin, 661
 Human immunodeficiency virus integrase, 78
 Human immunodeficiency virus protease, 80
 Human luteinizing hormone, 435, 436
 Human serum albumin, 13, 72, 304, 548
 anisotropy decay, 413–414
 intensity decay, 583, 584
 laser diode excitation, measurement with, 71, 72
 Hybridization, release of quenching, 310, 311
 Hydration, 367
 Hydrogen peroxide, 278, 279
 Hydrogen pulse lamps, 113
 Hydrophobic surface, calmodulin, 226–227
 7-Hydroxycoumarin (umbelliferone), 79
 8-Hydroxypyrene-1,3,6,8-trisulfonate. *See* HPTS
 17 β -Hydroxysteroid dehydrogenase, 66
 5-Hydroxytryptophan (5HW), 564, 565

I

IAEDANS
 distance distributions, 490–493
 Förster distances, 468
 immunoglobulin fragment labeled with, 371–372
 quenching-resolved spectra, 301–302
 IAF-CK, 662
 IAF [5-(Iodoacetamido)fluorescein], 68
 domain motion, 495
 Förster distances, 468
 ICT (internal charge transfer), 207, 220–221, 223–224, 229, 232
 Image correlation spectroscopy
 literature references, 837–838
 Imaging
 intracellular, 306–307
 in vivo, 656–658
 Imidazole and imidazolium, quenching by, 278
 Imidazolium, 336, 341
 Immunoassays, 658–663
 ELISA, 659
 energy-transfer, 660–661

- fluorescence polarization, 661–663
- metal–ligand complexes, 691–693
- surface plasmon-coupled emission, 867
- time-resolved, 659–660
- Immunoglobulin G, 854
- Immunoglobulins
 - anisotropy decay, 396–397
 - domain-to-domain motions in, 690
 - fragment, Perrin plot, 371–372
 - rotational correlation time, 367
- Immunophilin KFB59-1, 592–593
- Impulse response function, 106–107, 158, 246
- Inchworm motion, 784
- Incomplete labeling effects, energy-transfer studies, 452, 487–489
- Indicators, principles, 16–17
- Indo-1, 647, 648, 649, 650
- Indole
 - covalent adduct formation, 314
 - decay times, 489
 - electronic state resolution, 360–361
 - frequency-domain lifetime measurements, 178–180, 185
 - intensity decays, 579
 - mixture lifetime resolution, 138–141
 - quenching, 11, 278, 279, 341, 537
 - RET in three dimensions, 509–510
 - solvent effects, 533–534
 - spectral relaxation, 596
 - time-domain lifetime, multi-exponential decays, 133, 134
- Infrared and NIR fluorescence
 - dyes, 74–75
 - light sources, 32
- Inner filter effects, 55–56, 290
- In situ DNA hybridization, 715–717
- Instrumentation, 21–24
 - corrected emission spectra, 52–54
 - comparison with known emission spectra, 52–53
 - conversion between wavelength and wavenumber, 53–54
 - correction factors obtained with standard lamp, 53
 - quantum counter and scatterer use, 53
 - corrected excitation spectra, 51–52
 - dual-color fluorescence cross correlation spectroscopy, 824
 - excitation and emission spectra, 21–24, 27–31
 - distortions in, 30–31
 - ideal spectrofluorometer, 30
 - fluorescence correlation spectroscopy, 22–23
 - frequency-domain lifetime measurements, 163–168, 194–175
 - cross-correlation detection, 166
 - frequency synthesizers, 167
 - history, 163–164
 - laser diode excitation, 174
 - LED excitation, 174–175
 - light modulators, 165–166
 - 200-MHz fluorometers, 164–165
 - photomultiplier tubes, 167–168
 - principles of measurement, 168
 - radio-frequency amplifiers, 167
 - simple frequency-domain instruments, 173–175
 - light absorption and deviation from Beer-Lambert law, 58–59
 - light sources, 31–34
 - arc and incandescent lamps, 31–34
 - literature references, 838
 - monochromators, 34–38
 - calibration of, 38
 - polarization characteristics of, 36
 - second-order transmission in, 37
 - stray light in, 36–37
 - wavelength resolution and emission spectra, 35
 - multiphoton excitation, 21–22
 - optical filters, 38–41
 - bandpass, 39
 - combination, 40
 - for fluorescence microscopy, 41
 - neutral density, 40
 - signal purity and, 41–44
 - thin-film, 39–40
 - photomultiplier tubes, 44–49
 - CCD detectors, 49
 - failure of, symptoms, 49
 - hybrid, 49
 - photon counting vs. analog detection of fluorescence, 48–49
 - PMT design and dynode chains, 46–47
 - polarizers, 49–51
 - spectral response, 45–46
 - time response of, 47
 - quantum counters, 51–52
 - quantum yield standards, 54–55
 - sample geometry effects, 55–57
 - sample preparation, common errors in, 57–58
 - single-molecule detection, 23–24, 764–768
 - time-correlated single-photon counting (*See* Time-correlated single-photon counting (TCSPC))
 - two-photon and multiphoton excitation, 21–22
- Instrument response function (IRF), 100, 105–106, 387, 487
- Insulin, 813
- Integrins, energy transfer, 518–519
- Intensity-based sensing, 645
- Intensity decay, 98, 577–578
 - aromatic amino acids, 578
 - correlation time imaging, 406–407
 - least-squares analysis, 161–162
 - microsecond luminescence decays, 129
 - multi-exponential model, 101–102
 - of NADH, 172
 - RET in three dimensions, 509–511
 - ribonuclease T_1 and single-exponential intensity, 584, 585
 - time-domain lifetime measurements, 145–148
 - chlorophyll aggregates in hexane, 146–147
 - FAD, 147–148
 - green fluorescent protein, systematic data errors, 145–146
 - picosecond decay time, 146
 - single-tryptophan protein, 145
 - tryptophan, 580–583
 - decay-associated emission spectra, 581
 - neutral tryptophan derivatives, 581–582
 - rotamer model, 578–580
 - tyrosine, 580–583
 - neutral tyrosine derivatives, 582–583
- Intensity decay laws, 141–144
 - lifetime distributions, 143
 - multi-exponential decay, 141–143
 - stretched exponentials, 144
 - transient effects, 144–145
- Intensity fluctuations, 798–799, 800
- Interference filters, 39–40
- Interferon- γ
 - resonance energy transfer, 540–542

Internal charge transfer (ICT) state, 207, 220–221, 223–224, 229, 232
 Internal conversion in fluorophores, 5
 Intersystem crossing, 5–6, 334–335, 815–816
 Intracellular protein folding, 454–455
 Intramolecular quenching, 314–317
 Intrinsic fluorophores, 15
 Intrinsic/natural fluorescence, 15, 63–67
 enzyme cofactors, 63–65
 multiphoton excitation, 613–616
 of proteins, 594–596
 In-vivo imaging, sensors, 656–658
 Iodide
 absorption spectra, 303
 autocorrelation function in fluorescence correlation spectroscopy, 816
 quenching by, 18, 278, 279, 287, 288, 290, 303–304, 306
 chloride probe, 631
 proteins, 290, 546–547
 Iodine, 5
 Iodoacetamides, 68
 Ionic quenchers, 290. *See also* specific ions
 Ion indicators/probes/sensors. *See also* specific elements/ions
 analyte recognition probes, 644–650
 calcium and magnesium, 647–650
 cation probe specificity, 644
 sodium and potassium, 645–647
 chloride, 631–632
 energy-transfer mechanisms, 635–636
 oxygen, 627–630
 photoinduced electron-transfer (PET) probes, 316, 318, 335–336, 627, 641–643
 Ionization
 naphthol, 260–262
 tyrosine, 534–535
 IR-125, 74
 IR-144, 174
 Iridium metal–ligand complexes, 684
 I7S, 539
 Isomers, rotational, 253–255, 529, 578
 Isoxanthopterin (IXP), 75, 76
 Iterative reconvolution, 131

J

Jablonski, Alexander, 4–5
 Jablonski diagram, 3–6
 collisional quenching and resonance energy transfer, 11
 lanthanide probe, 87
 metal-enhanced fluorescence, 842–843
 red-edge excitation, 257
 solvent effects, 207
 solvent relaxation, 206, 238
 JF9, 780

K

Karyotyping, spectral, 730–732
 Kasha's rule, 7, 359
 Kerr lens mode locking, 109
 Δ^5 -3-Ketosteroid isomerase (KSI), 557
 KFU 111, 635, 636
 Kinase, intracellular, 823
 Kinesin, 784
 Kinetics, literature references, 838

Klenow fragment of DNA polymerase, 417
 Kretschmann configuration, 862

L

Labeling, incomplete, energy-transfer studies, 452, 487–489
 α -Lactalbumin, 806
 Lactate dehydrogenase, 559–560, 584
 Lactoglobulin, 368
 LaJolla Blue, 719
 Lamps. *See* Light sources
 Lanthanide MLCs, 87–88
 long-lifetime probes, 87–88
 quenching, 523
 retinal energy-transfer study, 523
 Lanthanides, 3, 467
 fingerprint detection, 683
 as fluorophores, 679–683
 nanoparticles, 682
 near-infrared emitting, 682, 683
 resonance energy transfer, 680–681
 as sensors, 681–682
 Laplace method, 130
 Laser diodes, 21
 DNA technology, 711
 frequency-domain lifetime measurements, 174
 human serum albumin measurement with, 71, 72
 instrumentation, 33, 34
 time-domain lifetime measurements, 107–108
 Laser line filter, 39
 Lasers
 DNA technology, 711
 dual-color fluorescence cross correlation spectroscopy, 824
 frequency-domain lifetime measurements, 173–174
 monochromators, 34
 multiphoton excitation, 577
 time-correlated single-photon counting
 film, 748–750
 picosecond dye devices, 105–107
 solid-state devices, 107
 time-resolved protein fluorescence, 577
 Laser scanning confocal microscopy (LSCM), 764
 Laser scanning microscopy (LSM), 748–750
 frequency-domain, 750–751
 imaging of cellular biomolecules, 750
 Lateral diffusion in membranes, 300–301, 812–813
 Laurdan, 219, 220, 221
 Least-squares analysis, 160, 487
 frequency-domain lifetime measurements, 161–162
 Stern–Volmer plots, 304
 time-domain lifetime measurements, 129–130
 TRES, 254
 Least-squares fitting, 103
 Lecithin:cholesterol acyltransferase, 454
 Lecithin vesicles, 248
 LED. *See* Light-emitting diodes
 Leucine, 294
 L-format anisotropy measurement or single-channel method, 361–363
 Lifetime-based probes and sensing, 626
 DNA sequencing, 712
 metal–ligand complexes, 88 (*See also* Metal–ligand complexes (MLCs))
 oxygen, 628–629

- Lifetime (decay time), 5–6
 antibodies, 498
 collisional quenching and, 256–257
 estimation, single-molecule detection, 787–788
 fluorescence-lifetime imaging microscopy, 741–752
 frequency-domain (*See* Frequency-domain lifetime measurements)
 long-wavelength long-lifetime fluorophores, 695–697
 meaning of, 99
 metal-enhanced fluorescence, 842–843
 metal–ligand complexes, 683–695
 natural, 10, 537
 phase-modulation
 apparent lifetimes, 191–192
 phase angle and modulation, 192–194
 principles, 9–12
 quenching, 12
 timescale of molecular processes in
 solution, 12
 protein folding and, 558
 quantum yield and, 537
 solvent effects, 222–223
 steady-state intensity and, 14
 time-domain (*See* Time-domain lifetime measurements)
- Lifetime distributions, time-domain lifetime measurements, 143
- Lifetime imaging, 743
- Lifetime reference, 133
- Lifetime-resolved anisotropy, 435–436
- Lifetime-resolved emission spectra, relaxation dynamics, 255–257
- Lifetime standards, 169
- Lifetime-weighted quantum yield, 142
- Ligand analogs, 80
- Ligand-centered absorption, 687
- Light absorption and deviation from Beer-Lambert law, 59
- Light diffraction, 37
- Light-emitting diodes, 33
 frequency-domain lifetime measurements, 174–175, 189
 instrumentation, 33–34
 time-domain lifetime measurements, 108
- Light-generated DNA arrays, 734
- Light-generated probe arrays, DNA hybridization, 734
- Light modulators
 frequency-domain lifetime measurements, 165–166
 monochromators, 34–35
- Light sources, 28
 instrumentation, 31–34
 lamps in corrected emission spectra, 34
 time-correlated single-photon counting, 107–114
 femtosecond titanium:sapphire lasers, 108–109
 flashlamps, 112–114
 picosecond dye lasers, 110–112
 synchrotron radiation, 114
- Linear-focused dynode chain PMTs, 118
- Linearity, time-to-amplitude converter (TAC), 115–116
- Lipid probes, 690–691
- Lipids
 energy transfer, 521–522
 membrane (*See* Membranes)
 metal–ligand complex probes, 690
 pyrenyl-labeled, 72
 pyrenyl-PC, 72
- Lipids, boundary
 lipid-water partitioning effects, 298–300
- Lipids, membrane
 boundary, 298
 distributions around Gramicidin, 463–465
 energy transfer, 513
 exchange of, 465
- Lipobeads, 656
- Lipocalin, 561, 563
- Lippert equation, 208–213
 application of, 212–213
 derivation of, 210–212
- Lippert-Mataga equation, 208–210
- Lippert plots, solvent effects, 215–216
- Liquid crystals, 377
- Lissamine rhodamine B, 70
- Liver alcohol dehydrogenase (LADH), 395, 584
- Localized quenchers, membranes, 332
- Locally excited state, 220–221
- Longitudinal relaxation times, 250, 252
- Long-lifetime probes, 86–88
- Long-pass filters, 38, 39
- Long-wavelength long-lifetime fluorophores, 695–697
- Lorentzian distributions, 487
 correlation time, 393
- Lorentzian lifetime distributions, 143
- Low-frequency polarization, 210
- Low-pressure mercury lamps, 33
- Lucigenin, 631
- Lumazine, 589
- Luminescence, defined, 1
- Luminescence decays, 129
- Lysozyme, 288
- M**
- MACA (N-methylacridinium-9-carboxamide), 631
- Macromolecules, detection of conformational dynamics, 820–821
- Magic-angle conditions, 43
- Magic-angle polarizer conditions, 364
- Mag-INDO-1, 646
- Magnesium indicators/probes/sensors, 17, 187–188, 647–650
- Magnesium Orange, 646, 649
- Magnesium oxide scatterer, 53
- Magnetic resonance imaging (MRI), 406, 742
- Mag-Quin-2, 187–188
- Malachite green, 514
- Maleimides, 68
- Maltose binding protein (MBP), 457–458, 653
- Manganese, 278
- Maximum entropy analysis (MEM), 185–186
- Maximum entropy method, 148–149
- Melittin, 20, 547, 548
 anisotropy decay, 398, 453, 590–591
 association reactions
 detection from homotransfer, 374
 distance distributions, 483–485
 frequency-domain lifetime measurements, 171, 188–189
 phosphorescence, 599
 RET distance measurements, 451–452
 rotational correlation time, 590
- Membrane binding site polarity, solvent effects on emission spectra, 206–207

- Membrane-bound fluorophore
 - anisotropy, 353
 - solvent effects on emission spectra, 215–216
- Membrane-bound receptors, 813–815
- Membrane fusion and lipid exchange, 465
- Membrane potential probes, 72–74
- Membrane probes, 72
 - absorption and emission spectra, 16
 - anisotropy decay, time-dependent, 401–402
- Membranes, 37
 - acceptor location in lipid vesicles, 521–522
 - affecting anisotropy, 366
 - anisotropy, 374–377
 - distribution of membrane-bound proteins, 375–376
 - membrane microviscosity, 374–375
 - anisotropy decay, hindered rotational diffusion in, 399–402
 - diffusion in lateral, 300–301
 - diffusive motions in biopolymers, 501
 - energy transfer, 462–465
 - lipid distributions around Gramicidin, 463–465
 - membrane fusion and lipid exchange, 465
 - relative donor quantum yields, 518
 - tyrosine-to-tryptophan in membrane-bound protein, 543
 - multiphoton excitation for membrane-bound fluorophore, 613
 - phase transitions, 217–219
 - quenching, 18
 - boundary lipid, 298
 - depth-dependent, 296, 297–298
 - lipid–water partitioning effects, 298–300
 - localization of tryptophan residues, 294–295
 - localized quenchers, 295–296
 - oxygen diffusion, 293–294
 - parallax quenching in, 296–298
 - red-edge excitation shifts, 258–259
 - RET in rapid-diffusion limit
 - retinal location in rhodopsin disk membranes, 522–524
 - shear stress on viscosity, 225
 - TNS spectrum, 17–18
 - TRES, 245–249
- Mercaptoacetic acid, 675
- Mercury lamps, 33, 38
- Merocyanine, 72–73
- Metal colloids, optical properties, 845–846
- Metal-enhanced fluorescence, 841
 - applications of, 851–855
 - DNA hybridization, 853
 - release of self-quenching, 853–854
 - silver particles on resonance energy transfer, 854–855
 - distance dependence of, 851–853
 - experimental results, 848–851
 - DNA analysis, 848–851
 - Jablonski diagram, 842–843
 - mechanism, 855–856
 - perspective on, 856
 - review of, 843–845
 - theory for fluorophore–colloid interactions, 846–848
- Metal ion and anions sensors, 641–643
- Metal–ligand complexes (MLCs), 1
 - energy transfer, 520
 - frequency-domain lifetime measurements, 174
 - long-lifetime, 683–695
 - anisotropy properties, 685–686
 - biomedical applications, 688–691
 - energy gap law, 687–688
 - immunoassays, 691–693
 - introduction to, 683–685
 - sensors, 694–695
 - spectral properties of, 686–687
 - long-wavelength long-lifetime fluorophores, 695–697
 - microsecond anisotropy decay, 408–409
 - oxygen sensors, 627–630
- Metalloprotease, 550–551
- Metals
 - effects on fluorescence, 843–845
 - excitation in metal-enhanced fluorescence, 842–843
 - interactions with fluorophores, 846–848
 - quenching by, 305
 - radiative decay engineering, 842
- Metal-to-ligand charge transfer (MLCT), 684–685, 687, 694
- Metaphase chromosomes, 730
- Methanol, 230, 510
 - dielectric properties, 250
 - Stokes shift, 209
- Methionine, 278, 558
- Methionyl-tRNA synthetase, 370–371
- Method of moments (MEM), 124, 130
- 2-Methylanthracene, 293, 294
- 9-Methylanthracene, 185, 186
- N-Methylanthraniloyl amide (NMA), 398
- Methyl 8-(2-anthroyl)octanoate, 215
- Methylindole, 590
- Methylmercuric chloride, 279
- N-Methylnicotinamide, 278
- N-Methylquinolinium iodide (MAI), 306
- O-Methyltyrosine, 583
- Methylviologen, 309–310, 336, 340, 341
- 200-MHz fluorometers, 164–165
- Micelles, 300
- Microbeads, 727, 728
- Microchannel plate photomultiplier tubes (PMT), 47, 117–118, 176
- Microplate readers, 29–30
- Microscopy
 - fluorescence lifetime imaging, 741–752
 - laser scanning, 748–750
 - laser scanning confocal, 764
 - with LED light source, 189
- Microsecond anisotropy decays, 408–409
 - long-lifetime metal–ligand complexes, 408–409
 - phosphorescence, 408
- Microsecond luminescence decays, 129
- Microviscosity, membrane, 374–375
- Mirror image rule, exceptions to, 8–9
- Mixtures
 - fluorescence-lifetime imaging microscopy, 748
 - quenching-resolved emission spectra, 301–302
 - sample preparation errors, 57–58
 - solvent, emission spectra effects, 229–231
 - TRES and DAS comparison, 255
- MLC. *See* Metal–ligand complexes (MLCs)
- Mode locking, laser, 110
- Modulation lifetimes, 99–100
 - apparent, 191–192
 - phase-modulation fluorometry, 198, 266–267
- Modulation spectra, 189–191

- Molecular beacons, 311, 720–724
 based on quenching by gold, 723–724
 emission spectra, 757–758
 with fluorescent acceptors, 722
 hybridization proximity beacons, 722–723
 intracellular detection of mRNA, 724
 with nonfluorescent acceptors, 720–722
 quenching by gold colloids, 313–314
 quenching by gold surface, 314, 315
 single-molecule detection, 782
- Molecular biology quenching applications, 310–313
- Molecular chaperonin cpn60 (GroEL), 371
- Molecular information from fluorescence, 17–19
 emission spectra and Stokes shift, 17–18
 fluorescence polarization of anisotropy, 19
 quenching, 18–19
 resonance energy transfer, 19
- Molecular weight effect on diffusion coefficients, 806–807
- Moments and higher orders
 literature references, 838
- Monellin, 548
 anisotropy decay, 432, 588
 phosphorescence, 599
- Monochromators, 28, 34–35
 instrumentation
 calibration of, 38
 polarization characteristics of, 36
 second-order transmission in, 37
 stray light in, 36–37
 time-correlated single-photon counting, 121
 wavelength resolution and emission spectra, 35
- Monte Carlo simulations
 energy transfer, 517
 parameter uncertainty, 135
- Motions of molecular motors, 784
- MQAE [N-(ethoxycarbonylmethyl)-6-methoxyquinolinium], 79, 632
- MR121, 311, 782
- mRNA
 intracellular detection of by molecular beacons, 724
- M13 peptide, single-molecule calcium sensor, 784
- Multi-alkali photocathode, 46
- Multichannel analyzer (MCA), 116, 121
- Multicolor fluorescence in-situ hybridization (m-FISH), 731
- Multi-exponential decay
 emission center of gravity, 583
 frequency-domain lifetime measurements, 171, 178–186
 global analysis of two-component mixture, 182–183
 maximum entropy analysis, 185–186
 melittin, 171
 three-component mixture, resolution limits, 183–185
 three-component mixture, resolution of 10-fold range of decay times, 185
 two closely spaced lifetimes, 180–182
 two widely spaced lifetimes, 178–180
- multi-tryptophan proteins, 584
- resolution, 103
- solvent effects, 229–231
- time-domain lifetime measurements, 133–141
 anthranilic acid and 2-aminopurine, 137–138
 global analysis, multi-wavelength measurements, 138
 goodness of fit comparison, F-statistic, 133–134
 intensity decay laws, 141–143
 multi-exponential or heterogeneous decays of, 101–103
 number of photon counts, 135, 137
 parameter uncertainty-confidence intervals, 134–135, 136
 p-terphenyl and indole, 133
 resolution of three closely spaced lifetimes, 138–141
- Multi-exponential phosphorescence, 599
- Multi-exponential relaxation
 measurement, 252–253
 in water, 251–252
- Multiphoton excitation, 607–619, 822
 cross-sections for, 609
 instrumentation, 21–22
 of intrinsic protein fluorescence, 613–616
 for membrane-bound fluorophore, 613
 microscopy, 616–619
 calcium imaging, 616–617
 excitation of multiple fluorophores, 618
 imaging of NAD(P)H and FAD, 617–618
 three-dimensional imaging of cells, 618–619
 two-photon absorption spectra, 609–610
 two-photon excitation of fluorophore, 610–612
- Multiphoton excitation anisotropy, 612–613
- Multiphoton microscopy, 607, 616–619
 calcium imaging, 616–617
 excitation of multiple fluorophores, 618
 imaging of NAD(P)H and FAD, 617–618
 three-dimensional imaging of cells, 618–619
- Multiple decay time quenching, 291
- Multiple intensity decay, 122
- Multiplexed microbead arrays: suspension arrays,
 726–727, 728
- Multiplex-FISH, 731
- Multiscalars, 129
- Multi-wavelength excitation, time-dependent anisotropy
 decay, 429–430
- Myb oncoprotein, 553–554
- Myelin basic protein, 548
- Myoglobin, 243, 584, 596
- Myosin light-chain kinase (MLCK), 372, 456–457
- Myosin S-1, 452
- Myosin S-1 subfragment, 770–771
- N**
- NADH, 16, 63–65
 frequency-domain lifetime measurements, 172, 177, 178
 imaging of, multiphoton microscopy, 617–618
 protein binding, 65–67
 quenching by adenine moiety, 278
- Nanoengineering, surface plasmon-coupled emission, 870
- Nanoparticles
 lanthanides, 682
 protein binding to, 457–458
 semiconductor, 675–678
- Nanosecond flashlamp, 112–113
- Naphthalene, 279
 Förster distances, 468
- 1,8-Naphthalimide, 340, 341
- Naphthalocyanines, 75
- Naphthol
 dissociation, time-domain studies of, 264–265
 excited-state reactions, 260–262
- Naphthyl-2-acetyl, 495
- Naphthylamine derivatives, 213

- Naphthylamines and sulfonic acids
 excited-state reactions, 610
 quenchers of, 279
- Naphthylamine sulfonic acids, 71. *See also* ANS; TNS
 (2-(p-toluidinyl)naphthalene-6-sulfonic acid)
- NATA (N-acetyl-L-tryptophanamide), 217
 anisotropy decay of, 588
 decay-associated spectra, 582
 intensity decay, 120, 579–580, 581–582
 lifetime reference, 100
 quenching, 285, 341, 547, 548
 rotational correlation times, 590
 structure, 579
- Natural fluorescence of proteins, 594–596
- Natural lifetime, 10, 537
- NATyrA (N-acetyl-L-tyrosinamide), 531–532
 intensity decay of, 582–583
- NBD derivatives
 Förster distances, 468
 lipids
 quenching, 279, 299, 300
 red-edge excitation shifts, 258–259
- NBD (7-nitrobenz-2-oxa-1,3-diazole)
 quenchers of, 279
- NBS (nitrobenzenesulfenyl)
 Förster distances, 468
- Nd:YAG lasers, 108, 109–111
- Near-field scanning optical microscopy (NFSOM),
 763–764, 765, 778
 literature references, 793
- Near-infrared emitting lanthanides, 682, 683
- Near-IR. *See* Light-emitting diodes
- Near-IR probes, DNA sequencing, 710–711
- Negative pre-exponential factor, 597
- Nelder-Mead algorithm, 131
- Neodymium, 682–683
- Neodymium:YAG lasers, 110
- Neuro-2a, 455
- Neuronal receptor peptide (NRP), 551–552
- Neutral density filters, 40
- Neutral Red (NR), 223, 338, 339
- N-Hydroxysuccinimide, 68
- Nickel, 278, 279
- Nicotinamide, 348
- Nicotinamide adenine dinucleotide. *See* NADH
- Nile Blue, 514–515
- Nitric oxide, 278, 279
- Nitrite, 348
- Nitrobenz-2-oxa-1,3-dioxol-4-yl. *See* NBD
- Nitrogen as flashlamp, 113
- Nitromethane, 279
- Nitrous oxide, 632–633
- Nitroxide-labeled 5-doxytstearate, 299
- Nitroxide-labeled phosphatidylcholines, 295, 296
- Nitroxide quenching, 278, 279, 295
- Nonlinear least-squares analysis. *See*
 Least-squares analysis
- Nonlinear least squares (NLLS), 124
- Non-radiative decay, 842–843
- Non-radiative decay rate, 222–223
- Non-spherical fluorophores, 391
- Notch filters, 39, 40
- Nuclease, 548
- Nucleic acids, 65
 anisotropy decay, time-dependent, 402–406
 DNA binding to HIV integrase, 404–406
 DNA oligomer hydrodynamics, 403
 intracellular DNA dynamics, 403–404
 aptamers, 724–726
 energy transfer, 459–461
 labeling methods, 707–708
 quenching, 284
- Nucleotides, 65
 quenching by, 341–342
- O**
- Oblate ellipsoids of revolution, 422–423
- Occupation numbers, 804
- Octadecapentaenoic acid, 401–402
- Octadecyl rhodamine B (ORB), 512–513
- Octadecyl rhodamine (ODR), 519
 Förster distances, 468
- Octanol, 210, 215
- Off-center illumination, 55
- Olefins, 278, 279
- Oligonucleotides
 anisotropy decay, 416
 energy transfer, 710
- Oligosaccharides, distance distributions, 495–496
- One-photon excitation, 171, 608–609
 absorption spectra, 610
 cross-sections for, 609
- Optical bias, 166
- Optical density, 55
- Optical filters, 29, 766–768
 bandpass, 39
 colored, 38–39
 combination, 40
 for fluorescence microscopy, 41
 interference, 38–39
 neutral density, 40
 signal purity and, 41–44
 thin-film, 39–40
- Optical properties
 of metal colloids, 845–846
 of tissues, 625
- Optics
 confocal, 761–762, 763
 internal reflection, 760–761
 single-molecule detection, 762–764
- Oregon Green, 516, 639, 648
- Orientation factor (k^2), 448–450
 energy transfer, 465, 489
 on possible range of distances, 448–449, 452–453
- Orientation imaging of R6G and GFP, 777–778
- Orientation polarizability, 209, 211
- Oriented fluorophores, transition moments,
 353, 377–378
- Oscillator strength, 59
- Osmium metal–ligand complexes, 684, 685, 686
 energy gap law, 688
- Osmium MLCs, 88
- Overlap integral, 445, 449–450
- Oxazine dyes, 74
- Oxonal, 73

- Oxygen
 - intersystem crossing, 816
 - quenching by, 334
 - Oxygen imaging
 - literature references, 754
 - Oxygen probes/sensors, 17
 - blood gas measurement, 637
 - camphorquinone, 672
 - collisional quenching mechanism, 627–630
 - lifetime-based, 628–629
 - mechanism of oxygen selectivity, 529
 - Oxygen quenching, 277, 278, 279
 - diffusion coefficient, 293–294
 - DMPC/cholesterol vesicles, 256–257, 293–294
 - DNA-probes, 286
 - intensity decays, 346
 - lifetime-resolved anisotropy, 435–436
 - membrane lipids, 293–294
 - monellin, 432
 - of phosphorescence, 317–318
 - of proteins, 548–549
 - quenching efficiency, 281
 - transient effects, 346
 - of tryptophan, 283–284
 - Oxytocin, 178, 399
- P**
- Papain, 584
 - Parallel component, 776
 - Parallax quenching in membranes, 296–298
 - Parameter uncertainty, time-domain lifetime measurements, 134–135
 - Parinaric acid, 72, 415
 - Parvalbumin, 548, 599
 - Patman, 217, 218
 - membrane TRES, 245–246, 247, 248
 - Pebble sensors, 655–656
 - Pentagastrin, 590
 - Pepsinogen, chicken, 597
 - Peptides
 - calmodulin binding, 372–373
 - distance distributions, 479–481
 - concentrations of D–A pairs and, 482
 - cross-fitting data to exclude alternative models, 481–482
 - donor decay without acceptor, 482
 - energy transfer
 - aggregation of β -amyloid peptides, 515–516
 - membrane-spanning, 294–295
 - rigid vs. flexible hexapeptide, 479–481
 - Peroxides, quenching by, 279
 - Perrin equation, 13, 366–370
 - examples of Perrin plots, 369–370
 - Perrin plots, 369–370, 453
 - immunoglobulin fragment, 371–372
 - molecular chaperonin cpn60 (GroEL), 371
 - segmental motion effects, 436
 - tRNA binding to tRNA synthetase, 370–371
 - Perylene, 3, 4, 5, 10, 226, 391
 - anisotropy, 427–428, 429, 434, 435
 - rotational diffusion and, 422
 - anisotropy decay, 429–430
 - emission spectra, 7
 - energy transfer, 450
 - photoinduced electron energy transfer, 342–343
 - quenchers of, 279
 - pH, indicators/probes/sensors, 17, 175
 - blood gases, optical detection of, 637
 - energy-transfer mechanisms, 633–634
 - fluorescein, 637–639
 - GFP sensors, 655
 - HPTS, 639–640
 - literature references, 754
 - metal–ligand complexes, 694
 - pH sensors, 637–641
 - SNAFL and SNARF, 640–641
 - two-state, 637–641
 - Phase angles, 99, 162
 - frequency-domain anisotropy decays, 385, 386–387
 - frequency-domain lifetime measurements, 189–191
 - lifetime relationship to, 192–194
 - phase-modulation resolution of emission spectra, 198
 - solvent relaxation, 246
 - Phase lifetimes, apparent, 191–192
 - Phase modulation
 - fluorescence equations, derivation of, 192–194
 - lifetime relationship to, 192–194
 - Phase-modulation fluorometry, 265–270
 - apparent phase and modulation lifetimes, 266–267
 - wavelength-dependent phase and modulation values, 267–269
 - Phase-modulation lifetimes
 - HPLC, 175
 - time-domain lifetime measurements, 98
 - Phase-modulation spectra
 - frequency-domain lifetime measurements, 194–196
 - Phase-sensitive and phase-resolved emission spectra, 194–197
 - fluorescence-lifetime imaging microscopy, 743
 - phase-modulation resolution of emission spectra, 197–199
 - from phase and modulation spectra, 198–199
 - phase angle and modulation-based, 198
 - phase or modulation lifetime-based, 198
 - theory of phase-sensitive detection, 195–196
 - examples of PSDF and phase suppression, 196–197
 - high-frequency or low-frequency, 197
 - Phase shift, 159
 - Phase transition in membranes, 217–219
 - Phenol
 - excited-state reactions, 259–260
 - intensity decays, 578
 - quantum yield standards, 54
 - Phenol red, 633
 - Phenylalanine, 63
 - calcium binding to calmodulin using phenylalanine and tyrosine, 545–546
 - mutants of triosephosphate isomerase, 555, 556
 - quantum yield standards, 54
 - quenching of indole, 537
 - resonance energy transfer in proteins, 542, 543–545
 - spectral properties, 530, 531
 - tryptophan quenching of, 537, 592–593
 - 2-Phenylindole, 269, 610
 - N-Phenyl-1-naphthylamine (NPN), 226, 227
 - Phorbol myristoyl acetate (PMA), 746
 - Phosphate, tyrosine absorption and emission, 534, 535
 - Phosphatidic acid, energy transfer, 463–464

- Phosphatidylcholine
 brominated, 295
 dansyl, energy transfer, 463–465
 parinaroyl, 415
- Phosphatidylethanolamine
 energy transfer, 522
- Phosphine ligand, 693
- Phosphoglycerate kinase, 494–495, 501, 690
- Phospholipase A₂, 395, 548, 583
- Phospholipids, 295
- Phosphorescence
 defined, 1
 microsecond anisotropy decays, 408
 protein, 598–600
 quenching, 317–318
- Phosphoryl-transfer protein (PTP), 587
- Photobleaching, 34, 299, 523–524, 608–609, 769
 fluorescence recovery after, 814–815
 literature references, 793
- Photocathodes (PD), 44, 45–46, 765
- Photo-counting streak camera (PCSC), 126–127, 128
- Photodiodes (PD), 177
 amplification, 115
 fast, 176
 single-photon-counting avalanche, 755
 time-correlated single-photon counting, 118–119
- Photoinduced electron transfer (PET)
 energetics of, 336–341
 examples of, 338–340
 in linked donor–acceptor pairs, 340–341
 quenching
 in biomolecules, 341–342
 single-molecule, 342–343
- Photoinduced electron-transfer (PET) probes, 316, 318, 335–336, 627, 641–643
- Photomultiplier tubes (PMTs), 44–49
 amplification, 115
 constant fraction discriminators, 114–115
 frequency-domain lifetime measurements, 167–168
 instrumentation, 44–49
 CCD detectors, 49
 designs and dynode chains, 46–47
 failure of, symptoms, 49
 hybrid, 49
 photon counting vs. analog detection of fluorescence, 48–49
 spectral response, 45–46
 time response of, 47
 multi-anode, 122
 pulse pileup, 116–117
 single-molecule detection, 765
 time-correlated single-photon counting, 103–104
 dynode chain, 118
 microchannel plate, 117–118
- Photon antibunching, 829–830
- Photon burst, 715, 716
- Photon counting histograms, 818
 literature references, 839
- Photon counting rate, 124
- Photon migration imaging (PMI), 657
- Photophysics of single-molecule detection, 768–770
- Photoselection, 12, 357–358
 for two-photon excitation, 612–613
- Photostability of fluorophores, 70–71
- pH sensors. *See* pH, indicators/probes/sensors
- Phthalocyanines, 75
- Phycobiliproteins, 84–86
- Phycocyanine, 84
- Phycocerythrin, 84
- Phycocerythrin, 84
- Phycocerythrin, 84
- Phytochromes, 83–84
- Phytofluors, 83–84
- Picolinium salts, quenching by, 278, 279
- Picosecond dye lasers, time-correlated single-photon counting, 110–112
- Picosecond intensity decays, 146
- Picosecond relaxation in solvents, 249–252
 multi-exponential relaxation in water, 251–252
 theory of time-dependent solvent relaxation, 250–251
- Picosecond rotational diffusion, oxytocin, 399
- Planar fluorophores with high symmetry, anisotropy, 435
- Plasma emission, 39
- Plasmons, 861, 869
- Platelet-derived growth factor (PDGF), 725, 726
- Platinum (II) octaethylporphyrin ketone, 629
- Point-by-point detection, 763
- Poisson distribution, 798
- Poisson noise, 103
- Polarity
 protein, 531, 533–534
 solvent effects on emission spectra, 206, 533–534
 Lippert equation, 210–211
 membrane-bound fluorophore, 206–207
- Polarization, 12–13. *See also* Anisotropy
 anisotropy measurement, 19, 354
 definition, 354–355
 fluorescence immunoassay, 661–663
 generalized, 218
 instrumentation, 36
 mobility of surface-bound fluorophores, 786–787
 monochromator characteristics, 36
 of single immobilized fluorophores, 786
 single-molecule detection, 775–777
 literature references, 794
 surface plasmon-coupled emission, 865
- Polarization assays, DNA hybridization, 719
- Polarization spectra
 electronic state resolution from, 360–361
 tyrosine and tryptophan, 531–533
- Polarized excitation, 778
- Polarizers, 29, 49–51, 364
- Polycyclic aromatic hydrocarbons, 279
- Poly-L-proline, 449
- Polymerase chain reaction (PCR), 720, 808
- Polymer beads, 656
- Polymer films, 433–434
- Polymers
 fluorescence correlation spectroscopy
 literature references, 839
- Poly(methylmethacrylate) (PMMA), 763
- Polynuclear aromatic hydrocarbons, 175
- Polyvinyl alcohol film, 359
- POPOP, 2, 3, 185, 186
- Porphyrin, 465
- Porphyrin ketone derivative, 629
- Position sensitive detection
 literature references, 754
- Potassium-binding benzofuran isophthalate (PBFI), 645–646, 647

- Potassium dehydrogen phosphate (KDP), 251
Potassium probes, 635–636, 645–647
PPD (2,5-diphenyl-1,3,4-oxadiazole), 105
PPO, 279
Presenilin I, 750
Primol 342, 369
Principles of fluorescence, 1–26
 anisotropy, fluorescence, 12–13
 biochemical fluorophores, 15–16
 emission characteristics, 6–9
 excitation wavelength independence, 7–8
 mirror image rule, exceptions to, 8–9
 Stokes shifts, 6–7
 fluorescence sensing, 3
 indicators, 16–17
 Jablonski diagram, 3–6
 lifetimes and quantum yields, 9–12
 molecular information from fluorescence, 17–20
 emission spectra and Stokes shift, 17–18
 fluorescence polarization of anisotropy, 19
 quenching, 18–19
 resonance energy transfer, 19–20
 phenomenon, 1–3
 quenching, 11
 resonance energy transfer, 13–14
 steady-state and time-resolved fluorescence, 14–15
Prion proteins, 827
Probes. *See* Fluorophores
Prodan, 70, 221
 apomyoglobin spectral relaxation, 244–245
 solvent effects, 219
 fatty acid binding proteins, 217
 LE and ICT states, 221
 phase transitions in membranes, 217–219
Prodan derivatives, 217, 218
Proflavin, 286–287
Programmable gain amplifier (PGA), 105
Propanol, 210, 250, 252
Propidium iodide, 713
Propylene glycol, 346, 347, 510
 anisotropic rotational diffusion, 428, 429
 excitation anisotropy spectra, 359, 360
 rotational correlation times in, 590
 solvent relaxation, 217
 tryptophan anisotropy spectra in, 532
Protein binding and association reactions. *See* Association reactions
Protein fluorescence, 529–567
 aromatic amino acids, spectral properties, 530–535
 tryptophan, solvent effects on emission, 533–534
 tyrosinate emission from proteins, 535
 tyrosine, excited-state ionization, 534–535
 tyrosine and tryptophan, excitation polarization of, 531–533
 association reactions, 551–554
 calmodulin, binding to target protein, 551–552
 calmodulin, tryptophan mutants, calcium binding site resolution, 552
 interactions of DNA with proteins, 552–554
 calcium binding to calmodulin, 545–546
 energy transfer, 539–545
 interferon- γ , tyrosine-to-tryptophan energy transfer in, 540–541
 membrane-bound protein, tyrosine-to-tryptophan energy transfer in, 543
 phenylalanine-to-tyrosine, 543–545
 RET efficiency quantitation, 541–543
 general features, 535–538
 genetically engineered proteins, spectral properties, 554–557
 barnase, 556–557
 ribonuclease mutants for, 558–559
 triosephosphate isomerase, 555, 556
 tyrosine proteins, 557
 indole, 531
 phenylalanine, 545
 protein folding, 557–560
 cellular retinoic acid binding protein I (CRABPI), 560
 lactate dehydrogenase, 559–560
 protein structure and tryptophan emission, 560–562
 tryptophan emission in apolar environment, 538–539
 azurins, emission spectra of molecules with one or two tryptophan, 539
 azurins, site-directed mutagenesis of single-tryptophan, 538–539
 tryptophan quenching, 546–551
 emission maximum, effects of, 547–549
 emission spectra resolution by, 550–551
 fractional accessibility in multi-tryptophan proteins, 549–550
Protein fluorescence, time-resolved, 577–600
 anisotropy decays, 583–588
 annexin V, 585–587
 melittin, 590–591
 protein with two tryptophans, 587–588
 representative proteins, 589–591
 ribonuclease T₁, 584, 585
 decay-associated spectra, 591
 intensity decays, 578–580
 perspectives, 600
 phosphorescence, 598–600
 protein folding, conformational heterogeneity, 588–589
 protein unfolding, 588–589
 conformational heterogeneity, 588–589
 representative proteins
 disulfide oxidoreductase DsbA, 591–592
 heme proteins, intrinsic fluorescence, 594–596
 immunophilin FKB59-1, phenylalanine quenching of tryptophan fluorescence, 592–593
 thermophilic β -glycosidase, 594
 tryptophan repressor, site-directed mutagenesis, 593–594
 spectral relaxation, 596–598
 tryptophan, intensity decays, rotamer model, 578–580
 tryptophan and tyrosine, intensity decays, 580–583
 decay-associated tryptophan emission spectra, 581
 neutral tryptophan derivatives, intensity decays, 581–582
 neutral tyrosine derivatives, intensity decays, 582–583
Protein folding, 292–293, 453–455, 557–560
Protein kinase C, 654, 690, 746–747
Protein phosphorylation, 459
Proteins. *See also* Fluorophores
 anisotropy
 Perrin equation, 367–369
 Perrin plots, 370–372
 anisotropy of membranes and membrane-bound proteins, 374–377
 association of tubulin subunits, 807–808
 binding of NADH, 65–67
 binding to chaperonin GroEL, 807
 conformation (*See* Conformation)
 diffusive motions in biopolymers, 501

- Proteins [cont'd]
- distance distributions, 482–485
 - analysis with frequency domain data, 479–482
 - melittin, 452, 483–485
 - representative literature references, 504
 - from time-domain measurements, 487
 - domain-to-domain motions, 690
 - energy transfer, 509, 681
 - orientation of protein-bound peptide, 456–457
 - protein binding to semiconductor nanoparticles, 457–458
 - RET and association reactions, 455–456
 - RET imaging of fibronectin, 516
 - single-protein-molecule distance distribution, 496–497
 - fluorescence correlation spectroscopy
 - literature references, 839
 - labeling
 - probes, non-covalent, 71–72
 - reagents, 67–69
 - Stokes shift in, 69–70
 - literature references, 794
 - metal–ligand complexes, domain-to-domain motions in, 690
 - protein kinase C activation, 746–747
 - quenching
 - distance dependent, 348
 - radiation boundary model, 344–346
 - substrate binding to ribozyme, 311–312
 - quenching applications to, 290–300
 - colicin E1 folding, 292–293
 - conformational changes and tryptophan accessibility, 291
 - effects of quenchers on proteins, 292
 - endonuclease III, 290–291
 - multiple decay time quenching, 291–292
 - as sensors, 88–89, 651–652
 - based on resonance energy transfer, 652–654
 - single-molecular resonance energy transfer, 773–775
 - specific labeling of intracellular, 86
 - time-resolved emission spectra (TRES)
 - apomyoglobin, 243–244
 - membranes, 245–249
 - spectral relaxation in, 242–243
- Proteins, anisotropy decay
- collisional quenching, analysis with, 431–432
 - frequency-domain, 397–399
 - apomyoglobin, rigid rotor, 397–398
 - melittin, 398
 - oxytocin, picosecond rotational diffusion, 399
 - time-domain, 394–397
 - alcohol dehydrogenase, 395
 - domain motions of immunoglobulins, 396–397
 - free probe, effects of, 397
 - phospholipase A₂, 395
 - Subtilisin Carlsberg, 395–396
- Proteins, fluorescent, 81–86
- green fluorescent protein, 81–83, 307–309
 - phycobiliproteins, 84–86
 - phytofluors, 83–84
- Protonation, 643
- Protons
- excited-state reactions, 259
 - quenching by, 279
- Pulsed laser diodes, 577
- Pulsed xenon lamps, 32
- Pulse lasers, 21
- Pulse picker, 110
- Pulse pileup, 116–117
- Pulse repetition rate, 124
- Pulse sampling or gated detection, time-resolved measurements, 124–125
- Purines, 278, 284
- Purothionines, 535
- PyDMA, 126
- Pyrene, 86, 126
 - DNA technology, 718
 - emission spectrum, 9
 - excited-state reactions, 610
 - Förster distances, 468
 - lipids labeled with, 86, 296, 297
 - pyrenyl-PC, 72
 - quenchers of, 279, 300
 - release of quenching upon hybridization, 310, 311
 - rotational diffusion, 371
- Pyrenedodecanoic acid (PDA), 293
- 1-Pyrenesulfonylchloride, 371
- Pyridine, 278, 279
- Pyridine-1, 2, 3
- Pyridine-2, 112
- Pyridinium, 336
- Pyridinium hydrochloride, 278
- Pyridoxal 5-phosphate, 64
- Pyridoxamine, 64
- Pyrimidines, 278, 284
- Pyrophosphate, 316
- Q**
- Quantum counters
 - corrected spectra, 52–53
 - instrumentation, 51–52
- Quantum dots, 457, 675
 - labeling cells, 677–678
 - multiplexed arrays, 727
 - resonance energy transfer, 678
 - spectral properties, 676–677
- Quantum yields, 9
 - and lifetime, 537
 - long-wavelength long-lifetime fluorophores, 695
 - in membranes, 518
 - principles, 9–12
 - quenching, 10
 - timescale of molecular processes in solution, 12
 - protein fluorescence, 536–537
 - resonance energy transfer in proteins, 541–542
- Quantum yield standards, 54–55
- Quartz-tungsten halogen (QTH) lamps, 33
- Quenchers, 278. *See also* specific agents
- Quenching, 11, 18, 277–318, 401–402
 - and association reactions, 304–305
 - accessibility to quenchers, 312–313
 - specific binding reactions, 304–305
 - bimolecular quenching constant, 281–282
 - collisional, 171–172
 - collisional, theory of, 278–282
 - bimolecular quenching constant, interpretation of, 281–282
 - Stern-Volmer equation, derivation of, 280–281

- comparison with resonance energy transfer, 331–334
 - distance dependence, 332–333
 - encounter complexes and quenching efficiency, 333–334
 - by dabcyI, 722
 - energy transfer, 519
 - energy transfer, χ_0 changes from, 480
 - fractional accessibility, 288–290
 - experimental considerations, 289–290
 - Stern-Volmer plots, modified, 288–289
 - by gold, molecular beacons, 723–724
 - on gold surfaces, 313–314
 - molecular beacon by gold colloids, 313–314
 - molecular beacon by gold surface, 314
 - intramolecular, 314–317
 - DNA dynamics, 314–315
 - electron transfer in flavoprotein, 315–316
 - sensors based on photoinduced electron transfer, 316, 318
 - of lanthanides, 523
 - mechanisms of, 334–336
 - electron-exchange, 335
 - intersystem crossing, 334–335
 - photoinduced electron transfer, 335–336
 - molecular biology applications, 310–313
 - molecular beacons by guanine, 311
 - release of quenching upon hybridization, 310, 311
 - substrate binding to ribozymes, 311–312
 - molecular information from fluorescence, 18–19
 - of phosphorescence, 317–318
 - photoinduced electron transfer, 336–341
 - examples of, 338–340
 - in linked donor–acceptor pairs, 340–341
 - photoinduced electron transfer quenching in biomolecules, 341–342
 - DNA bases and nucleotides, 341–342
 - quenching of indole by imidazolium, 341
 - proteins
 - anisotropy decays, 431–432
 - tryptophan position and, 550
 - proteins, applications to, 290–300
 - colicin E1 folding, 292–293
 - conformational changes and tryptophan accessibility, 291
 - effects of quenchers on proteins, 292
 - endonuclease III, 290–291
 - multiple decay time quenching, 291–292
 - quenchers, 278
 - quenching-resolved emission spectra, 301–304
 - fluorophore mixtures, 301–302
 - Tet repressor, 302–304
 - self-, metal-enhanced fluorescence, 853–854
 - sensing applications, 305–310
 - amplified, 309–310
 - chloride-sensitive fluorophores, 306
 - chloride-sensitive green fluorescent protein, 307–309
 - intracellular chloride imaging, 306–307
 - simulated intensity decay, 101
 - single-molecule photoinduced electron transfer, 342–343
 - sphere of action, 285–286
 - static, theory of, 282
 - static and dynamic, 282–283
 - examples of, 283–284
 - steric shielding and charge effects, 286–288
 - DNA-bound probe accessibility, 286–287
 - ethenoadenine derivatives, 287–288
 - Stern-Volmer equation, deviations from, 284–285
 - transient effects, 343–348
 - experimental studies, 346–348
 - proteins, distance-dependent quenching in, 348
 - tryptophan fluorescence, by phenylalanine, 537
 - Quenching, advanced topics, 293–301
 - membranes, 293–300
 - boundary lipid, 298
 - lipid-water partitioning effects, 298–300
 - localization of membrane-bound tryptophan residues, 294–295
 - in micelles, 300
 - oxygen diffusion, 293–294
 - partitioning, 298–300
 - membranes, applications to
 - localized quenchers, 295–296
 - parallax and depth-dependent quenching, 296–298
 - membranes, diffusion in, 300–301
 - lateral, 300–301
 - probe accessibility to water- and lipid-soluble quenchers, 286–287
 - quenching efficiency, 281, 333, 543
 - Quenching constants, 309, 348, 548–549
 - Quenching efficiency, 281, 333, 542
 - encounter complexes, 333–334
 - Quin-2, 648, 649
 - fluorescence-lifetime imaging microscopy, 744–745
 - Quinine, 2, 7
 - chloride sensors, 631
 - Quinine sulfate, 51–52, 53, 56, 196, 197
 - Quinolinium, 279
- R**
- R_0 , *See* Förster distance
 - Rac activation, 459, 460
 - Radiating plasmon model, 856, 868
 - Radiation boundary condition (RBC) model, 344–346
 - Radiation patterns, 778–779
 - Radiative decay, 842–843
 - Radiative decay engineering, 841–870
 - introduction, 841–843
 - Jablonski diagram, 842–843
 - optical properties of metal colloids, 845–846
 - surface plasmon-coupled emission, 861–870
 - Radiative decay rate, 223, 537
 - Radiative transfer, 366
 - Radio-frequency amplifiers, frequency-domain lifetime measurements, 167
 - Raman notch filter, 39
 - Raman scatter, 39, 42, 43, 289
 - Rapid diffusion limit, 467
 - Ras in single-molecule detection, 24
 - rATP, 725
 - Rayleigh scatter, 42, 59, 289, 766
 - Reaction coordinate, 238
 - Reaction kinetics, 758–759, 799
 - Receptors, membrane-bound, 813–815
 - Red and near-IR dyes, 74–75
 - Red-edge excitation shifts, 257–259
 - energy transfer, 259
 - membranes, 258–259
 - Red fluorescent protein, 81
 - Red shift, solvent effects on, 533–534
 - Reflectivity in surface-plasmon resonance, 862–863
 - Refractive index, 50, 208, 209

- Rehm-Weller equation, 337
- Relaxation, 7, 12
- Relaxation dynamics, 237–270
 - analysis of excited-state reactions, 265–270
 - continuous and two-state spectral relaxation, 237–239
 - phase modulation studies of solvent relaxation, 265–267
 - excited-state ionization of naphthol, 260–262
 - excited-state processes, overview, 237–240
 - excited-state reactions, 259–262
 - lifetime-resolved emission spectra, 255–257
 - multi-exponential spectral relaxation, measurement, 252–253
 - picosecond relaxation in solvents, 249–252
 - multi-exponential relaxation in water, 251–252
 - theory of time-dependent solvent relaxation, 250–251
 - red-edge excitation shifts, 257–259
 - energy transfer, 259
 - membranes, 258–259
 - solvent relaxation vs. rotational isomer formation, 253–255
 - time-resolved emission spectra (TRES)
 - analysis, 246–248
 - anthroxyloxy fatty acids, 248–249
 - labeled apomyoglobin, 243–244
 - measurement, 240–242
 - membranes, spectral relaxation in, 245–249
 - overview, 239–240
 - proteins, spectral relaxation in, 242–243
 - synthetic fluorescent amino acid, 244–245
 - time-resolved emission spectra (TRES) measurement
 - direct recording, 240–241
 - from wavelength-dependent decays, 241–242
 - TRES vs. DAS, 255
- Resonance, surface-plasmon, 861–865
- Resonance energy transfer (RET), 13, 144, 375, 443. *See also*
 - Energy transfer
 - applications, 20–21, 490–496
 - characteristics of, 443–445
 - comparison with quenching, 331–334
 - distance dependence, 332–333
 - encounter complexes and quenching efficiency, 333–334
 - Dexter interaction, 335
 - and diffusive motions in biopolymers, 501
 - effects on anisotropy, 364–365
 - efficiency, 333
 - literature references, 839
 - molecular information from fluorescence, 19–20
 - principles, 13–14
 - sensors, 626
 - time-resolved RET imaging, 497–498
- Restricted geometries, energy transfer, 516–519
- Restriction enzymes, 712–713, 826
- Restriction fragment length polymorphisms (RFLPs), 713
- RET. *See* Resonance energy transfer (RET)
- Retinal, 522–524
- Reversible two-state model, 262–264
 - differential wavelength methods, 264
 - steady-state fluorescence of, 262–263
 - time-resolved decays for, 263–264
- Rhenium complex, 520
- Rhenium metal–ligand complexes, 88, 684, 686
 - immunoassays, 692–693
 - spectral properties, 687
- Rhod-2, 645
- Rhodamine, 2, 3, 20, 314, 315
 - anisotropy decay, 394, 416
 - DNA technology, 723, 725, 729
 - glucose sensor, 635
 - quantum yield standards, 54
 - time-resolved RET imaging, 498
- Rhodamine 800, 74
- Rhodamine B, 51, 279
 - metal-enhanced fluorescence, 848
- Rhodamine derivatives, 74, 76
 - Förster distances, 468
 - structures of, 74–75
- Rhodamine 6G, 122, 514
 - concentration in fluorescence correlation spectroscopy, 805–806
 - single-molecule detection, 759–760
- Rhodamine 6G dye laser. *See* R6G laser
- Rhodamine green (RhG), 824
- Rhodamines, 68–69
- Rhodopsin disk membranes, retinal in, 522–524
- Riboflavin, 64
- Ribonuclease A, 501, 558–559
- Ribonuclease T₁, 536, 548, 588–589
 - anisotropy decays, 584, 585
- Ribozymes
 - energy transfer, 460
 - hairpin, 493
 - representative literature references, 505
 - in single-molecule detection, 23–24, 775
- Ribozyme substrate binding, 311–312
- Rigid rotor, 397–398
- Rigid vs. flexible hexapeptide, distance distributions, 479–481
- RNA
 - energy transfer, 459–461
 - imaging of intracellular RNA, 460–461
- Room-temperature phosphorescence of proteins, 599
- Rose bengal, 848
- Rotamers (rotational isomers), 253–255, 529, 578–580
- Rotational correlation time, 102–103, 353
 - ellipsoids, 423–425
- Rotational diffusion, 12, 13, 102, 168, 365, 422–423, 828–830
 - anisotropy decay
 - ellipsoids, theory, 425–426
 - frequency-domain studies of, 427–429
 - non-spherical molecules, 418–419
 - time-domain studies of, 426–427
 - membranes, hindered, 399–402
 - oxytocin, 399
 - Perrin equation, 366–370
 - rotational motions of proteins, 367–369
 - stick vs. slip rotational diffusion, 425
- Rotational isomer formation, 253–255, 529, 578–580
- Rotational motion
 - measurement of, 102
 - single-molecule detection, 775–779
- Rotors
 - hindered, 391–392
 - rigid, 397–398
- R6G laser, 111, 112, 120
 - fluorescence intensity distribution analysis, 818, 819
 - single-molecule detection, 777–778
- R3809U, 117

- Ru(bpy)₂phe-C₁₂, 189, 190
Rugate notch filters, 766
Ruthenium metal–ligand complexes, 88, 684, 686
- S**
- Sample geometry effects, 55–57
Sample preparation, common errors in, 57–58
Second-order transmission, monochromator, 37
Scanning fluorescence correlation spectroscopy
 literature references, 839
Scattered light, 366, 766
 phase-sensitive detection, 196, 197
Scattered light effect, frequency-domain lifetime measurements, 172–173
Second-order transmission, monochromator, 37
Segmental mobility, biopolymer-bound fluorophore, 392–393
Selex, 725
Self-quenching, 69–70
 metal-enhanced fluorescence, 853–854
Semiconductor nanoparticles, 675–678
Seminaphthofluoresceins (SNAFLS), 640–641
Seminaphthorhodofluors (SNARFS), 640–641
Senile plaques, 498
Sensing and sensors, 78–79, 623–663
 analyte recognition probes, 643–650
 calcium and magnesium, 647–650
 cation probe specificity, 644
 intracellular zinc, 650
 sodium and potassium, 645–647
 theory of, 644–645
 calcium, 784
 cardiac, 662
 chloride, 631–632
 clinical chemistry, 623–624
 by collisional quenching, 627–633
 chloride, 631–632
 miscellaneous, 632
 oxygen, 627–630
 energy transfer
 glucose, 634–635
 ion, 635–636
 pH and CO₂, 633–634
 theory for, 636–637
 energy-transfer, 633–637
 GFP sensors, 654–655
 intrinsic, 655
 using resonance energy transfer, 654–655
 glucose-sensitive fluorophores, 650–651
 immunoassays, 658–663
 ELISA, 659
 energy transfer, 660–661
 fluorescence polarization, 661–663
 time-resolved, 659–660
 in-vivo imaging, 656–658
 lanthanides, 659, 681–682
 literature references, 795
 mechanisms of sensing, 626–627
 metal–ligand complexes (*See* Metal–ligand complexes (MLCs))
 molecular information from fluorescence, 17–20
 new approaches to, 655–656
 pebble sensors and lipobeads, 655–656
 pH, two-state sensors, 637–641
 blood gases, optical detection of, 637
 pH sensors, 637–641
 phosphorescence, 629
 photoinduced electron-transfer (PET), 316, 318
 photoinduced electron-transfer (PET) probes for metal ions and anions, 641–643
 probes, 79–81
 proteins as sensors, 651–652
 based on resonance energy transfer, 652–654
 RET, 458–459
 spectral observables, 624–626
 lifetime-based sensing, 626
 optical properties of tissues, 625
 Serotonin, 615–616
 Serum albumin, 13, 71, 72, 304, 584, 589, 678
 anisotropy decay of, 413–414
 intensity decay of, 583, 584
 laser diode excitation, measurement with, 71, 72
 metal-enhanced fluorescence, 851–853
 rotational correlation time, 368
 Shear stress on membrane viscosity, 225
 β-Sheet structure, 561–562, 563
 Side-window dynode chain PMTs, 118
 Signaling, intracellular, 459
 Signal-to-noise ratio in single-molecule detection, 784–786
 Silicone, oxygen sensor support materials, 627, 628, 629
 Silver, 278, 279
 effect on resonance energy transfer, 854–855
 Silver colloids, 845–846
 Silver island films, 848
 Simazine, 660
 Simulated intensity decay, 101, 102
 Single-channel anisotropy measurement method, 361–363
 Single-exponential decay, 120, 121
 spherical molecules, 367
 time-dependent intensity, 198
 Single-exponential decay law, 346
 Single-exponential fit, FD intensity decay approximation, 479
 Single-exponential intensity and anisotropy decay of ribonuclease T₁, 584, 585
 Single-molecule detection, 23–24, 757–788
 advanced topics, 784–788
 lifetime estimation, 787–788
 polarization measurements and mobility of surface-bound fluorophores, 786–787
 polarization of single immobilized fluorophores, 786
 signal-to-noise ratio in single-molecule detection, 784–786
 biochemical applications, 770–773, 780–784
 chaperonin protein, 771–773
 conformational dynamics of Holliday junction, 782–783
 enzyme kinetics, 770
 molecular beacons, 782
 motions of molecular motors, 784
 single-molecule ATPase activity, 770–771
 single-molecule calcium sensor, 784
 turnover of single enzyme molecules, 780–781, 782
 detectability of single molecules, 759–761
 instrumentation, 764–768
 detectors, 765–766
 optical filters, 766–768
 internal reflection and confocal optics, 760–762
 confocal detection optics, 761–762
 total internal reflection, 760–761
 literature references, 788, 791–795
 optical configurations for, 762–764

- Single-molecule detection [cont'd]
 photophysics, 768–770
 resonance energy transfer, 773–775
 single-molecule orientation and rotational motions, 775–779
 imaging of dipole radiation patterns, 778–779
 orientation imaging of R6G and GFP, 777–778
 time-resolved studies of single molecules, 779–780
- Single-molecule detection (SMD), 342–343
- Single-particle detection, 85
- Single-photon counting, 103. *See also* Time-correlated single-photon counting
- Single-photon-counting avalanche photodiode (SPAD), 755, 763
- Single-photon excitation, green fluorescent protein, 171
- Single-stranded DNA binding protein, 552–554
- Singlet state, 334
- Site-directed mutagenesis, azurins, 538–539. *See also* Genetically engineered proteins
- Skeletal muscle troponin C, 490–492
- Skilling-Jaynes entropy function, 148
- Smoluchowski model, 281, 344, 345–346, 347
- SNAFL, 640–641
- SNARF, 640–641
- Sodium analyte recognition probes, 645–647
- Sodium-binding benzofuran isophthalate (SBFI), 645, 647
- Sodium Green, 16, 17, 646, 647
- Sodium probes, 17, 635–636, 643, 645–647
- Soleillet's rule, depolarization factor multiplication, 436–437
- Sol gels, 634
- Solvent effects on emission spectra, 205–235, 533–534
 additional factors, 219–223
 changes in non-radiative decay rates, 222–223
 excited-state intramolecular photon transfer, 221–222
 locally excited and internal charge transfer states, 219–221
 biochemical examples
 calmodulin, hydrophobic surface exposure, 226–227
 cyclodextrin binding using dansyl probe, 227–228
 fatty acid binding proteins, 226
 with solvent-sensitive probes, 226–229
 development of advanced solvent-sensitive probes, 228–229
- Lippert equation, 208–213
 application of, 212–213
 derivation of, 210–212
- Lippert-Mataga equation, 208–210
- Lippert plots, specific solvent effects, 215–216
- mixtures, effects of, 229–231
- overview, 205–208
- polarity surrounding membrane-bound fluorophore, 206–207
- probe–probe interactions, 225–226
- Prodan
 phase transitions in membranes, 217–219
 specific, 213–215
 spectral shift mechanisms, 207–208
 summary of, 231–232
 temperature effects, 216–217
 tryptophan, 533–534
 viscosity effects, 223–225
 shear stress on membrane viscosity, 225
- Solvent relaxation, 12. *See also* Relaxation dynamics; Solvent effects on emission spectra
 vs. rotational isomer formation, 253–255
- Solvent-sensitive probes, 226–229
- Soybean peroxidase (SBP), 595
- SPA (N-sulfopropylacridinium), 631
- Species-associated spectra (SAS), 269–270
- Spectral diffusion in single-molecule detection, 767
- Spectral karyotyping, 730–732
- Spectral observables, sensors, 624–626
- Spectral overlap, two-state model, 661
- Spectral relaxation, 239, 596–598. *See also* Relaxation dynamics
- Spectral response, PMTs, 45–46
- Spectral shift mechanisms, solvent effects on emission spectra, 207–208
- Spectrofluorometer, 3, 27–29
 for high throughput, 29–30
 ideal, 30
 schematics of, 28
- Spectroscopy
 fluorescence correlation, 757, 797–832
 general principles (*See* Principles of fluorescence)
- Sperm whale myoglobin, 584
- Sphere of action, 285–286
- Spin-labeled naphthalene derivative, 314
- Spin-labeled PC, 298
- Spin-orbit coupling, quenching, 278
- Spotted DNA microarrays, 732–734
- SPQ [6-methoxy-N-(3-sulfopropyl)quinolinium]
 chloride sensors, 171–172, 631–632
 quenching, 279
- Squirrel cage, 46
- Stains, DNA, 712–715
 energy-transfer stains, 715
 fragment sizing by flow cytometry, 715
 high-affinity bis, 713–715
- Standard lamp, correction factors obtained with, 53
- Standards
 corrected emission spectra, 52–53
 emission spectra correction, 52–53
 quantum yield, 54–55
- Staphylococcal nuclease, 346, 347, 536, 558, 560, 564–565
 anisotropy, 588
 frequency-domain lifetime measurements, 171
 intensity decay of, 583
- Staphylococcus aureus* metalloprotease, 550–551
- Static quenching, 11, 65, 277. *See also* Quenching
 combined with dynamic quenching, 282–283
 examples, 283–284
 theory of, 280, 282
- Steady-state and time-resolved fluorescence principles, 14–15
- Steady-state anisotropy
 calculation of, 367
 DPH in DPMC vesicles, 302
 proteins, tryptophan position and, 551
- Steady-state intensity, 15
- Steady-state measurements
 continuous relaxation model, 238
 light sources, 31–34
 vs. time-resolved measurements, 97
- Steric shielding, quenching, 281, 286–288
- Stern-Volmer equation, 278, 283–284
 derivation of, 280–281
 deviations from, 284–285
- Stern-Volmer plots, 549–550
- Stern-Volmer plots, modified, 288–289
- Stern-Volmer quenching, 11
- Stern-Volmer quenching constant, 18, 279
- Steroid analogs, 80
- Steroid binding protein (SBP), 286

- Steroids, quenching, 284, 286–287
Stilbene, 223–224, 309, 310
Stokes, G.G., 6, 7
Stokes-Einstein equation, 281
Stokes shift, 6–7, 119
 - advanced solvent-sensitive probes, 228–229
 - dielectric constant and refractive index effects, 207, 208
 - emission spectra and, 17–18
 - in protein labeling, 69–70
 - solvent effects, 208–210, 222Stratum corneum, 751
Stray light, 36–37
Streak camera fluorescence-lifetime imaging microscopy, literature references, 754
Streak cameras, 125–128
Streptavidin, 565–566, 678
Streptococcal protein G, 244
Stretched exponentials, time-domain lifetime measurements, 144
Stroboscopic sampling, 124–125
Structural analogs of biomolecules, 80
Structural motifs
 - tryptophan spectral properties and, 561–562Structure
 - protein (*See* Conformation; Protein folding)
 - steric shielding and quenching, 286–288Stryryl, 72
Substrate binding to ribozymes, 311–312
Subtilisin, 583
Subtilisin Carlsberg, 395–396
Succinimide, 278, 279, 281
Succinyl fluorescein, 707, 708
Sudan III, 633
Sulfa antibiotic sulfamethazine (SHZ), 660
Sulfonyl chlorides, 68
Sulforhodamine, 656, 657
Sulforhodamine, 865, 866
Sulfur dioxide, 279, 632
Support materials, oxygen sensors, 627, 628, 629
Support plane analysis, 134
Surface-bound assays, 867
Surface plasmon-coupled emission (SPCE), 861–870
 - applications of, 867–868
 - expected properties, 865
 - experimental demonstration, 865–867
 - future developments, 868–870
 - phenomenon of, 861
 - surface-plasmon resonance, 861–865
 - theory, 863–865Surface-plasmon resonance (SPR), 861–865
Suspension arrays, multiplexed microbead, 726–727, 728
Syber Green, 720
Synchrotron radiation, 114
Syto 14, 189, 190
- T**
- TAMRA, 724, 726
Taqman, 720
Temperature effects
 - excited-state lifetime, 221
 - LE and ICT states of Prodan, 216–217
 - metal–ligand complexes, 685
 - room-temperature phosphorescence of proteins, 599
 - rotational motions of proteins, 368, 369
 - solvent relaxation, 216–217Terbium, 3, 87, 523–524
 - energy transfer, 467, 521
 - as fluorophores, 679
 - Förster distances, 468Terbium probes, 87
p-Terphenyl, 120, 133, 134, 178
 - resolution of two widely spaced lifetimes, 178–180Tetraethylorthosilicate (TEOS), 634
Tetrahydrorhodamine, 454
Tetramethylrhodamine-labeled lipid (TMR-POPE), 764
Tetramethylrhodamine-labeled nucleotide, 808–809
Tetramethylrhodamine (TMR), 313, 314, 707, 729, 769
 - RET imaging of fibronectin, 516Tetraoctylammonium hydroxide (TOAH), 634
Tet repressor, 145, 302–304
Texas Red, 41, 69, 70, 72, 707
Texas Red-PE, 72
T-format anisotropy measurement, 29, 363–364
Thallium, 279
Theory
 - anisotropy, 355–358
 - anisotropy decay, 414–415
 - energy transfer
 - for donor–acceptor pair, 445–448
 - homotransfer and heterotransfer, 450–451
 - orientation factor, 448–449
 - transfer rate dependence on distance, overlap integral, and orientation factor, 449–450
 - energy-transfer sensing, 636–637
 - frequency-domain lifetime measurements, 161–163
 - global analysis of data, 162–163
 - least-squares analysis of intensity decays, 161–162
 - phase-sensitive detection, 195–197
 - examples of PSDF and phase suppression, 196–197
 - quenching, 278–282
 - relaxation dynamics, time-dependent, 250–251
 - representative literature references, 504Thermophilic β -glycosidase, 594
Thiazole dyes, DNA technology, 715
Thiazole orange, 74–75
Thin-film filters, 39–40
Thiocyanate, 279, 631
Three-decay time model, 178, 179
Three-dimensional imaging of cells, 618–619
Three-photon excitation, cross-sections for, 609
Thymidine kinase, 497
TICT (twisted internal charge transfer), 207, 220, 221, 627, 645
Time-correlated single-photon counting (TCSPC), 103–107, 241
 - convolution integral, 106–107
 - detectors
 - color effects in, 119–121
 - DNA sequencing, 123–124
 - dynode chain PMTs, 118
 - microchannel plate PMTs, 117–118
 - multi-detector and multidimensional, 121–124
 - timing effects of monochromators, 121
 - electronics, 114–117
 - amplifiers, 115
 - analyte-to-digital converter (ADC), 115
 - constant fraction discriminators, 114–115
 - delay lines, 116

- Time-correlated single-photon counting [cont'd]
 - multichannel analyzer (MCA), 116
 - photodiodes as, 118–119
 - pulse pileup, 116–117
 - time-to-amplitude converter (TAC), 115–116
- examples of data, 105–106
- laser scanning microscopy, 748–750
- light sources, 107–114
 - femtosecond titanium:sapphire lasers, 108–109
 - flashlamps, 112–114
 - laser diodes and light-emitting diodes, 107–108
 - picosecond dye lasers, 110–112
 - synchrotron radiation, 114
- principles, 104–105
- Time-correlated single-photon counting (TCSPC) detectors, 117–121
 - compact PMTs, 118
- Time-dependent anisotropy decays. *See* Anisotropy decays, time-dependent
- Time-dependent solvent relaxation, theory of, 250–251
- Time-domain decays
 - anisotropy, time-dependent, 383–387
- Time-domain lifetime measurements, 97–155
 - alternative methods for time-resolved measurements, 124–129
 - microsecond luminescence decays, 129
 - streak cameras, 125–128
 - transient recording, 124–125
 - upconversion methods, 128–129
 - applications of time-correlated single-photon counting (TCSPC)
 - chlorophyll aggregates in hexane, 146–147
 - FAD intensity decay, 147–148
 - green fluorescent protein, systematic data errors, 145–146
 - picosecond decay time, 146
 - applications of time-correlated single-photon counting (TSCPC), 145–148
 - single-tryptophan protein, 145
 - biopolymers, multi-exponential or heterogeneous decays of, 101–103
 - data analysis, 129–133
 - assumptions of nonlinear least-squares method, 130
 - autocorrelation function, 132–133
 - goodness of fit (χ_R^2), 131–132
 - least-square analysis, 129–131
 - maximum entropy method, 148–149
 - frequency-domain measurements, 98–100
 - examples of time-domain and frequency-domain lifetimes, 100
 - lifetime or decay time, meaning of, 99
 - phase modulation lifetimes, 99–100
 - global analysis, 144–145
 - intensity decay laws, 141–144
 - lifetime distributions, 143
 - multi-exponential decay, 141–143
 - stretched exponentials, 144
 - transient effects, 144–145
 - multi-exponential decays, analysis of, 133–141
 - anthranilic acid and 2-aminopurine, 137–138
 - global analysis, multi-wavelength measurements, 138
 - goodness of fit comparison, F-statistic, 133–134
 - number of photon counts, 135, 137
 - parameter uncertainty-confidence intervals, 134–135, 136
 - p-terphenyl and indole, 133
 - resolution of three closely spaced lifetimes, 138–141
- vs. steady-state measurements, 97
 - time-correlated single-photon counting (TCSPC), 103–107
 - convolution integral, 106–107
 - examples of data, 105–106
 - principles, 104–105
- time-correlated single-photon counting (TCSPC) detectors, 117–121
 - color effects in, 119–121
 - compact PMTs, 118
 - DNA sequencing, 123–124
 - dynode chain PMTs, 118
 - microchannel plate PMTs, 117–118
 - multi-detector and multidimensional, 121–124
 - photodiodes as, 118–119
 - timing effects of monochromators, 121
- time-correlated single-photon counting (TCSPC) electronics, 114–117
 - amplifiers, 115
 - analyte-to-digital converter (ADC), 115
 - constant fraction discriminators, 114–115
 - delay lines, 116
 - multichannel analyzer (MCA), 116
 - pulse pileup, 116–117
 - time-to-amplitude converter (TAC), 115–116
- time-correlated single-photon counting (TCSPC) light sources, 107–114
 - femtosecond titanium:sapphire lasers, 108–109
 - flashlamps, 112–114
 - laser diodes and light-emitting diodes, 107–108
 - picosecond dye lasers, 110–112
 - synchrotron radiation, 114
- Time-domain measurements
 - anisotropy decay, 394–397, 415–417
 - protein distance distributions from, 487
- Time-resolved emission spectra (TRES), 596–597, 598. *See also* Relaxation dynamics
 - analysis, 246–248
 - vs. DAS, 255
 - frequency-domain data for calculation of, 264–265
 - labeled apomyoglobin, 243–244
 - membranes, spectral relaxation in, 245–249
 - overview, 239–240
 - synthetic fluorescent amino acid, 244–245
- Time-resolved emission spectra (TRES) measurement, 240–242
- Time-resolved energy transfer. *See* Energy transfer, time-resolved
- Time-resolved fluorescence
 - anisotropy decay, 102, 367
 - Förster distance determination, 499
 - light sources, 31
 - principles, 14–15
 - protein (*See* Protein fluorescence, time-resolved)
 - reasons for, 14
 - reversible two-state model, 263–264
- Time-resolved fluorescence correlation spectroscopy, 819–820
- Time-resolved immunoassays, 659–660
- Time-resolved measurements, 779–780
- Time-to-amplitude converter (TAC), 104, 105, 115–116, 121, 122
- TIN, 715
- TIRF, 56
- Tissues
 - in-vivo imaging, 656–658
 - optical properties of, 625
- Titanium:sapphire lasers, 108–109, 128, 577
 - for multiphoton microscopy, 614
- TMA, 500–501
- TMA-DPH, 72

- TMR (tetramethylrhodamine), 468
fluorescence intensity distribution analysis, 818, 819
Förster distances, 468
time-resolved fluorescence correlation spectroscopy, 819
- TNB (trinitrophenyl)
Förster distances, 468
- TNS [6-(p-toluidinyl)naphthalene-2-sulfonate]
red-edge excitation, 256
vesicles, TRES, 256
- TNS [2-(p-toluidinyl)naphthalene-6-sulfonic acid], 71–72
anisotropy decay, 397–398
- TNS [6-(p-toluidinyl)naphthalene-2-sulfonic acid], 17–18
- TO, 715
- TO-8, 118
format of photomultiplier tubes, 46
- [2-(p-Toluidinyl)naphthalene-6-sulfonic acid] (TNS). *See* TNS
(2-(p-Toluidinyl)naphthalene-6-sulfonic acid)
- Total internal reflection (TIR), 56, 760–761, 762, 821–822, 862
literature references, 839
- TOTIN, 715
- TOTO, 75, 714, 715
- Transfer efficiency, 446, 447
- Transferrin, energy transfer, 521
- Transient effects, time-domain lifetime measurements, 143
- Transient recording, 124–125
- Transition metal–ligand complexes. *See* Metal–ligand complexes
(MLCs); specific elements
- Transition moments, anisotropy, 355, 356, 377–378, 433–435
- Transit time spreads (TTS), 47, 117–118, 119
- Translation diffusion and fluorescence correlation spectroscopy,
802–804
- TRES. *See* Time-resolved emission spectra (TRES)
- Trichloroethanol (TCE), 278, 292
- Trifluoperazine, 89
- Trifluoroacetamide (TFA), 288
- Trifluoroethanol (TFE), 304
- Triosephosphate isomerase, 555, 556
- tRNA binding to tRNA synthetase, 370–371
- Tropomyosin, 681
- Troponin C, 614
calcium-induced conformation changes, 490–493
- Troponin I, 589
- Trp repressor-DNA binding anisotropy, 373
- Trypsin, 368
- Tryptophan, 11, 15, 63, 490
absorption and emission spectra, 16, 17
acceptor decay, 489
challenge of, 566–567
conformational changes and accessibility, 288–289
decay-associated emission spectra, 581
emission, 536
emission and protein structure, 560–562
genetically inserted amino-acid analogues, 565–566
tryptophan spectral properties and structural motifs, 561–562
emission in apolar environment, 538–539
emission spectra, 44
energy transfer, 450, 451
excitation polarization spectra, 531–533
frequency-domain lifetime measurements, 188–189
intensity decays, 145, 580–583
multiphoton excitation of, 614
mutants, 552, 555, 556
pH and, 579
phosphorescence of, 598–600
protein fluorescence, 529–530
quantum yield standards, 54
resonance energy transfer in proteins, 540–541, 542
rotamers, 578–579
rotational correlation times, 590
simulated intensity decay, 101–102
solvent effects on emission spectra, 533–534
spectral properties, 530, 531, 561–562
spectral relaxation, 596–598
structure, 579
tryptophan analogs, 562–567
unfolding and exposure to water, 588–589
- Tryptophan analogs, protein fluorescence, 562–567
- Tryptophan quenching, 279, 280, 283–284, 546–551. *See also*
specific proteins
accessibility of quencher, 18, 288, 291, 549–550
emission maxima, effects of, 547–549
emission spectra resolution by, 550–551
endonuclease III, 290–291
localization of membrane-bound residues, 294–295
by phenylalanine, 592–593
quenching constant, 281–282, 548–549
- Tryptophan repressor, site-directed mutagenesis, 593–594
- Tubulin subunits, 807–808
- TU2D, 500–501
- Turbidity, 365–366
- Twisted internal charge transfer (TICT) state, 207, 220, 221, 627, 645
- Two-channel method anisotropy measurement, 363–364
- Two-component mixture, global analysis, frequency-domain lifetime
measurements, 182–183
- Two-photon excitation, 171, 608, 822–823
absorption spectra, 609–610
cross-sections for, 609
diffusion of intracellular kinase, 823
excitation photoselection, 612–613
of fluorophore, 610–612
instrumentation, 21–22
- Two-state pH sensors, 637–641
- Two-state relaxation, 246, 262–263
model, 237
- Tyr-NO₂
Förster distances, 468
- Tyrosinate-like emissions, 535
- Tyrosine, 63, 316
calcium binding to calmodulin using phenylalanine and
tyrosine, 545–546
dipeptides, 542
emission from proteins, 535
emission spectra, 44
excitation polarization spectra, 531–533
excited-state ionization of, 534–535
intensity decays, 580–583
protein fluorescence, 529
quantum yield standards, 54
quenchers of, 279
resonance energy transfer in proteins, 540–541, 542, 543–545
spectral properties, 530, 531
structure, 579
vasopressin, 178
- Tyrosine kinase, 459
- Tyrosine proteins, genetically engineered, 557

U

Umbelliferone (7-hydroxycoumarin), 79
 Umbelliferyl phosphate (7-UmP), 79, 659
 Underlabeling, 488–489
 Upconversion methods, time-resolved measurements,
 128–129
 Uridine quenching, 284

V

Valinomycin, 635
 Vasopressin, 177, 178
 Vesicles
 giant unilamellar, 465, 466
 Patman-labeled, TRES, 246–247, 248
 Prodan, 219
 red-edge excitation, 258–259
 RET in rapid-diffusion limit, 521–522
 TNS-labeled, TRES, 256
 Vibrational structure of fluorophores, 5
 Viscosity
 and rotational diffusion, 366
 rotational motion of proteins, 367–368
 solvent effects, 223–225
 Viscosity probes, 80–81
 Voltage and fluorophores, 73–74
 Volume calculation in fluorescence correlation
 spectroscopy, 804

W

W71, 556
 W92, 558–559
 W94, 556–557
 Water
 dielectric properties, 251
 multi-exponential relaxation in, 251–252

phosphorescence quenching, 317
 polarizability properties, 209
 Wavelength, 27
 dye lasers, 112
 emission spectrum, 4
 excitation, emission characteristics, 6–8
 Wavelength-dependent decays, 239–240
 TRES measurement from, 241–242
 Wavelength-ratiometric probes, 79, 624, 645, 651, 741, 742
 Wavelength-to-wavenumber conversion, 53–54
 Wavenumber, 27
 Weber, Gregorio, 68, 69
 W168F mutant, 555
 Wide-field frequency-domain film, 746–747
 Window discriminator (WD), 105

X

Xenon, 279
 Xenon lamp, 28, 31–32
 pulsed, 32

Y

Y-base, 65
 Yellow fluorescent protein (YFP), 81, 307–309, 397,
 398, 458, 497, 654
 YFP5, 747
 Yt-base, 230–231
 solvent relaxation, 251–252
 Ytterbium, 682, 683

Z

Z (collisional frequency, fluorophore-quencher), 281
 Zener diode, 167
 Zinc-finger peptide, 88, 89, 501